Politecnico di Torino

Politecnico Di Torino

Master's Degree

Energy and Nuclear Engineering

Sustainable Nuclear Energy

FIRST NEUTRONIC EVALUATION OF A HIGH TEMPERATURE SODIUM COOLED REACTOR

Academic Tutor:
Prof. Sandra DULLA

Candidate:
Vanessa NIGRO

CEA Supervisors:
Dr. Cyril PATRICOT
Dr. Sandrine COCHET
Dr. Roland LENAIN

2023/2024

Politecnico di Torino

Politecnico Di Torino

Master's Degree

Energy and Nuclear Engineering

Sustainable Nuclear Energy

FIRST NEUTRONIC EVALUATION OF A HIGH TEMPERATURE SODIUM COOLED REACTOR

Academic Tutor:
Prof. Sandra DULLA

Candidate:
Vanessa NIGRO

CEA Supervisors:
Dr. Cyril PATRICOT
Dr. Sandrine COCHET
Dr. Roland LENAIN

2023/2024

To my land
to my sea.

Acknowledgements

This thesis is the culmination of my internship at the CEA Saclay center. The experience I gained during these six months is truly invaluable. It allowed me the opportunity to work in my specialized field for the first time, to live in Paris, and last but certainly not least, the chance to meet many kind persons, who were not just professional nuclear engineers, but also wonderful people always ready to help me and to share with me the their knowledge.

Fist of all I want to thank my academic tutor, Sandra Dulla for making this experience possible, the professor Piero Ravetto, who gave me the passion in reactor physics and the Politecnico di Torino for the education I received.

I want to thank the SERMA people with whom I collaborate and who gave me priceless suggestion during my work. A special thanks to the laboratory LPEC of which I was a part and its laboratory chief Amélie Rouchon.
I am extremely grateful to my tutor Cyril Patricot, for being by my side all the internship, helping me and leading me during this six month, to Sandrine Cochet for always being kind and available to answer the many questions I asked and to follow me during the construction of all the scripts in APOLLO2®. I am also grateful to Roland Lenain for being present in the last period of work.

Special thanks to my co-workers Lèo and Alexis, for making these months even more memorable.
I could not have undertaken this journey without my good friend Rebecca, with whom I spent all the time, during work and beyond.

I could not be here and be what I am if it were not for the people who have contributed with their love and support to make who I am now.

A special thank to my parents, for giving always great support, for believing in my potential from the beginning. Thanks for the priceless lessons you gave me during all these years.

Thank to my sister, Brenda, for being always my point of reference, for her kindness and noble character.

Thank to my dearest friend Fabiana, who supported me in any case, for any reason and for being by my side since forever. My best adventure girl.

A big thank you goes to my sweet friends Nina and Margherita, with whom I spent all my university experience and share memorable moments that bonded us forever.

I'm grateful to Flavia, the perfect roommates, for being by my side in any occasion during the last months.

Finally, I want to extend my deepest gratitude to Lorenzo. Thank you for being constantly close to me, even from miles away. The person I am today owes much to you.

Abstract

The focus of this work is to perform an preliminary neutronic assessment of a Sodium-Cooled High-Temperature Reactor (HTR-Na cooled). This involves the development of a deterministic calculation schemes, followed by a detailed physical analysis and the formulation of some design proposals. The concept of the HTR-Na cooled draws inspiration from the Japanese High Temperature Test Reactor (HTTR), a High-Temperature Gas Reactors (HTGRs). The key objective is to downsize the reactor by employing liquid sodium as a coolant to replace the helium, while simultaneously rising the core power to collect thermal energy for industrial application, such as hydrogen generation.
The work is divided into three main parts: first the construction of the assembly calculation scheme, then a comprehensive physical analysis at lattice level and finally the core calculation scheme. The evaluations are carried out using the CEA's deterministic codes APOLLO2® and APOLLO3®.
The assembly calculation scheme includes the static and the depletion calculations. Through the use of Method of Characteristics (MOC), the transport equation is solved allowing a detailed analysis of the reactor behaviour. Various neutronic parameters are studied, including reactivity, temperature coefficients for fuel, moderator and coolant both at beginning and end of fuel life and the cycle length. Different assembly designs are considered, assessing their behavior at the lattice level by altering geometrical parameters and properties. The analysis highlights significant aspects, particularly the impact of packing fraction, which represents the ratio between the volume occupied by the TRi-stuctural ISOtropic (TRISO) particles and the graphite matrix. Results indicate how this geometrical parameter influences the overall behavior of the fuel assembly. Additionally, other findings provide insights into the general reactor behavior at the assembly level. Next, core calculations are performed and compared with the preliminary core analysis performed from the assembly calculation to predict core behaviour.

Contents

List of Figures

List of Tables

Acronyms

ACS Auxiliary Cooling System

BPs Burnuble poisons

BWRs Boiling Water Reactors

C/V Reactor Containment Vessel

CEA Atomic Energy and Alternative Energies Commission

CFPs Coated Fuel Particles

CP2C Criticality Competence Team

CPM Collision Probability Method

DES Direct des Energies

DM2S Systems and Structures Modelling Department

EDF Electricity of France

FPs Fission Products

Gen-IV Generation IV

GFR Gas-cooled Fast Reactor

GIF Generation IV International Forum

GUI Graphical User Interface

He helium

HTGRs High-Temperature Gas Reactors

HTR-Na cooled Sodium-Cooled High-Temperature Reactor

HTRs High Temperature Reactors

HTTR High Temperature Test Reactor

IPyC Inner Pyrolitic Carbon

ISAS Institute of Applied Sciences and Simulation for Low-Carbon Energy

JAERI Japan Atomic Energy Research Institute

LFR Lead-cooled Fast Reactor

LLPR Laboratory of Software for Reactor Physics

LPEC Laboratory of Physics and studies of Cores

LTSD Stochastic Transport and Data Laboratory

LWRs Light Water Reactors

MCS Main Cooling System

MOC Method of Characteristics

MSR Molten Salt Reactor

OPyC Outer Pyrolitic Carbon

PDFs Partial Differential Equations

PWRs Pressurized Water Reactors

RPV Reactor Pressure Vessel

RVCS Reactor Vessel Cooling System

SCWR Super-critical Water-cooled Reactor

SEMT Mechanical and Thermal Studies Department

SERMA Reactor Studies and Applied Mathematics Department

SFR Sodium-cooled Fast Reactor

SiC Silicon Carbide

STMF Thermal Hydraulics and Fluid Mechanics Department

TDT Two-and Three-Dimensional Transport

TRISO TRi-stuctural ISOtropic

VHTR Very-High-Temperature Reactor

Introduction

1.1 CEA Research Center

The Atomic Energy and Alternative Energies Commission (CEA)[1] is a public research organization and one of the key actors in technological research and innovation in France. Created in 1945, from the beginning, it has covered an important role in research, development and innovation.
It is currently active in four areas:

- Low-carbon energy (nuclear and renewable),
- Digital technologies,
- Technologies for medicine field,
- Defence and security.

The CEA is a complex organization with multiple research centers and divisions. There are 9 centres throughout France. It is developing numerous partnerships with other research organisations, local authorities and universities.

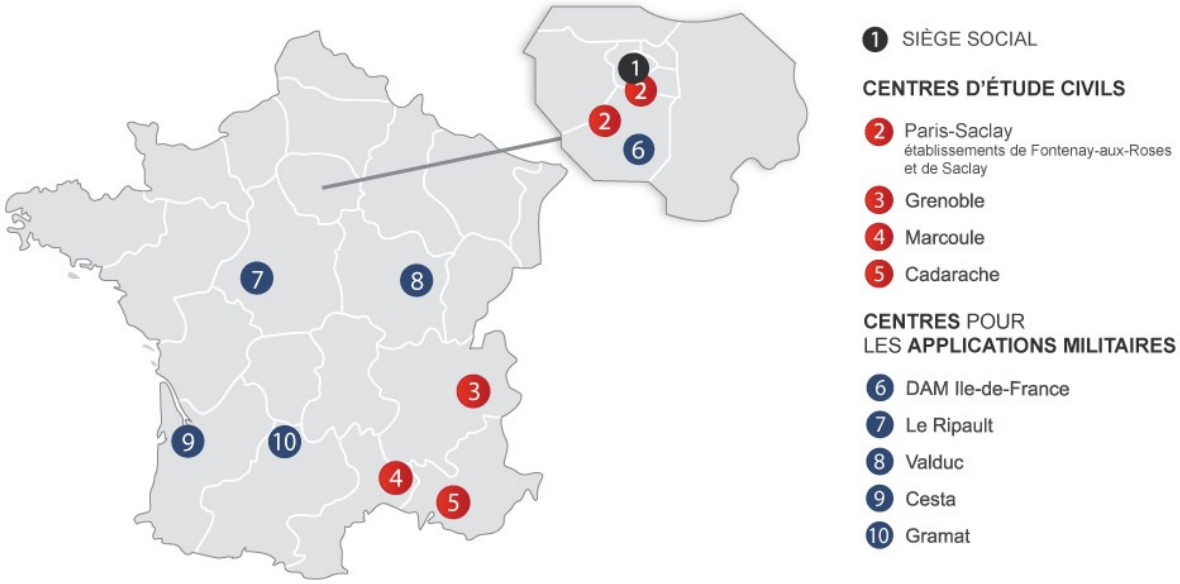

Figure 1.1: CEA Research Centres

It is organized into various research divisions or centers, each focusing on specific areas of research and innovation. Some of the prominent research centers include:

- **CEA Saclay**: Known for fundamental research in physics, materials science, nanotechnology, and energy.
- **CEA Grenoble**: Specializing in microelectronics, nanotechnology, and advanced materials.
- **CEA Cadarache**: Focused on nuclear energy research, including nuclear fusion.
- **CEA Marcoule**: Concentrating on research related to nuclear fuel cycle and waste management.

CEA Saclay is one of the major research centers. Located in Saclay, a suburb of Paris, CEA Saclay is renowned for its contributions to fundamental research in various scientific fields, including physics, materials science, nanotechnology, and energy. It is one of the key scientific hubs in France and Europe, known for its advanced facilities and collaborations with research institutions and industries.

One of the main institution in CEA Paris-Saclay is Institute of Applied Sciences and Simulation for Low-Carbon Energy (ISAS).

ISAS

The goal of ISAS is to develop predictive science in the fields of materials for low-carbon energy production systems, assessment of energy production structures and systems (experimentation, modelling and simulation), physical chemistry, mechanics, thermohydraulics and neutronics. The main department of this institution is Systems and Structures Modelling Department (DM2S).

DM2S

DM2S develops simulation tools and methodologies for the design and assessment of nuclear systems. To do this, it relies on appropriate tests and high-performance software platforms, developed in-house or in partnership with other CEA units or external organisations. It implements them as part of the studies it is commissioned to carry out, particularly in the fields of nuclear reactor core behaviour in normal and accident situations, the strength and integrity of nuclear facility structures under extreme conditions, protection against radiation, the long-term strength of geological nuclear waste repositories, and the design of new-generation reactors. The department has four services. The Mechanical and Thermal Studies Department (SEMT), the Thermal Hydraulics and Fluid Mechanics Department (STMF), the SGLS and the Reactor Studies and Applied Mathematics Department (SERMA).

SERMA is a service that develops calculation codes in the fields of criticality, radiation protection and neutronics. It also carries out neutronics studies for the design and optimisation of nuclear reactors, as well as criticality and radiation protection studies. The department comprises four laboratories. The Stochastic Transport and Data Laboratory (LTSD) carries out research and development on calculation codes for particle transport and simulation. The probabilistic code TRIPOLI-4® (Monte-Carlo) is developed in this laboratory. This laboratory is also responsible for processing nuclear data (cross sections, etc.) for all the codes developed at SERMA.

The Laboratory of Software for Reactor Physics (LLPR)[1] focuses on the development of deterministic codes for reactor core physics and radiation protection (with, for example, CRONOS, APOLLO3 codes and the OPERA platform), as well as source estimation and evolution tools (with the DARWIN and MENDEL codes). The Laboratory of Physics and studies of Cores (LPEC) works on the physics of reactors, including experimental reactors, 4th generation reactors (future reactors) and current reactors (nuclear power plants and PWR reactors). In addition, the laboratory develops experimental devices and is interested in the design of nuclear fusion reactors. Activities are also carried out on the propagation of uncertainties. Finally, the laboratory is also working on the design of new calculation schemes based on Monte-Carlo calculations and on the development of physical and numerical methods for reactor cores. The Criticality Competence Team (CP2C) works on controlling the risk of criticality, as well as carrying out studies into radiation protection, clean-up and dismantling. On this second theme, it looks at improving radiological protection, the neutron fluence of the reactor vessels in the French fleet and the dismantling of reactors.

In Figure1.2 is shown the internal structure of the Department of System and Structure Modelling (DM2S).

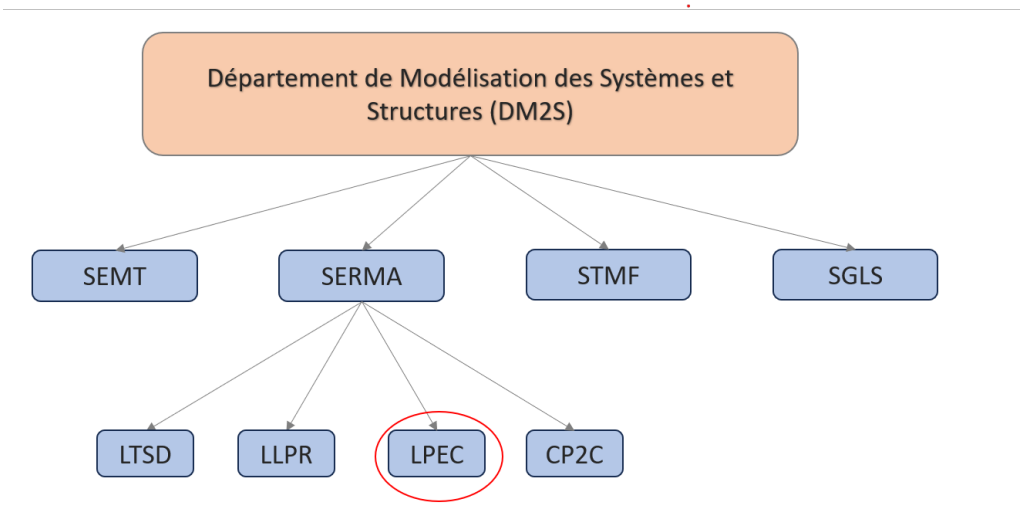

Figure 1.2: DM2S departments structure[1]

Objectives of the CEA

A key principle of the CEA is centered around the development of innovative advanced technologies, all aimed at realizing the goal of reaching low carbon targets. The term "low carbon target" embodies the objective of decreasing carbon dioxide (CO_2) emissions in order to mitigate climate change and allows the transition toward a more sustainable and environmentally friendly energy system. Nuclear power is an important low-emission source of electricity, providing about 10%[2]of global electricity generation in the World. For those countries where it is accepted, it can complement renewable sources in reducing power sector emissions. It is also an option for producing low-emission heat and hydrogen.

The CEA is a prominent player in nuclear research and has been involved in the development of advanced nuclear reactor technologies, including the Generation IV (Gen-IV) reactors.

The Gen-IV of nuclear reactors is a class of advanced reactor designs that aims to provide a solution for some of the problems of earlier generation of reactor improving, in this way, the safety, sustainability, and efficiency. These reactors are still in the research and development phase. As major player, the CEA has been very active in this framework, particularly it has been involved in the Sodium-cooled Fast Reactor (SFR) and the Gas-cooled Fast Reactor (GFR). The SFR uses liquid sodium as a coolant, while the GFR uses helium or carbon dioxide. Both of these concepts are intended to be more efficient and have improved safety characteristics compared to older reactor types. Moreover, CEA is also involved in research and development related to High Temperature Reactors (HTRs). HTRs are a type of nuclear reactor that operates at higher temperatures compared to conventional nuclear reactors, providing potential benefits in terms of safety, efficiency, and versatility. In fact, the HTRs have potential applications beyond electricity generation. They can be used for industrial processes as hydrogen production through high-temperature electrolysis, providing a carbon-free pathway to produce hydrogen for various applications, as the transport sector.

1.2 Overview on HTGR reactor

The HTGRs are a class of reactors that operate at higher temperature with respect to traditional nuclear reactors. The major characteristics are:

1. **Operating Temperature:** HTGRs are designed to operate at significantly higher temperature than traditional Light Water Reactors (LWRs). The latter works usually at around 300°C and 350°C whereas the HTGRs can reach the temperature in the range of 600°C and 1000°C, or even higher.

2. **Fuel:** HTGRs use a special type of fuel known as TRISO particle. The TRISO particle consists in a small fuel kernel surrounded by layers of carbon and ceramic materials. These layers provide multiple barriers for the fission products retention, enhancing safety.

3. **Coolant:** HTGRs typically use helium gas as coolant, which has important neutronic properties as the low absorption cross-section.

4. **Safety:** Due to the use of the TRISO particles, HTGRs are know to be intrinsically safe. The fuel multiple layers can withstand high temperature and prevent the release of radioactive materials even under severe accident scenarios.

5. **Moderator:** The HTGRs usually use as moderator graphite, with the aim of slowing down the neutron until they reach the thermal energy region, encouraging the self-sustainable chain reaction.

6. **Application:** The HTGRs have many potential application as the electricity generation, heating generation, hydrogen production through high temperature electrolysis for industrial applications.

7. **Passive safety:** As Gen-IV reactor, the HTGRs are intrinsically safe. The passive safety is referring to regulation of abnormal situations without active human intervention or complex systems.

Two design concepts of HTGRs are of particular interest due to their structural and operational characteristics: the prismatic block type and the spherical pebble bed type fuel. The first has been used in prototype and commercial HTGRs in USA and currently used in the design of the HTTR in Japan. The latter will serve as the foundational starting point for this comprehensive study.

1.2.1 HTGRs concept choice

HTGRs, in their existing design, have an intrinsic and robust safety profile, avoiding the potential for serious accidents due to their design and engineering structure.This fundamental safety aspect is a distinguishing mark of HTGRs, ensuring that even under extreme circumstances, their operation remains within a secure and controlled domain. However, given the nature of being gas-cooled reactors, the structural dimensions required can be a disadvantage.

The current design of HTGRs is characterised by the use of a gaseous coolant, helium (He). Although this choice is in line with the strict safety parameters of HTGRs, it contributes to a lack of compactness. The gaseous nature of helium requires a larger volume for heat transfer and effective cooling, which in turn affects the overall compactness of the reactor. This trade-off between safety and compactness underlines the complexity of reactor design.

One of the main features of HTGRs is the use of the TRISO particles, which improves fuel utilisation and facilitates efficient energy extraction, contributing to overall efficiency.

1.3 Goals of the internship and structure of the thesis

1.3.1 CEA's role

Within the scope of Gen-IV reactor development, a primary objective of CEA is the research and assessment of novel reactor concepts. This commitment aims to enhance the deployment of these reactor types within the French economic framework. Generation IV reactors serve a crucial role by expanding the scope of nuclear power plant applications beyond conventional electricity generation as the heat production for industrial processes. Among these developments, various departments within CEA have undertaken new studies to counter greenhouse gas emissions and to support the growth of the French energy sector.

HTGRs was selected to be the main object of this thesis. This is in line with the mission to promote sustainable and versatile nuclear technologies as the production of high quality heat for industrial processes and transportation application. Moreover, CEA have very good experience in the framework of SFR's research with sodium as coolant and these background studies could help in the understanding of the new concept HTR-Na cooled.

1.3.2 Thesis goals

In a constant quest for optimisation and innovation, a new concept has emerged that proposes an alternative to the conventionally used gaseous refrigerant. This alternative involves the adoption of liquid sodium as coolant medium. This choice introduces a substantial change in design, allowing a more robust extraction of energy from the reactor system.

The prospect of employing liquid sodium as coolant brings with it the potential to enhance the compactness of HTGRs. This alternative concept represents a delicate interplay between engineering, safety and performance optimisation. By embracing this innovative approach, HTGRs could delete existing limitations, opening a new path for power generation and reactor design that couples the evolution of energy demand and the sustainability.

The purpose of this thesis is to make a contribution to the initial neutron evaluation of a HTR-Na cooled. This task covers a complete path, beginning with the fundamental fuel cell scheme and ending with the complete implementation of the reactor core. The reference design is inspired by the Japanese HTTR. This design structure provides the basis on which the initial sketches and subsequent developments are based. The aim of the thesis is to advance understanding of the characteristics and neutron behaviour of a HTR-Na cooled.

1.3.3 Thesis structure

The present thesis includes eight macro-objectives:

- **Chapter 2: HTGR background study.** The HTGRs background study is carried out to describe in general the core design and the characteristics that make the reactor the one chosen for this study. A meticulous description is proposed in this chapter about what is the HTTR and how it is composed, starting with the core.
- **Chapter 3: Theoretical background.** The theoretical background includes the Boltzmann equation, the deterministic methods with particular attention to the methods used for this study and the specific treatment with which the method is modified to take into account the TRISO particles.
- **Chapter 4: Logic scheme of the thesis** In this chapter a logic scheme is shown to better summarize the steps and the breakpoints of this work, highlighting the main path and the main calculation performed.
- **Chapter 5: Assembly calculation.** In this chapter the Assembly calculation is presented; It starts with general information on the reference assembly design, then the geometry implemented in the calculations is showed and at the end the physical analysis performed. After the latter, the static and the depletion calculation schemes are described pointing out all the steps done to built the models together with validation calculation.
- **Chapter 6: Physical analysis.** A comprehensive physical analysis is performed to assess the reactor behaviour at assembly level for different geometries, evaluating the reactivity, effective and infinite multiplication factor, temperature coefficients at beginning and at the end of fuel life, cycle length. All the results are explained and commented.
- **Chapter 7: Core Calculation.** The Core calculation chapter start with the preliminary analysis performed starting from the assembly level to evaluate the reactivity of the whole core. The latter is, then, compared to the one performed directly for the core, including the reflectors and the control rods.
- **Chapter 8: Conclusions and perspective.** The conclusions of the work is carried out in the last chapter, in which several results are underlined and in which the prospective are considered to give ideas of how to continue the studies.

HTGR background study

2.1 Generation IV reactors

Nuclear power plants, which produce low-carbon electricity at stable and competitive costs, constitute an element of the solution to global warming. Further developments of nuclear technology is needed to meet future energy demand.

The development of nuclear reactors can be categorized into many generations, each representing a stage of technological advancement and improvement in safety features[3]. The generation of nuclear reactors are:

1. First Generation: The first-generation nuclear reactors were the early experimental and commercial reactors built from the 1950s to the 1960s. They were primarily focused on proving the feasibility of nuclear energy for electricity generation. These reactors were based on natural uranium or slightly enriched uranium fuel and used graphite or heavy water as moderators.

2. Second Generation: Second-generation reactors were developed from the 1960s to the 1990s and saw more widespread commercial use. They featured improved safety and operational characteristics compared to the first generation. LWRs became the dominant type, including Pressurized Water Reactors (PWRs) and Boiling Water Reactors (BWRs). These reactors were designed to produce electricity efficiently, but their safety systems often required active human intervention.

3. Third Generation: Third-generation reactors were developed from the late 1990s through the 2010s. They were designed with enhanced safety features and increased efficiency. Passive safety systems, which can respond to accidents without the need for active human intervention, were a significant characteristic of this generation.

4. Fourth Generation: Fourth-generation reactors are still in the research and development phase. They represent the next step in nuclear reactor technology and aim to further improve safety, sustainability and waste management. Fourth-generation reactors focus on innovative concepts such as fast neutron reactors, molten salt reactors, and gas-cooled fast reactors. These reactors have the potential to use alternative fuels and contribute to nuclear waste reduction.

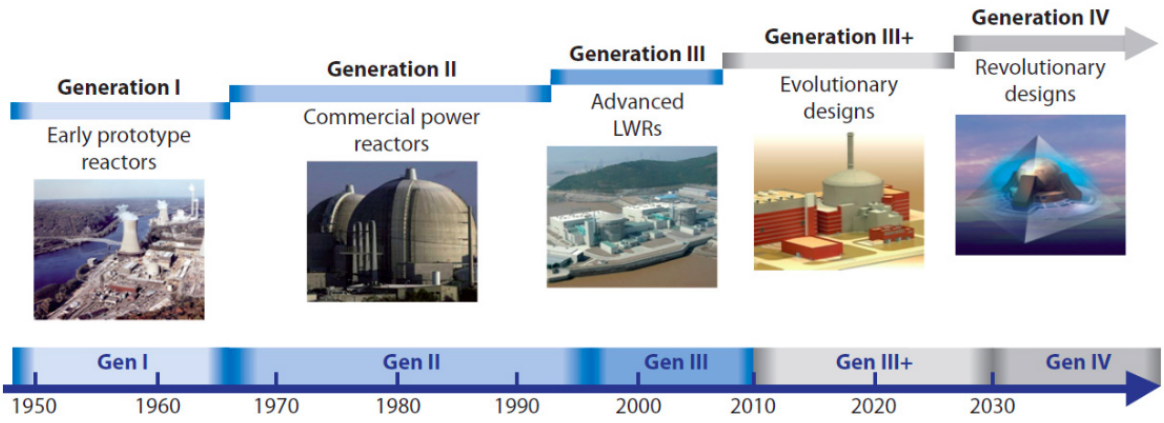

Figure 2.1: Timeline of generations of nuclear power[4]

Closing of the nuclear fuel cycle is an important component for achieving the sustainability goal. It is based on the reprocessing the spent nuclear fuel and the management of each fraction with the best possible strategy. Fissile material, for example, can be recovered from the spent fuel and used to make new fuel. With advanced fuel cycles using fast-spectrum reactors and extensive recycling, it may be possible to breed fissile fuel from fertile material and thus produce equal or more fissile material than the reactor consumes. This would also significantly reduce the footprint of deep geological repositories for the disposal of ultimate waste.
The selected design concepts to be the main reactors of the Gen-IV generation are the following:

- Gas-cooled Fast Reactor GFR;
- Lead-cooled Fast Reactor (LFR);
- Molten Salt Reactor (MSR);
- Sodium-cooled Fast Reactor SFR;
- Super-critical Water-cooled Reactor (SCWR);
- Very-High-Temperature Reactor (VHTR);

2.2 High Temperature Gas-Cooled Reactor

The Generation IV International Forum (GIF) was created in January 2000 and it define four goal areas to advance nuclear energy into its next fourth generation: sustainability, safety and reliability, economic competitiveness, proliferation resistance and physical protection[5]. Among the concepts is the HTGRs with an outlet temperature in the range of 900°C and 1000°C. The high temperature enhances the efficiency of the thermal conversion cycles. The thermal efficiencies reached in some of the design of the HTGRs are greater than 45%.

In general, HTGRs offer many advantages compared to LWRs, especially in terms of safety. Firstly, the significant mass of the graphite moderator provides good heat capacity. The helium coolant has inert property and the core materials are composed of ceramics that demonstrate excellent performance at elevated temperatures.

However, HTGRs pose significant challenges in terms of material selection. Due to the high operating temperatures, both the structural materials and the primary circuit components must withstand extreme thermal conditions without degrading over time. This necessitates the utilization of advanced materials that can maintain their physical and chemical properties under such condition. Another major challenge involves the coolant's performance. The advantages in using helium as coolant are represented by its neutron transparency and chimical inertness. The negative aspects, instead, are its low density and low volumetric specific heat leading to the necessity of high pumping power[6]. Additionally, the manufacturing of TRISO particles, which are used in HTGRs fuel, also has a significant impact on core efficiency. Any structural defects in these particles can lead to a decrease in fuel performance. In order to face these challenges, research and development (R&D) play an essential role.

2.2.1 HTGR Characteristics

As outlined in the overview, the HTGRs stands as a nuclear reactor capable of generating high-temperature heat energy ranging between 750°C and 950°C. Its characteristics encompass a spherical fuel structure coated with ceramics as carbon and silicon carbide. This reactor employs helium gas as a coolant and graphite as a moderator. The features of HTGRs as the structure and the characteristics will be described.

Fuel

The HTGRs use Coated Fuel Particles (CFPs) inside which is located the kernel of uranium oxide. The kernel is enveloped by multiples layers of pyrolytic carbon and silicon carbide. These coatings contain the Fission Products (FPs) generated during the operational condition. The heat resistance of CFPs allows them to withstand temperatures up to 1600°C, representing their upper temperature limit. Depending on the shape of the fuel, there are two different HTGRs design: the prismatic type and a pebble bed type. In prismatic cores, graphite is formed into chair sized hexagonal blocks with hole for cylindrical fuel pellets and separate holed for coolant channels[7]. In the pebble bed type fuel, the CFPs are sintered into a spherical shape after mixing with graphite powder. The HTTR is prismatic type, also called "pin-in-block" where fuel rods with fuel compacts in a graphite sleeves are inserted into hexagonal columnar graphite block.

Coolant

Helium gas, serves as the HTGRs coolant. The exceptional behavior of helium is attributed to its chemical inertness, avoiding reactions with fuel and structural

materials even under the high temperatures experienced during normal operations. Additionally, helium has another key attribute: it is neutronic transparent.

Moderator

HTGRs uses graphite as moderator. There are many advantages to the use of gaphite as moderator. Firstly it is a suitable core structural material because of its great properties such as low neutron absorption, high resistance to radiation, high heat resistance and high thermal conductivity. The disadvantage of using graphite is that a large volume is needed as it has less slowing-down power with respect the water.

Heat application

HTGRs can reach high temperature thank to the materials, fuel type, coolant and moderator used. Compared to LWRs they reach a temperature from 750°C to 950°C. The high temperature heat can be used for highly efficient gas turbine power generation. There are other applications, in particular the hydrogen generation by thermo-chemical water splitting process.

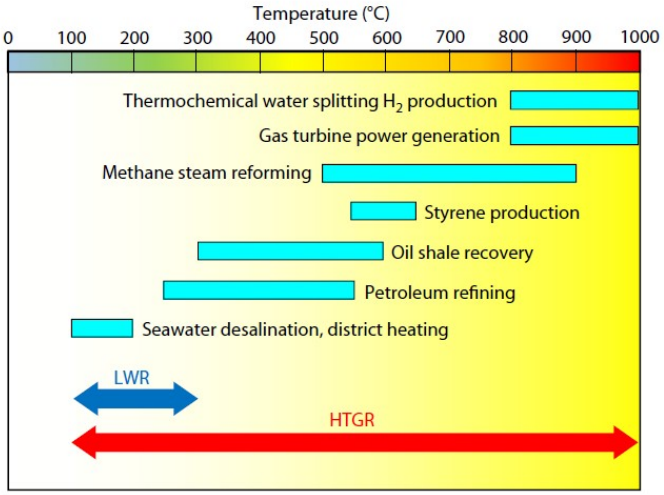

Figure 2.2: Potential Heat applications and HTGR supply Temperature[5]

Safety

One of the key highlights in the design of HTGRs is their inherent safety. The use of helium gas as a coolant prevents any chemical reactions with the fuel and core materials. This means that the risk of hydrogen production, which can lead to explosions in other types of reactors, is eliminated in HTGRs.

Another important safety feature comes from the type of fuel used. The ceramic-coated fuel particles in HTGRs can withstand incredibly high temperatures, even exceeding 2000℃, without releasing any fission products. To ensure an extra layer of safety, the system is designed with a safety margin, setting the limit at 1600°C. This means that even in accidents, the fuel temperature won't go beyond this point, preventing fuel damages. This careful approach significantly reduces the chances of a core meltdown accident, where the reactor's core would become damaged due to overheating.

In addition to the safety features, the HTGRs can remove the residual heat of the core indirectly thanks to the low reactor power density and graphite core structure as the latter has large heat capacity and high thermal conductivity. Then the decay heat of fuel transfers to reactor vessel through the core graphite structure by thermal conduction. This will prevent to rise the fuel temperature up to 1600°C. The HTGRs does not need to provide excess emergency safety system.

Adaptability to environment

Due to the use of the coated fuel particles, the HTGRs has high radiation resistance to the high FPs containment performance. Thanks to this characteristics, the average burnup ratio of the HTGRs can be 120 GWd/t, almost three times higher than in LWRs in which the metal cladding tube is used. This lead to a lower amount of high level radioactive waste, about 1/4 of those produced by LWRs.

2.3 TRISO particles

TRISO (TRi-stuctural ISOtropic) fuel particles were invented in United Kingdom during The Dragon reactor project[8]. It was the first experimental HTGRs built in the 1960s. Since then, the fuel particles has been used in many different reactors. They are the choice for the next generation HTGRs.

The TRISO coated fuel particle is a spherical shape wrapped with multiples layers. The layer are composed by the kernel in the center, buffer, Inner Pyrolitic Carbon (IPyC), Silicon Carbide (SiC) and the last one is the outer Outer Pyrolitic Carbon (OPyC). All together contribute to retain fission products under nuclear reactor condition. The dimensions are typically in the range 750 to 830 µm in diameter and they can vary depending on the kernel type manufacturing process. The TRISO particles then are combined with a carbon matrix to make an individual fuel compact. There are two different fuel compact's forms, the spherical and the cylindrical. The first one is called, usually, "pebbles" and, they are about 6 cm diameter and are used in pebble-bed type reactor. The second is used in circular cylinder. They are use in the prismatic reactor type.

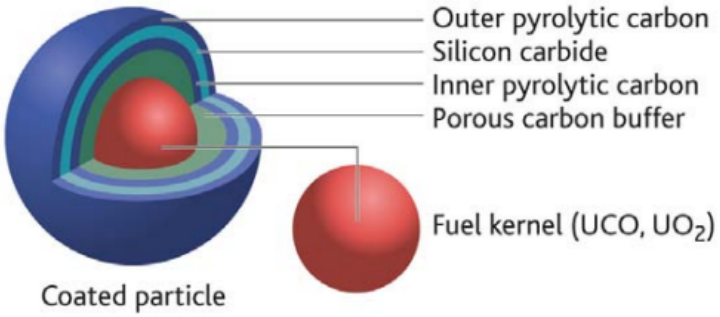

Figure 2.3: TRISO particle structure[9]

2.3.1 Layers Description

Kernel

The core of the particles is the kernel, which contains the fissionable material. Beyond its role as fuel, the kernel plays a crucial function in preventing the release of radioactive fission products by immobilizing and by delaying fission products. The type of fission fuel could be: UO_2, $(U,TH)O_2$, UC,$(U,Th)C$, PuO_2 and UCO. The difference between UO_2 and UCO is that UCO kernels limit oxygen activity reducing in this way the generation of CO and CO_2 and consequently reducing the gas pressure in the particle allowing for higher burnup limits and thermal gradients.

Buffer

Surrounded the kernel there is a porous carbon buffer with the rule of mitigating fission and providing void space to embrace the fission products. The main aspect of

the layer is that it absorbes the kinetic energy of fission fragments coming out from the kernel surface and then it collect them. It is also used in between the kernel and IPyC to accommodate kernel swelling.

IPyC

The IPyC has about 85% porosity. It has several purposes. First of all it protects the kernel from corrosive gases liberating during the SiC coating process, it provides also structural support for SiC layer and protects the latter from the fission products trapped in the inner layers.

SiC

The SiC layer had an high density and high strength properties. The main function is to give to the particle the structural strength.

OPyC

The OPyC layer has high density with respect the layer situated in the inner part of the particles. The main rule is to protect the particles during the formation of the fuel compact. Also it provides an additional barrier to the fission products, in case of SiC layer failure. Over all, as the matrix material of the fuel compact and the SiC layer don't bond, the OPyC give a bonding surface between the TRISO particles and the graphite matrix.

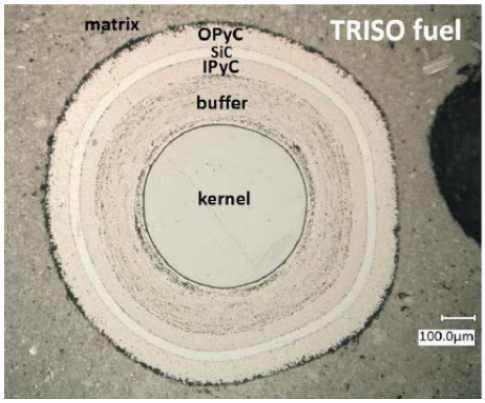

Figure 2.4: TRISO particles structure layers[10]

2.4 High Temperature Test Reactor

The HTTR is a test reactor built in Japan by the Japan Atomic Energy Research Institute (JAERI)[11][12]. JAERI has carried out the research and development on HTGRs and high temperature application since 1960s. The construction of the HTTR started in 1991 in the Oarai Research and Development Institute of JAERI. The first criticality was reached on November 10 1998 and it achieved a full power of 30MW with a reactor outlet temperature of 850°C and reached an outlet temperature of 950°C in 2003, for the first time in the World. The destination usage of HTTR, after conducing safety demonstration tests, will be as heat source of a hydrogen production system. The HTTR's main aim is to develop JAERI technology and carry out essential research on high-temperature radiation. The key factor driving this goal is the need for research and development in hydrogen production. This is important because hydrogen holds a significant role as a crucial energy source in the future.
The method that has already been validate for the hydrogen production is the water "splitting iodine-sulfur (IS)". This appears to be an effective and exceptionally clean system. Ultimately, using nuclear heat for hydrogen generation has the potential to completely eliminate dioxide emissions, leading to a significantly cleaner and more efficient of use of energy.

2.4.1 HTTR plant layout

The HTTR is located on JAERI's Oarai Research Establishment site that is about 100km extended, in the north of the Tokyo metropolitan area, near the Pacific ocean. The dimension of the entire plant are are $200m \ x \ 300m$. It includes the reactor building, the spent fuel storage building, a machinery building, cooling towers, exhaust stack, a high temperature process heat utilization system and complementary facilities.

In the center of the reactor building there is a steel Reactor Containment Vessel (C/V) with 18.5m in diameter and 30m in height. Its major functions are to contain FPs and limit the amount of air ingress into the core during a potential primary pipe rupture accident. The Reactor Pressure Vessel (RPV) together with the C/V constitute the HTTR's safety barrier. In the Figure 2.5 is shown the internal structure of the HTTR.

In the Figure 2.6 is shown the HTTR cooling system structure. The system is composed by the Main Cooling System (MCS), an Auxiliary Cooling System (ACS) and two Reactor Vessel Cooling System (RVCS). The role of the MCS is to remove heat energy from the reactor during the normal operation. The ACS and the RVCS are instead used as safety features to remove the heat after the reactor scram.[13]

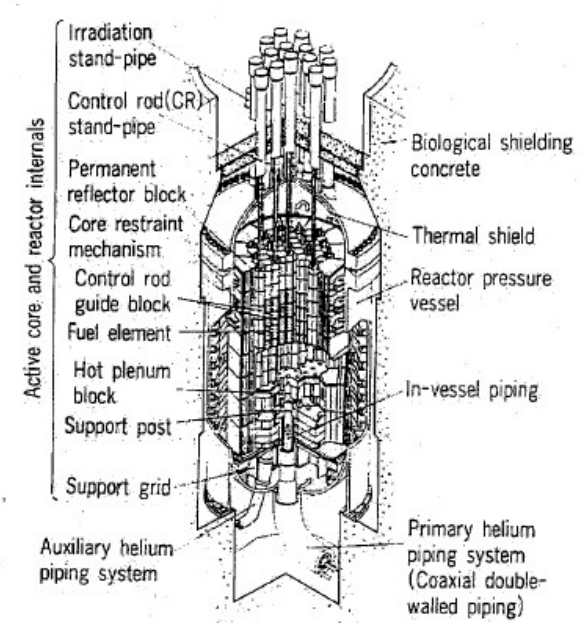

Figure 2.5: HTTR internal structure[13]

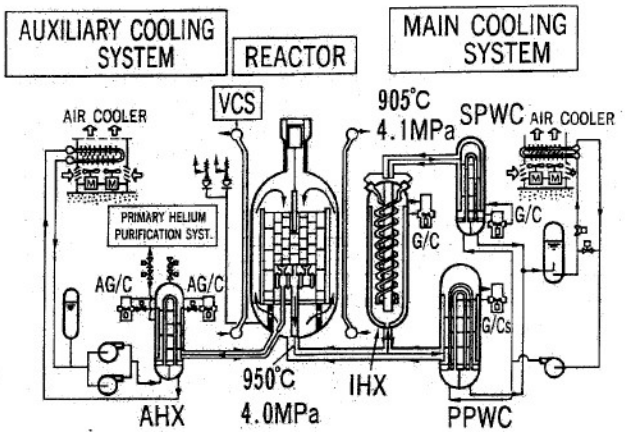

Figure 2.6: HTTR cooling system[13]

2.4.2 HTTR core configuration

At the heart of the HTTR's capabilities is its core.[13][14][15]. In the Figure 2.7 is possible to appreciate the dimension and the internal structure of the HTTR.

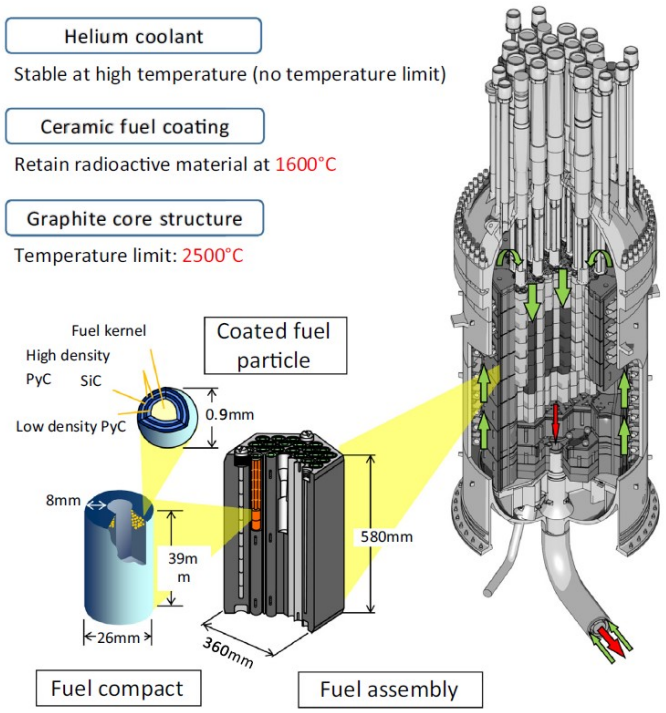

Figure 2.7: HTTR pressure vessel and internals[5]

The structure of the HTTR core is represented in the Figure 2.8. The dimension are small compared to the traditional reactors: 2.30m in diameter and 2.90m in height. The core includes control rod blocks made of graphite to be inserted in the active core. The core consists in prismatic hexagonal blocks having size of 580mm in height and 360mm width. These include fuel assembly block, control rod guide block, replaceable reflector blocks and irradiation blocks. The core internals consist in of graphite and metallic core support structure and shielding blocks. The active core has 30 columns and 7 control rod guide columns. The replaceable reflector region consists in 9 control rod columns, 12 replaceable reflector columns and 3 irradiation columns which are surrounded by permanent reflector blocks. Each fuel column consist of 2 top reflector blocks, 5 fuel assembly blocks and 2 bottom reflector blocks. As it is possible to see in the Figure 2.8, in order to achieve the first criticality, the fuel elements are loaded into core starting from the outer region. This fuel-loading scheme is characterize by a strong neutron flux gradient at the core/reflector interface and represents a challenge for the core design modeling.

In the Figure 2.9 is shown the "pin-in-block" type fuel. In this particular structure, the fuel rod consists of a graphite sleeve containing 14 fuel compacts. The fuel rods are placed inside the channels where the coolant flows through the fuel graphite blocks. Each fuel compact contains around 13,000 TRISO particles. The amount of fuel enrichment changes across the core. In the upper and outer core regions,

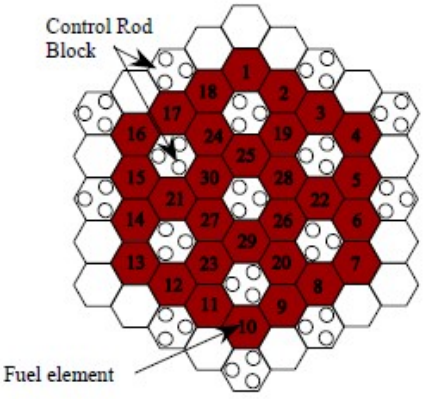

Figure 2.8: HTTR fuel-loading scheme[15]

there is high-enriched uranium to help to reduce the maximum fuel temperature. Within the assembly, the Burnuble poisons (BPs) rods are added. The BPs rod are composed by boron carbide and carbon and they are placed into two of the holes under the dowel pins in the fuel graphite blocks. Regarding the coolant, it flows downward through special channels formed by the graphite blocks and the fuel rods, helping the cooling process.

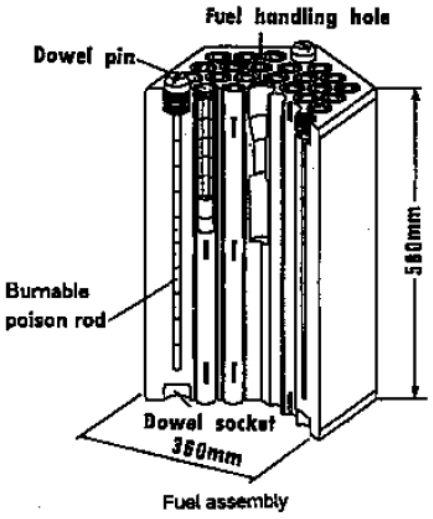

Figure 2.9: HTTR assembly structure[13]

There are two types of fuel graphite blocks, with either 31 or 33 fuel rods. These assemblies are categorized based on how enriched the uranium is, how many fuel rods there are, and what kind of BPs are used.

In Table2.1, are listed the main characteristics of the HTTR as dimensions, thermal power, type of fuel, and more.

Property	**Value**
Thermal Power	30 MW
Outlet coolant temperature	950 °C
Inlet coolant temperature	395 °C
Primary coolant pressure	4 MPa
Core structure	Graphite
Equivalent core diameter	2.3 m
Effective core height	2.9 m
Average power density	2.5 W/c^{3}m
Fuel	UO_2
Uranium enrichment	3 to 10 wt%
Type of fuel	Pin-in-block
Burn-up period (efpd)	600 days
Coolant material	Helium gas
Flow direction in core	Downward
Reflector thickness Top	1.16 m
Reflector thickness Side	0.99 m
Reflector thickness Bottom	1.16 m
Number of fuel assemblies	150
Number of fuel columns	30
Number of pairs of control rods In core	7
Number of pairs of control rods In reflector	9

Table 2.1: Properties of the HTTR[13]

Theoretical background

3.1 Neutron Transport Equation

Neutron physics is the study of how the neutrons behave in presence of matter, how they react with it and the reactions they make with other neutron and with heavy neutrons. The behaviour of a nuclear reactor is dominated by the distribution of neutrons in space, energy and time. To predict the neutron distribution, a neutron transport equation is used. It is called Boltzmann equation and It was obtained for the molecules of gases by Ludwig Boltzmann. The time indipendent equation is shown below[16]:

$$\begin{aligned} &\nabla \cdot \vec{\Omega}\Phi(\vec{r}, E, \vec{\Omega}) + \Sigma(\vec{r}, E)\Phi(\vec{r}, E, \vec{\Omega}) = \\ &\oint d\Omega' \int dE' \Sigma_s(\vec{r}, E')\Phi(\vec{r}, E', \vec{\Omega}') f_s(\vec{r}, E' \rightarrow E, \vec{\Omega}' \cdot \vec{\Omega}) + \\ &\oint d\Omega' \int dE' \Sigma_f(\vec{r}, E')\Phi(\vec{r}, E', \vec{\Omega}')\nu(\vec{r}, E')\frac{\chi(r, E)}{4\pi} + \\ &S(\vec{r}, E, \vec{\Omega}) \end{aligned} \tag{3.1}$$

The equation describe the behaviour of neutron flux ϕ in phase space $(\vec{r}, E, \vec{\Omega})$. The different terms contribute to complete the overall neutron distribution. In particular, streaming, scattering, fissions, external source and removal phenomena are taken under consideration. An explanation of each term will follow:

$\nabla \cdot \vec{\Omega}\Phi(\vec{r}, E, \vec{\Omega})$: it represents the streaming term and describes the net balance in the phase space between the outgoing and incoming neutrons.

$\Sigma(\vec{r}, E)\Phi(\vec{r}, E, \vec{\Omega})$: it is the removal term and counts all the collision that could happen, in particular absorption and scattering phenomena.

$\oint d\Omega' \int dE' \Sigma_s(\vec{r}, E')\Phi(\vec{r}, E', \vec{\Omega}') f_s(\vec{r}, E' \rightarrow E, \vec{\Omega}' \cdot \vec{\Omega})$: it rapresent the scattering terms. It counts all the neutrons that emerge from scattering in $d\vec{r}$, around the position $\vec{r}$ with energy E and direction $\vec{\Omega}$. The two integrals in front of the parametes are the integration over the whole energy domain and all the directions.

$\oint d\Omega' \int dE' \Sigma_f(\vec{r}, E')\Phi(\vec{r}, E', \vec{\Omega}')\nu(\vec{r}, E')\frac{\chi(r,E)}{4\pi}$: it represent the fission term. It counts the neutron the number of fissions that take place within the volume $d\vec{r}$ for neutrons

that have energy E' and direction Ω' and add to this information the probability that the neutrons are emitted within dE and $d\Omega$ and the information about how many neutrons are emitted for each fission interaction, indicated with $\nu(\vec{r}, E')$.

$S(\vec{r}, E, \vec{\Omega})$: it is the source term. Non negligible if sub-critical system is envolved.

It is an integro-differential equation and initial condition and boundary condition are needed to complete the description of the system under investigation. About the initial condition for time dependent problem:

$$\phi(\vec{r}, E, \vec{\Omega}, t = 0) = \phi_0(\vec{r}, E, \vec{\Omega}) \tag{3.2}$$

Regarding the boundary condition, it is necessary to impone an incoming flux equal to zero at the boundary since the neutrons that cross it, cannot come back inside the system and collide. In this way the boundary condition to be applied is:

$$\phi(\vec{r}_s, E, \vec{\Omega}_{incoming}, t) = 0 \tag{3.3}$$

where $\vec{r}_s$ express any point considered on the boundary and $\vec{\Omega}_{incoming}$ are the direction that go from the outside towards the inside region of the system through the boundary.

This equation can be analytically solved taking advantage of simplified system. Instead, It is not easy to solve as it is when nuclear studies are involced. For this reason, over the time, some approximation and numerical methods were been introduced. With this aim, the numerical methods developed, can be categorized in: *Deterministic* and *Stochastic* methods. The first mentioned are those in which discretization in energy, direction and in time is performed while the stochastic uses a probabilistic approach as the Monte Carlo method.

3.2 Effective moltiplication factor

The Effective moltiplication factor, denoted with k_{eff} is a fundamental paramenter to take into account when it is needed to impose the criticality of the system. It is added to the fission term in the tansport equation. It can be evaluated through the use of the so called "Four Factor Formula"[16]:

$$k_{eff} = \eta f \epsilon p P_{NL} = k_\infty P_{NL} \tag{3.4}$$

It express the total number of fission neutron produced on average by one fast neutron from a previous fission event. k_∞ instead refers to the multiplication constant of an infinite assembly without leakage. If one neutron, on average, survives to cause another fission, the system is critical ($k_{eff} = 1$), it means that neutron population in the assembly will remain constant. If less than one neutron survives, on average, to produce another fission event, the system is subcritical ($k_{eff} < 1$). The opposite case is when more than one neutron survives lead to an increase of the neutron population ($k_{eff} > 1$). Considering, now, the paramenter apperating in eq.3.4:

- η is defined as the ratio between the number of fast neutron generated by thermal fission and the number of neutron absorbed in the fuel.
- f is the ration between the number of neutron absorbed in the fuel and the total number of thermal neutron absorbed.
- (ηf) is the ration between the number of fast neutron generated by thermal fission and the total number of thermal neutrons absorbed
- p is defined as the ratio fast neutrons thermalized and the number of fast neutrons removed.
- ϵ is the ration between the number of fast neutrons generated by all fissions and the number of neutrons generatedd by thermal fission.

The Four factors formula is not used anymore since there was developed many codes thanks to which complex system can be taken under consideration. Still it is important to observe it for a physical point of view.

3.3 Deterministic Methods

Deterministic numerical methods aim obtain a numerical solution of the transport equation by implementing some approximation to make the problem solvable. This approximations consider the discretization domain for the variable which are involved. Having a fine discretization means also have a very accurate description of the system and consequently more accurate result.

3.3.1 Diffusion

Studying reactor physics means understand the distribution of neutron in the domain considered. To do so the neutron transport equation should be solved. The numerical methods provide a way to solve it by introducing some hypothesis and approximation. The most widely used one is the Diffusion theory. The overall effect of neutrons interacting with the environment can be seen as a sort of diffusion in the reactor core as the diffusion of a gas into another.
The derivation of the Diffusion equation depends on the well-known **Fick's law**[17]. The latter suggests that the neutron move from high concentration to low concentration within the medium. It is expressed, in three dimensions as:

$$\mathbf{J} = -\mathbf{D}\boldsymbol{\nabla}\boldsymbol{\Phi} \tag{3.5}$$

where:

1. **J** is the diffusion flux vector, expressed in $neutrons/cm^2/s$
2. D is the diffusion coefficient, expressed in cm and it is given by:

$$D = \frac{1}{3\Sigma_s(1-\bar{\mu})} = \frac{1}{3\Sigma_{tr}} = \frac{\lambda_{tr}}{3}$$

where λ_{tr} is the transport means free path, which is an average distance a neutron will move in its original direction after an infinite number of scatterig collision and $\bar{\mu}$ is the average value of the cosine of the angle in the lab system at which the neutrons are scattered in the medium. Σ_s and Σ_{tr} are, respectively the macroscopic scattering cross-section and macroscopic transport cross-section.

3. $\boldsymbol{\nabla}\Phi$ is the gradient of neutron flux.

The neutron diffusion theory is based also on the balance of neutrons in a differential volume element considering the rate of change of neutron density to be equal to the production rate, the absorption rate and the leakage rate. In equation 3.6 is presented the contenuity equation [18]:

$$\frac{\partial n}{\partial t} = -\Sigma_a \Phi - \boldsymbol{\nabla} \cdot J + S \tag{3.6}$$

where:

- n is the neutron density
- S is the rate of neutrons emmission from sources per cm^3, the source can be external or from fission events
- J is the neutron current density vector
- Φ is the scalar flux
- Σ_a is the macroscopic absorption cross-section

Considering both the Fick's law and the contenuity equation, the diffusion equation is given by equation 3.7:

$$\frac{1}{v}\frac{\partial \Phi}{\partial t} = D\boldsymbol{\nabla}\Phi - \Sigma_a \Phi + S \tag{3.7}$$

The diffusion equation, which is a second-order partial differential equation, can be solved taking into account the boundary conditions. They depends on the problem involved, in general for one-dimension problem the solution of diffusion equation contain two arbitrary constants. The most used boundary condition are: the vacuum boundary condition, finite flux condition, interface condistions, source condition and finally the Albedo boundary condition.
As already mentioned the diffusion theory is an approximation and to be used it needed that some condition are fullfilled [18]:

1. Infinite medium
2. No source or sinks
3. Isotropic scattering
4. Uniform medium
5. Low absoption medium
6. Time dependent flux

3.3.2 Multi-group formalism

Energy discretization is a fundamental step in solving the Transport equation[19][20][21]. It involves dividing the energy domain into discrete groups or sub-intervals, each numbered from 1 to N_g. It is common to group the neutron depending on their energy values. A brief overview of a physical description of the neutrons categorization:

1. **Thermal neutrons**: The thermal neutrons have energies on the order of eV. In particular they have energies comparable to the surrounding medium, thus they are in equilibrium. They travel with lower speed respect others and the probability to be capture by a fissile material as U^{235}, is very high. This is very important to maintain the self-sustaining of a chain reaction in the nuclear reactor. These neutrons grouped in the **thermal group**.

2. **Epithermal neutrons**: The epithermal neutrons have energies in the range of few eV to several keV. They have energy higher then the thermal neutrons but lower than the fast ones. They have substantial probability of undergoing scattering interaction and are represented by the **epithermal group**.

3. **Fast neutrons**: Fast neutron have energies in the order of MeV or higher. The neutron born from a fission reaction belong to this group. Their characteristic is that, as they travel at high velocity, the probability of undergoing elastic scattering is high. They can be used for nuclear transmutation process. These neutron are taken into account in the **fast group**.

The first step to derive the **multi-group transport equation** is to consider the Transport equation in steady-state form:

$$\begin{aligned} \vec{\Omega}\cdot\nabla\phi(\vec{r},E,\vec{\Omega}) + \Sigma_t(\vec{r},\vec{\Omega})\phi(\vec{r},E,\vec{\Omega}) = \\ \oint d\Omega' \int_E dE'\Sigma_s(\vec{r},E')\phi(\vec{r},E',\vec{\Omega'})f_s(\vec{r},E'\to E,\vec{\Omega'}\cdot\vec{\Omega}) + \\ \frac{1}{k_{eff}}\oint d\Omega' \int dE'\Sigma_f(\vec{r},E')\phi(\vec{r},E',\vec{\Omega}',t)\nu(\vec{r},E')\frac{\chi(r,t)}{4\pi} \end{aligned} \tag{3.8}$$

where the multiplication factor k_{eff} is been introduced to guarantee the steady-state condition.

Considering thus, the energy discretization in multi-groups, the angular neutron flux $\phi(\vec{r},E,\vec{\Omega})$ will be called the **multi-group angular flux** $\phi^g(\vec{r},\vec{\Omega})$ and it will correspond to:

$$\phi^g(\vec{r},\vec{\Omega}) = \int_g \phi(\vec{r},E,\vec{\Omega})\,dE \tag{3.9}$$

and the scalar flux to:

$$\Phi^g(\vec{r},\vec{\Omega}) = \int_g \Phi(\vec{r},E,\vec{\Omega})\,dE \tag{3.10}$$

The equations describing the exchange of particles between energy groups are derived by *equivalence* to the continuous-in-energy neutron transport equation. In order to maintain the reaction rate within each energy group, it's crucial to define the multi-group cross sections as the weighted averages of the actual cross sections at each point, with weights determined by the actual flux. This ensures that the reaction rate is preserved across the energy groups. The cross sections to be introduced are:

$$\Sigma_t^g(\vec{r},\vec{\Omega}) = \frac{\int_g dE \Sigma_t(\vec{r},E)\phi(\vec{r},E,\vec{\Omega})}{\phi^g(\vec{r}\vec{\Omega})} \tag{3.11}$$

$$\Sigma_s^{gg'}(\vec{r},\vec{\Omega},\vec{\Omega}') = \frac{\int_g dE \int_{g'} dE' \Sigma_s(\vec{r},E'\rightarrow E,\vec{\Omega}'\cdot\vec{\Omega})\phi(\vec{r},E',\vec{\Omega}')}{\phi^g(\vec{r},\vec{\Omega})} \tag{3.12}$$

$$\chi\nu\Sigma_f^{gg'}(\vec{r}) = \frac{\int_{g'} dE' \int_g dE \chi\nu\Sigma_f(\vec{r},E,E')\Phi(\vec{r},E',\vec{\Omega}')}{\Phi^g(\vec{r},\vec{\Omega})} \tag{3.13}$$

The equations 3.11, 3.12 and 3.13 are respectively the equivalent multi-group total and transfer cross section and the last one is the multi-group fission cross section.

The multi-group equivalence is performed using a reference scalar flux as weighting function. At the end the multi-group version of the neutron transport equation is:

$$(\Omega\cdot\nabla+\Sigma_t^g)\phi(\vec{r},\vec{\Omega}) = \sum_{g=1}^{G}\oint d\Omega\Sigma_s^{gg'}(\vec{r},\vec{\Omega},\vec{\Omega}')\phi^{g'}(\vec{r},\vec{\Omega}') + \frac{1}{k_{eff}}\sum_{g=1}^{G}\frac{\chi\nu\Sigma_f^{gg'}(\vec{r})}{4\pi}\Phi^{g'}(\vec{r}) \tag{3.14}$$

It is important to highlight that the flux in each energy groups is coupled to the fluxes of the other groups through the transfer and the fission operators while the transport operator only depends on the energy groups under investigation. The transfer matrix $\Sigma_s = mat\{\Sigma_s^{gg'}\}$ and the fission one $\Sigma_f = mat\{\chi\nu\Sigma_f^{gg'}\}$ are crucial in understanding the coupling between the equations.

3.3.3 MOC

The method of Characteristics is a mathematical technique used to solve first-order Partial Differential Equations (PDFs)[19][20][21][22]. It simplifies the problem considering curvilinear coordinate system. The PDFs are, hence, solved along "characteristic line" or more simple "characteristic", becoming an ordinary differential equation.

Starting from the transport equation written in multi-groups terms and considering the point $\vec{r}$ described by $\vec{r}(s) = \vec{r_0} + s\vec{\Omega}$ with $\vec{r_0}$ constant and $\vec{r_0}\perp\vec{\Omega}$, the streaming term can be defined as:

$$\vec{\Omega}\cdot\nabla\phi^g(\vec{r},\vec{\Omega}) = \frac{d\phi^g(\vec{r_0}+s\vec{\Omega},\vec{\Omega})}{ds} \tag{3.15}$$

Since the $\vec{\Omega}$ is fixed, the right-side of the equation is a total derivative.

The main trick used by MOC is to divide the domain D in a set of homogeneous regions D_i in which the multi-group cross section and the emission $q^g(\vec{r}, \vec{\Omega})$ are assumed to be spatially constant. The emission terms $q^g(\vec{r}, \vec{\Omega})$ includes both scattering and fission located in the right-hand-side of the equation3.14.

The continuous angular variable is discretized according with the S_N formalism. This approximation employs a quadrature set ω_n, Ω_n with $n = 1, .., N$ satisfying:

$$\int_{4\pi} d\Omega f(\vec{\Omega}) = \sum_{n=1}^{N} \omega_n f(\vec{\Omega}) \tag{3.16}$$

where N is the number of direction considered and ω_n are the weight associated to the n^{th} direction.

The mechanism in using the characteristic lines makes possible to subdivided the sub domain D_i in a set of rectangles with the size given by the chords identified by the characteristics and the transversal step given with the distance between two lines. The more number of characteristics line are considered, the closer the volume would be to the real one. By employing the method of characteristic lines, it becomes feasible to divide the pre-defined subdomain D_i into a collection of rectangles. These rectangles are determined by the chords identified through the characteristics and the transverse step defined by the spacing between two adjacent characteristic lines. In essence, this approach allows for a finer-grained subdivision of the subdomain. The level of detail in this subdivision depends on the number of characteristic lines taken into account. As more characteristic lines are considered, the resulting volume approximation becomes increasingly closer to an accurate representation of the actual physical geometry. In practical terms, this method provides a powerful tool for breaking down complex reactor geometries into more manageable regions, which can be systematically studied to gain insights into neutron behavior within the reactor.

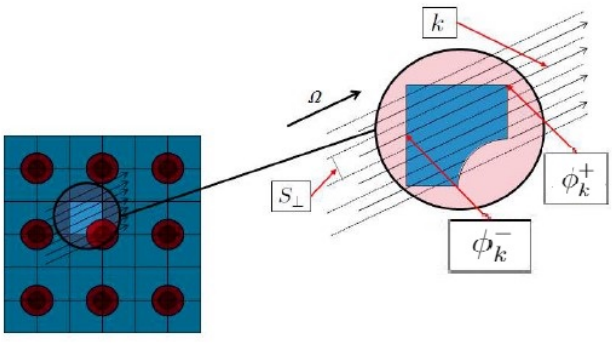

Figure 3.1: Numerical methods to solve the transport equation

In Figure3.1 is shown the characteristic lines crossing the domain. On the right a zoomed view of on a single region is shown. The characteristic line k is pointed together with the cross-sectional area $S_\perp$ and the angular flux ϕ_k^- entering in the

region ϕ_k^+ going out from the same. Taking a characteristic line k with direction $\vec{\Omega}$ inside a sub-region D_i, the solution of the transport equation in the multi-group formalism is:

$$\phi_k^g(s) = \phi_k^g(0)\exp\big(-\Sigma_{t,i}^g s\big) + q_i^g(\vec{\Omega})\frac{1-\exp\big(-\Sigma_{t,i}^g s\big)}{\Sigma_{t,i}^g} \tag{3.17}$$

where the $\phi_k^g(s)$ is constant over the cross section perpendicular to the line k, $S_\perp$.

Considering3.17 at the end of the chord, the **transmission equation** is obtained:

$$\phi_k^{g+} - \phi_k^{g-} = (\frac{q_i^g(\vec{\Omega})}{\Sigma_{t,i}^g} - \phi_k^{g-})[1-\exp\big(-\Sigma_{t,i}^g I_{t,i}\big)] \tag{3.18}$$

the physical quantities present are defined as folows:

1. $I_{t,i}$: chords length
2. ϕ_k^{g+}: angular flux at the entrance. It is negative as the scalar product between the normal vector to the surface and the direction is negative, i.e.opposite versus.
3. ϕ_k^{g-}: angular flux exiting from the region. It is signed as positive as the scalar product between the normal vector to the surface and the direction positive, i.e same versus.

Now, to obtain the average information about the whole characteristic line of the average flux on of the group g in the region i, the **balance equation** is considered:

$$\frac{\vec{\Omega}\cdot\int_{D_i} d\vec{r}\nabla\phi^g(\vec{r},\vec{\Omega})}{\int_{D_i} d\vec{r}} + \frac{\Sigma_{t,i}^g\int_{D_i} d\vec{r}\nabla\phi^g\vec{r},\vec{\Omega}}{\int_{D_i} d\vec{r}} = \frac{q_i^g(\vec{\Omega})\int_{D_i} d\vec{r}}{\int_{D_i} d\vec{r}} \tag{3.19}$$

The balanced equation makes possible to integrate the flux along the line preserving the total number of neutrons in the system. To consider then the contribution of all the characteristic lines of all the regions, the transverse variable $S_\perp$ and direction $\vec{\Omega}_\perp$ have to be taken into account.

Considering, at this point, a set of positions on the boundary of region i, denoted as $\vec{r_s}$, and V_i as the total volume of the region the following equation is obtained, using the divergence theorem:

$$\Sigma_{t,i}^g\bar{\phi}^g(\vec{\Omega}) = q_i^g(\vec{\Omega}) - \frac{1}{V_i}\int_{D_i} d\vec{r_s}\vec{\Omega}\cdot\hat{n}\phi^g(\vec{r_s},\vec{\Omega}) \tag{3.20}$$

Now, taking into account the subdivision of the region in the volume, the surface integral becomes:

$$\frac{1}{V_i}\int_{\partial D_i} d\vec{r_s}\vec{\Omega}\cdot\hat{n}\phi^g(\vec{r_s},\vec{\Omega}) = \frac{z(\vec{\Omega})}{V_i}\sum_{k\|\vec{\Omega},k\cap D_i}[\phi_k^{g+} - \phi_k^{g-}] = \Delta J_i^g(\vec{\Omega}) \tag{3.21}$$

Usually, the integration weight does not depend on the characteristic line but only on the direction $\vec{\Omega}$. In this way the3.21 becomes:

$$\Sigma_{t,i}^{g}\bar{\phi}^{g}(\vec{\Omega}) = q_i^g(\vec{\Omega}) - \Delta J_i^g(\vec{\Omega}) \tag{3.22}$$

Moreover, the emission term for a group g can be treated with the spherical harmonics and written as:

$$q_i^g(\vec{\Omega}) = \vec{A}(\vec{\Omega}) \cdot q_{g,i} \tag{3.23}$$

where the vector $\vec{A}(\vec{\Omega})$ is the vector of all spherical harmonics functions which, for an order of scattering anisotropy equal to K, it is equal to:

$$\vec{A}(\vec{\Omega}) = A_k^l(\Omega) \cdot q_{g,i} \tag{3.24}$$

with k=0 and l=-k,+k. The term $\vec{q}_{g,i}$ is define as:

$$\vec{q}_{g,i} = \sum_{s,i}^{gg} \vec{\Phi}_{g,i} + S_{g,ext} \tag{3.25}$$

with $S_{g,ext}$ being:

$$S_{g,ext} = \sum_{g' \neq g} \Sigma_{s,i}^{g'g} \vec{\Phi}_{g',i} + \partial_{0k}\mathcal{F}_{g,i}\vec{\Phi}_i^g \tag{3.26}$$

The latter is the vector of the $(K+1)^2$ angular moments. It count the contribution, for each moment, of the scattering event from the same group g, the one from the others groups and only for zero-order moment the fission contribution. The term denoted with $\Sigma_{s,i}^{g'g}$ is the diagonal scattering operator applied to the flux moment $\vec{\Phi}_{g',i}$.

Now, using the S_N quadrature formula, the average scalar flux for a group g and region i, can be written as:

$$\bar{\Phi}_i^g = \oint d\Omega \vec{\Omega} \bar{\phi}_i^g(\vec{\Omega}) \approx \sum_{n=1}^{N} \omega_n \vec{A}(\vec{\Omega}) \phi_i^g(\vec{\Omega}_n) \tag{3.27}$$

3.4 Treatment of the Double Heterogeneity with MOC

In this section an overview about how to treat the double heterogeneity[23][24] is carried out. The deterministic methods require a very fine description of the geometrical domain but in some application those methods cannot be applied. An example of this is when the geometrical location of the different components is not exactly known, as it happens with HTRs reactors fuel pellet, the TRISO particles. The double heterogeneity refers to the different regions of the assembly calculation and, contemporary, to the internal structure of the fuel compact (containing the TRISO particles). The problem to solve regards a stochastic dispersion of grains in

a homogeneous matrix. In the following, the analytical solution for grains is carried out denoting with 0 the matrix and with i, form 1 to M, where M are the types of different grains with given chord length distribution.

To find out the analytical solution, it is assumed that the matrix follow Markovian chords statistics $f_0(l) = \exp\{-l/\lambda_0\}/\lambda_0$. The grains considered are of spherical shape and surrounded by multi-layers. The asymptotic solution is:

$$\begin{cases} \phi_0^{out}(x) = \exp\{-\Sigma x\}\phi_{in} + (1 - \exp\{\Sigma x\})\phi_{as} \\ \phi_i^{out}(x) = \exp\{-\Sigma x\}\phi_{in}\widehat{T}_i^g + (\widehat{T}_i^g - \exp\{\Sigma x\}\widehat{T}_i^g)\phi_{as} + \phi_i^{out} \end{cases} \tag{3.28}$$

where

$$\begin{cases} \phi_{as} = (q_0 + \frac{1}{\Lambda_0}\sum_i t_i\phi_i^{out})/\widetilde{\Sigma} \\ \phi_i^{out} = \lambda_i \sum_k p_{ik}^g q_{ik} E_{ik}^g \end{cases} \tag{3.29}$$

p_0 is the volumetric fraction for matrix, p_i is the volumetric fraction for grain i, p_{ik}^g is the volumetric fraction for layer k of grain i, λ_i is the average chord length for grain i, q_0 is the angular emission in the matrix, q_{ik} is the angular emission in layer k of grain i, $\widehat{T}_i^g$ is the transmission probability for grain i with the total cross section diminished by Σ, $t_i = (\lambda_0 p_i)/(p_0\lambda_i)$ is the transition probability from matrix into grain i and finally E_{ik}^g si the escape probability from layer k of grain i. The cross section are evaluated as:

$$\begin{cases} \widetilde{\Sigma} = \Sigma_0 + \frac{1}{\lambda_0}\sum_i t_i(1 - T_i^g) \\ \Sigma = \Sigma_0 + \frac{1}{\lambda_0}\sum_i t_i(1 - \widehat{T}_i^g) \end{cases} \tag{3.30}$$

As the matrix follow the Markovian chord length statistics, the material flux for the matrix is equal to the transition flux $\phi_0(x) = \phi_0^{out}(x)$. The solution of the fluxes in the grains is

$$\phi_{ik}(x) = \exp\{-\Sigma x\}\phi_{in}\widehat{E}_{ik}^g + (E_{ik}^g - \exp\{-\Sigma x\}\widehat{E}_{ik}^g)\phi_{as} + \phi_{ik} \tag{3.31}$$

where

$$\phi_{ik} = \frac{1}{V_{ik}^g \Sigma_{ik}} \sum_l V_{il}^g q_{il} P_{ik;il}^g \tag{3.32}$$

in which V_{il}^g is the volume of layer k of grain i and $P_{ik;il}^g$ is the collision probability from layer l to k within grain i. The analytical solution is asymptotic as it is not valid in the boundary layer of thickness $\delta = 2\max_i R_i$ where R_i is the external radius of the grain i.

The analytical solution just demonstrated can be used to describe to implement a numerical solution with the method of characteristics for unstructured meshes MOC containing regions with stochastic materials. In the following line the numerical implementation will be performed, recalling the MOC considering a more numerical solution rather than a theoretical demonstration as done in the previous section.

The iterative solution for the MOC is carried out through the conservation and the transmission equation (3.18) along each trajectory crossing a region. The following equations are based on the assumption of sources and cross sections are uniform within the region:

$$\begin{cases} \phi_+ = (1 - \Sigma\beta)\phi_- + \beta q \\ \phi_+ - \phi_- + \Sigma L\bar{\phi} = Lq \end{cases} \tag{3.33}$$

where ϕ_+ and ϕ_- are respectively the outgoing and incoming fluxes along the trajectory, L is the length of the trajectory and $\bar{\phi}$ is the mean flux over the length, q is the source, Σ is the total cross section and β is the region transmission coefficient along the trajectory and it is defined as:

$$\beta = \frac{1 - \exp\{-\Sigma L\}}{\Sigma} \tag{3.34}$$

The iteration process is based in considering the system3.28 in which the outgoing flux is calculated starting from the incoming flux and from the value of the source from the previous iteration. The second equation in the system give the average flux over the chord. Then, these average chords are used at the end of the iteration to evaluate the cell average values:

$$\bar{\phi}_{cell}(\vec{\Omega}) = \frac{1}{V}\sum_{t\|\vec{\Omega}} \omega_\perp(t,\vec{\Omega}) \int_0^{L(t,\vec{\Omega})} dx\phi(x) = \frac{1}{V}\sum_{t\|\vec{\Omega}} \omega_\perp(t,\vec{\Omega})(L\bar{\phi})(t,\vec{\Omega}) \tag{3.35}$$

The average cell flux is then used to estimate new averaged cell sources for the next iteration. In3.35 are indicated the trajectory t with direction Ω that intersect the cell. The volume V of the cell and the $\omega_\perp$ is the angular quadrature weight times the trajectory cross section.

The treatment of the double heterogeneity is carried out by estimating the ϕ_+ as the mean flux of the ensemble exiting from the region along the trajectory. With the assumption of having the grains inside the region and that they cannot cross its boundary, the analytical solution for grain statistics ϕ_0^{out} can be written in the same form of MOC transmission equation:

$$\phi_+ = (1 - \Sigma\beta)\phi_- + \beta q \tag{3.36}$$

where the source $q = \Sigma\phi_{as}$ is the effective source in the stochastic region and the transmission factor β computed in this framework is with the stochastic cross section Σ.

The next steps is to establish equations for the calculation of the cell average fluxed for the matrix and for the different type of grains inside it. The values over the intersection of the trajectory with the region can be evaluated by integration.The solution of $\bar{\phi}_0$ will be:

$$\phi_+ - \phi_- + \Sigma L\bar{\phi} = Lq \tag{3.37}$$

and the mean chord flux for the grains can be evaluated as:

$$\bar{\phi}_{ik} = \widehat{E}^g_{ik}\bar{\phi}_0(\vec{\Omega}) + (E^g_{ik} - \widehat{E}^g_{ik})\phi_{as}(\vec{\Omega}) + \phi_{ik} \tag{3.38}$$

where $\widehat{E}^g_{ik}$ is the escape probability from layer k of grain i with total cross section Σ. Thanks to the (3.36) and to (3.38) it is possible to implement the stochastic region without need of modifying the MOC done for homogeneous regions containing deterministic medium. The only different is that it is necessary to calculate the effective source $q = \Sigma\phi_{as}$ before each iteration.

At the end of the iterations, the updated mean flux in the grains is evaluated as:

$$\bar{\phi}_{ik,cell}(\vec{\Omega}) = \widehat{E}^g_{ik}\bar{\phi}_{0.cell}(\vec{\Omega}) + (E^g_{ik} - \widehat{E}^g_{ik})\phi_{as}(\vec{\Omega}) + \phi_{ik}(\vec{\Omega}) \tag{3.39}$$

3.5 Stochastic Methods

The stochastic methods use a probabilistic approach to model and simulating the life of neutron from the beginning of their life until they get absorbed. The Monte Carlo Method is the most widely used in nuclear applcation.

Monte Carlo simulations are used for reactor physics, radiation shielding design, criticality safety analysis, and nuclear material tracking in fuel cycles.
The macroscopic behaviour, in this way, is recostructed analyzing what happen at the microscopic level. The advantage of using Monte Carlo Method is the accuracy, vesatility but it is computationally expensive, expecially when high number of samples are involved.

3.6 Calculation Scheme

When the goal is to solve the transport equation over a core reactor, a calculation scheme is needed. It is based on a choice of numerical methods, acceleration methods and homogenization phases that allows numerically solve the transport equation[25]. It is composed by the Assembly calcualtion and the Core calculation.

3.6.1 Assembly calculation

The Assembly calculation (or lattice calculation) refers to the analysis of individual fuel assemblies that constitute the core of a nuclear reactor. These calculations are fundamental to modeling and to predict the behavior of the assemblies, which are pivotal in the overall performance and safety of a nuclear reactor. To achieve this goal the assembly geomentry and composition is needed. Through these calculation it is possible to evaluate and understand the major nuclear paramentes as the neutron flux, the power distribution, the reactivy and the evolution of fuel composition over time.

The assemebly calculation involves precise steps: problem definition, assembly geometry, material composition, number of fuel rods involved and fuel characteristics, coolant properties, moderator properties.

The boundary condition are fundamental in setting the calculation. Through them it is possible to established the behaviour of neutron at the assembly's boundary.

In the assembly calculation there are some details that it is important to introduce: the condensation and the homogenization concept. The data needed to this type of calculation are the energy averages, performed by the condensation, and the space averages, performed with the homogenization approach. In many cases a complete homogenization of the assembly is required. If the latter is performed, it is not possible to have a fine rod-by-rod power distribution. In fact this should be evaluated *a posteriori* by considering the fine structure obtained from the assembly calculation.

3.6.2 Core calculation

The core calculation scheme is an important component to analyse the complex behaviour of nuclear reactors. Thought its use it is possible to evaluate, understand and optimise the performances of the entire reactor in terms of design, materials, fuel cycle and so on. The scope of the core calculation scheme is wide reaching and adaptable to several purposes. It is possible to understand how the power is distributed within the core, optimize the utilization of the nuclear fuel, keep the safety margins. As done in the assembly calculation scheme, the core one is composed in very precise steps in which all the problem and condition should be well defined.

In general when the core calculation is performed, a simpler model is selected with respect the assembly calculation. It is possible to say that in core calculation is used a "more rough" neutron physics. In many reactor is sufficient to consider two energy groups, as in PWRs. If more accurate calculation is required, more than two energy groups can be considered, or another model as the simplified transport calculation sP_N or S_N instead of Diffusion.

3.6.3 APOLLO2® and APOLLO3®

APOLLO2®[26][27] is a spectra multigroup two-dimensional computer code that solves the neutron equation using different methods:

1. **Collision probability**.
2. **Space nodal methods and angle S_N type methods**.
3. **Method of Characteristics**.

Most of APOLLO2® applications aim at achieving multi-parameterized libraries of space-homogenized, energy-condensed cross sections which are used as input data for core calculations. APOLLO3®[28] is a new multi-purpose deterministic code under development in the field of neutronics simulation project of the Direct des Energies (DES) of the CEA, with financial support from AREVA, Electricity of France (EDF) and Framatome. The new generation code system with the purpose

of analyzed the core physics with more accuracy, more flexibility, and with high computation performances. It wants to built a support for either *R&D* and industrial applications. It is object oriented, C++ and FORTRAN programming languages. The complex architecture design is a layered one consisting of several functional and modular components. It is written incorporating and extending the capabilities of the original code APOLLO2®. For lattice calculation, standard methods have been implemented as the collision probability model and the short/long characteristic method. The short (IDT) and the long Two-and Three-Dimensional Transport (TDT) characteristic methods are extended in 3D. For core calculations, several solvers can be used according to the problem.

3.6.4 Silène

Silène[29], a Java-based Graphical User Interface (GUI) developed by CEA, serves as a robust platform for assisting users in preparing input data for APOLLO2®. Silène was tailored specifically for TDT, accommodating unstructured geometries. Beyond data preparation, it offers a range of functionalities, including the capacity for post-processing analysis. Over time, its utility was expanded to provide support for Monte Carlo codes TRIPOLI4® as well.

Over the years, lattice transport computer codes were developed to increase the number of different problem to treat, thank to advancements in computer power and the algorithms' efficiency. The geometry and mesh design are crucial rules being the input of both deterministic and Monte Carlo computer code. Geometry are usually unstructured type and built to use MOC and Collision Probability Method (CPM) solves, which required tracking data for the angular discretization. The main difference between the unstructured and structured geometry is in the way data, for points, line and surface are stored: the structure one uses basic shapes as the polygons and circles described by equation whose coefficient can be modified by the user.

Complex geometries are treated, usually, starting from the its elementary parts. In fact, to build a fuel assembly it is used to start by defining the fuel cell. So it is possible to imagine the geometry as a nested structure that goes from the inner part towards the entire system. Silène was an original and intuitive product and it has achieved its final maturity. It finds particular application in two-dimensional calculations, which are typical for lattice calculation. This methodology is especially valuable in preparing homogenized cross-sections for subsequent full-core calculations. It is important to mention that Silène is also capable of apply to the defined region the boundary condition.

Logic scheme of the Thesis

To enhance the reader's comprehension of the thesis, a chronological flowchart has been constructed. Its purpose is to provide a clear, step-by-step overview of the processes undertaken.

As it is possible to see from the flow chart shown in Figure 4.1, the assembly calculations were carried out using APOLLO2® deterministic code while for the core calculation was used APOLLO3®. It was not possible to use APOLLO3® for the lattice calculation because of the the double heterogeneity (treated in the Section 3.4) needed in HTRs is not implemented yet in APOLLO3®. In addition an existing calculation scheme was validated on HTTR using APOLLO2®.

Referring to Figure 4.1, the initial focus was on the left branch, specifically the development of the static calculation scheme and its subsequent validation through Monte Carlo simulations using Serpent. The Serpent model was provided by the CEA Cadarache team for a single assembly.

After the static calculation scheme was validated, the depletion calculation was conducted. Subsequently, the SAPHYB files containing the cross-section librearies for the core calculation were created. These cross sections were created by incorporating information from both the static and depletion calculations. Then, they were integrated into the core calculation input to allows the simulation of the entire core.

Given the study's objectives of constructing a "Deterministic Scheme" and identifying an optimal configuration for the new sodium-cooled HTR concept, various geometries and evaluations were conducted. Alongside the static and depletion calculation schemes, physical analyses were performed to assess crucial parameters including reactivity, effective multiplication factor, temperature coefficient, and fuel depletion across all cases studied.

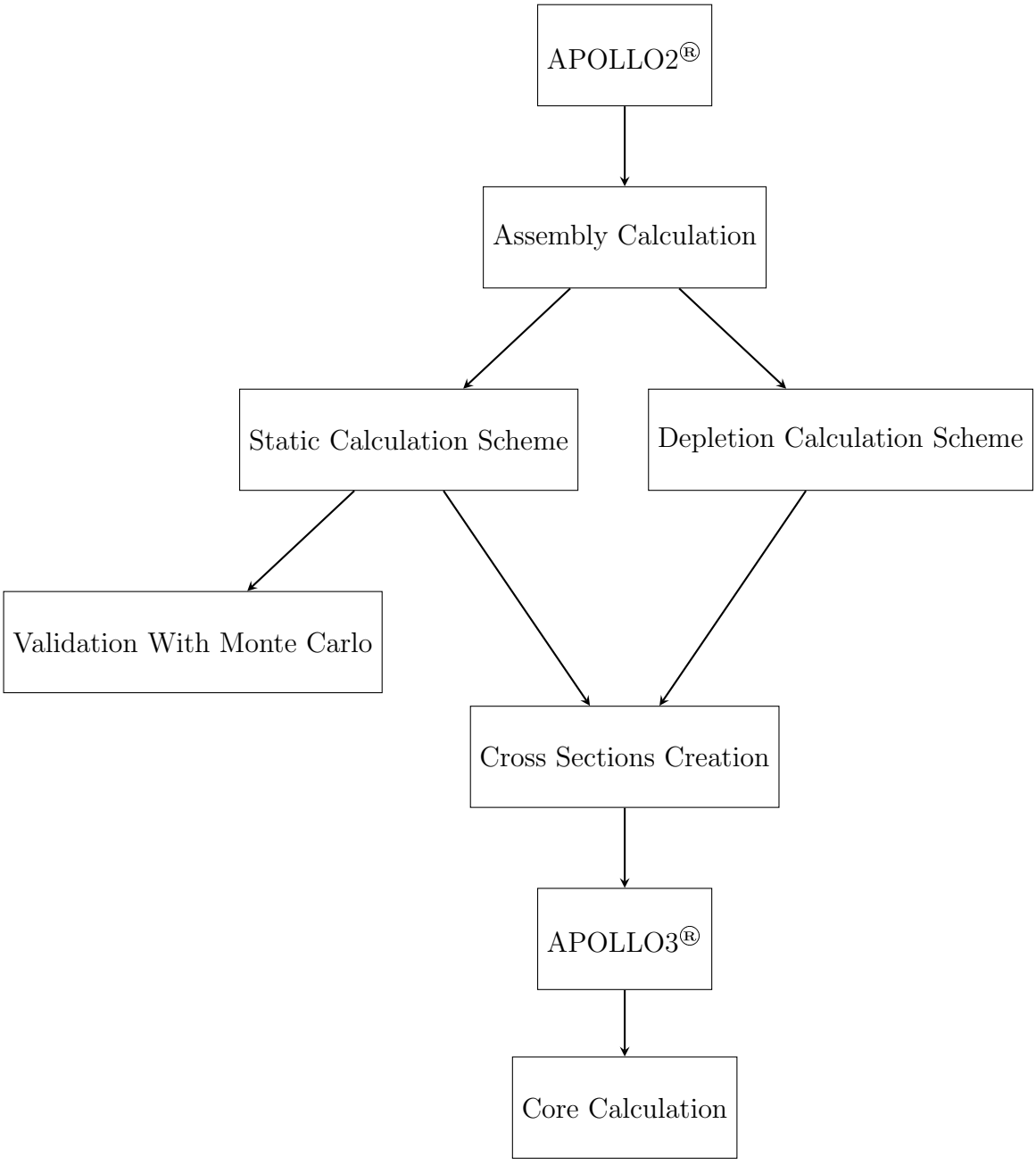

Figure 4.1: Thesis Logic Scheme

Assembly calculation

Assembly calculations, also known as lattice calculations, in nuclear engineering constitute a fundamental methodology for analyzing the behavior of nuclear reactor core at the assembly level. They play a crucial role in designing, optimizing, and understanding the performance of nuclear reactors. These calculations involve modeling the spatial distribution of nuclear materials, such as fuel assemblies and control elements, and simulating the neutron interactions within them. Lattice calculations are indispensable for predicting key parameters like neutron flux, power distribution, and reactivity, providing vital insights into reactor operation, safety, and efficiency.

In this section, the core focus of the thesis will be meticulously carried out, describing each step of the process. This will encompass the input data, the utilization of the deterministic code, the obtained results, the subsequent validation using Monte Carlo simulations.

5.1 Preliminary information

Before delving into the main body of this thesis, it's essential to introduce the initial context that support all the subsequent analyses. Starting from the knowledge of the HTTR design, a thermal-analysis has already been completed considering sodium instead of helium as coolant. A new geometry HTTR-like was built with some differences with respect the configuration of the HTTR reactor. Considering the sodium as coolant implied an additional layer of steel as the sodium cannot stay in contact with graphite otherwise they would give an exothermic reaction leading to corrosion and erosion damage, creation of insulation layers and other demages that can compromise the correct function of the reactor[30]. In the Figure 5.1, the HTTR assembly is shown. In the center there is the handling hole surrounded by the fuel hole and three sites are located the burnable poison hole.

The main objective was to increase the power density of the core while keeping all the materials under some constraint as the TRISO particle temperature limit (1800°C). It is important to remember that, in the HTTR configuration, the core is cooled by helium that is in contact with graphite and passes through the center hole and around the assembly. In the case analyzed, the cooled down process is supposed to be done by sodium from the outer frontier of the assembly.

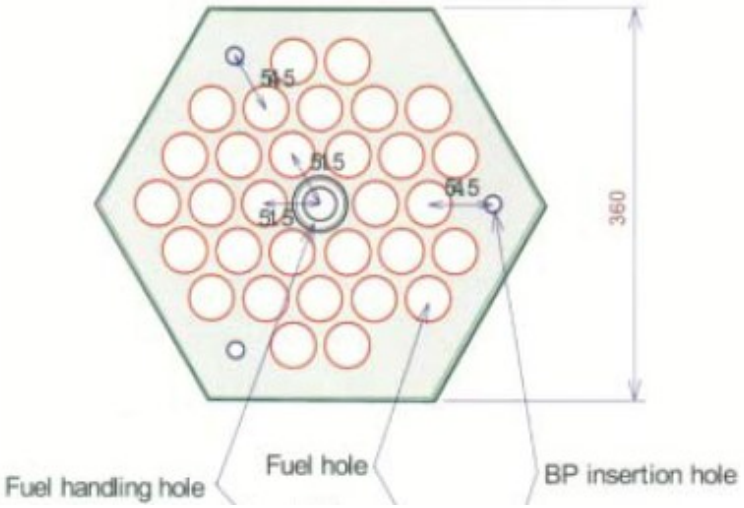

Figure 5.1: HTTR structural assembly[13]

In the Figure 5.2 is shown the assembly with a detail description with dimensions of a fuel compact.

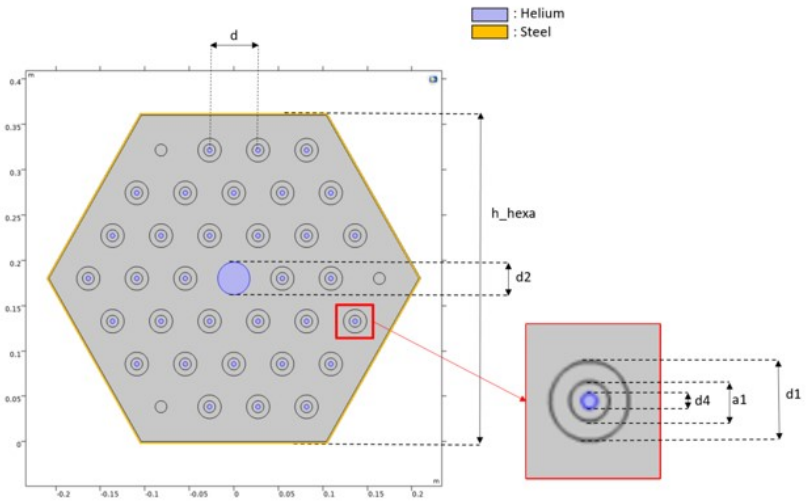

Figure 5.2: HTTR assembly[31]

The thermal analysis was conducted to assess the temperature distribution under the influence of the total core power. It was analyzed different configurations depending on the numebr of rings considered within one assembly. The best configuration in terms of thermal analysis performances was represented by the configuration with 5 rings.

In addition, this geometry was built to have the two outer rings with fuel and graphite in the entire inner part. The result is shown in the Figure 5.3. The reason of having the two outer region with fuel is to locate them as close as possible to the

coolant. It is important to note that in the Figure 5.3, the coolant region is not shown.

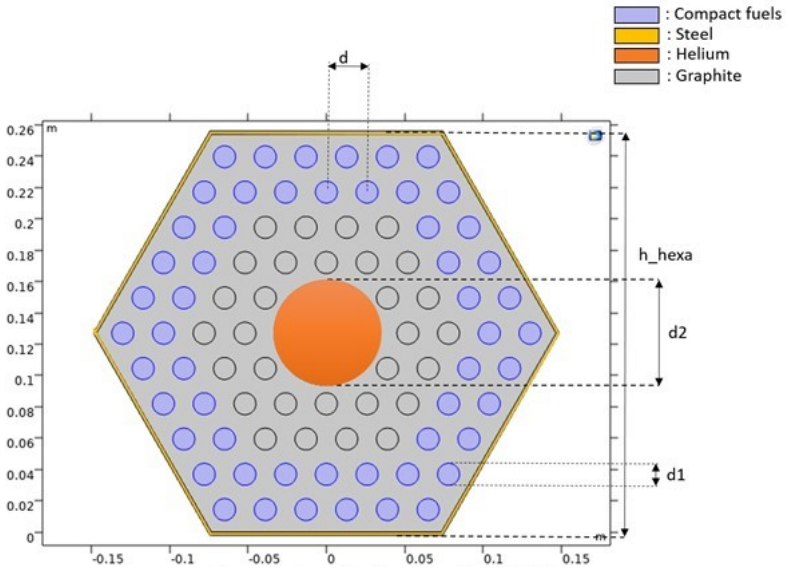

Figure 5.3: 5-ring geometry[31]

In the proposed geometry the changes were done conserving some parameters as the total fuel mass in the HTTR core and the moderating ratio (ratio between the fuel volume and the graphite volume), to have the neutron correctly thermalized. Performing the thermal analysis on this configuration, the maximum temperature reached was very low respect the previous proposed geometry (HTTR assembly). In conclusion, the starting geometry configuration of the study here presented is the one showed in the Figure 5.3.

5.2 Geometry

The goal of this thesis is to determine the optimal configuration for the new sodium-cooled HTR concept or at least give a first evaluation including different proposals. Within this framework, various geometries have been proposed, each differing in specific geometric aspects.

The new concept is based on the configuration of the HTTR, and in a hierarchical manner, the assembly consists of: fuel compacts, moderator matrix, a central handling hole, and the surrounding layers. Now, beginning from the innermost region: the fuel compacts are characterized by TRISO particles dispersed within a graphite matrix. Around the fuel compact are several layers made of different media: a helium layer, a graphite layer followed by another helium layer. It is possible to appreciate the fuel cell in details in Figure 5.4.

Proceeding in the assembly description, the fuel cells are located on the outer region of the assembly, in particular they occupy the two rings of the latter. The reason of this choice was discussed in the previous thermal analysis study and it

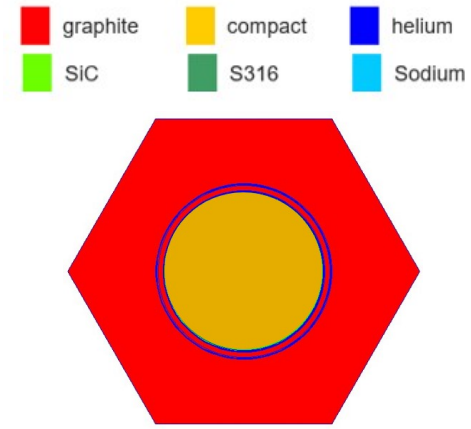

Figure 5.4: Fuel cell

is related to the replacement of helium coolant with sodium. Around the assembly, there are four layers: a thin helium layer, a more substantial silicon carbide (SiC) layer, an extremely thin layer of 316S steel, and, in the outermost region, the sodium. Figure 5.5 provides an illustration of an assembly with a closer view of the surrounding layers.

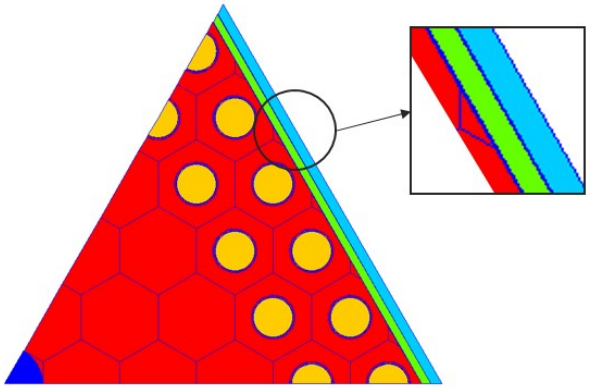

Figure 5.5: Detail of layers around the assembly

As the aim is to evaluate the core behaviour implementing different geometries, some geometric aspects are selected to be the main parameters of the physical analysis.

1. Size of the handling hole in the center of the assembly.
2. Thickness of the sodium layer.
3. Number of fuel rings.

All the geometry constructions were performed on Silène program. In Figure 5.6 are shown the four geometries analyzed changing the size of the central handling hole.

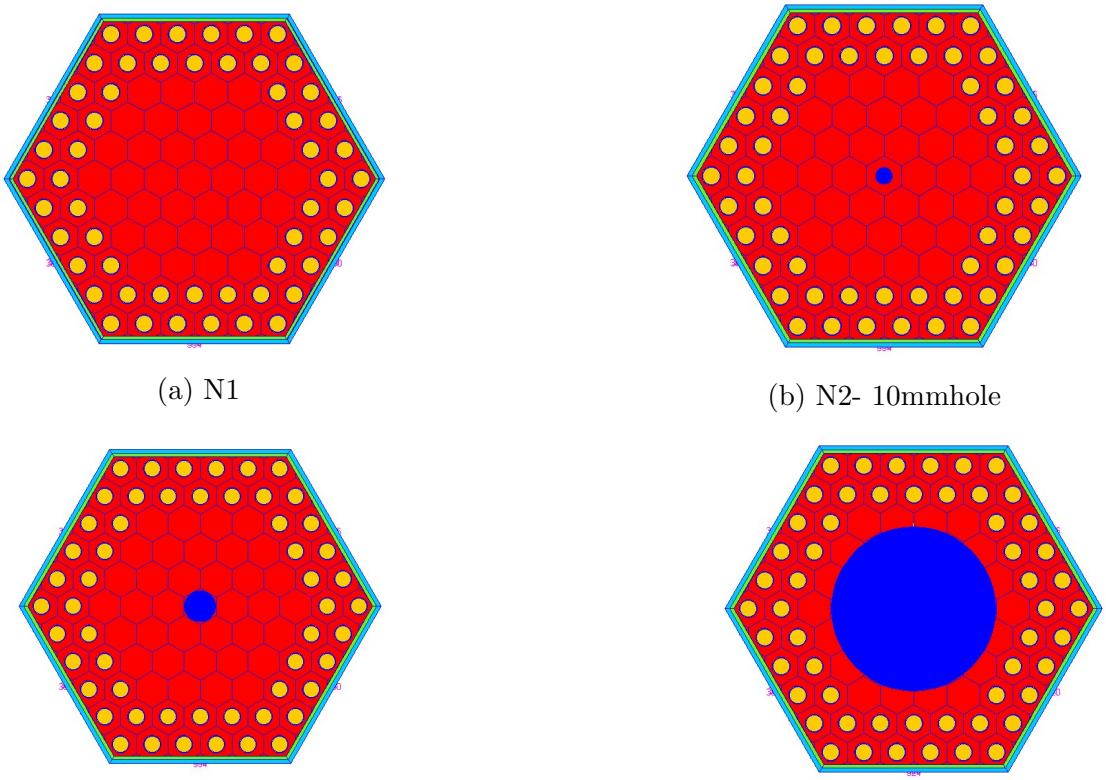

(a) N1

(b) N2- 10mmhole

(c) N3- 20mmhole

(d) N4- 100mmhole

Figure 5.6: Geometries with an increasing handling hole size

For a better implementation, a symmetry of 60° were adopted to minimize the calculation effort in APOLLO2®. In Figure 5.7 are shown the correspond 60° symmetries of the geometries in the Figure 5.6. This choice was selected also to assign the geometry type for the generation of the TDT geometry and to assign the boundary condition on each sides. For the latter was selected the "axial symmetry" by imposing the starting node and the angle.

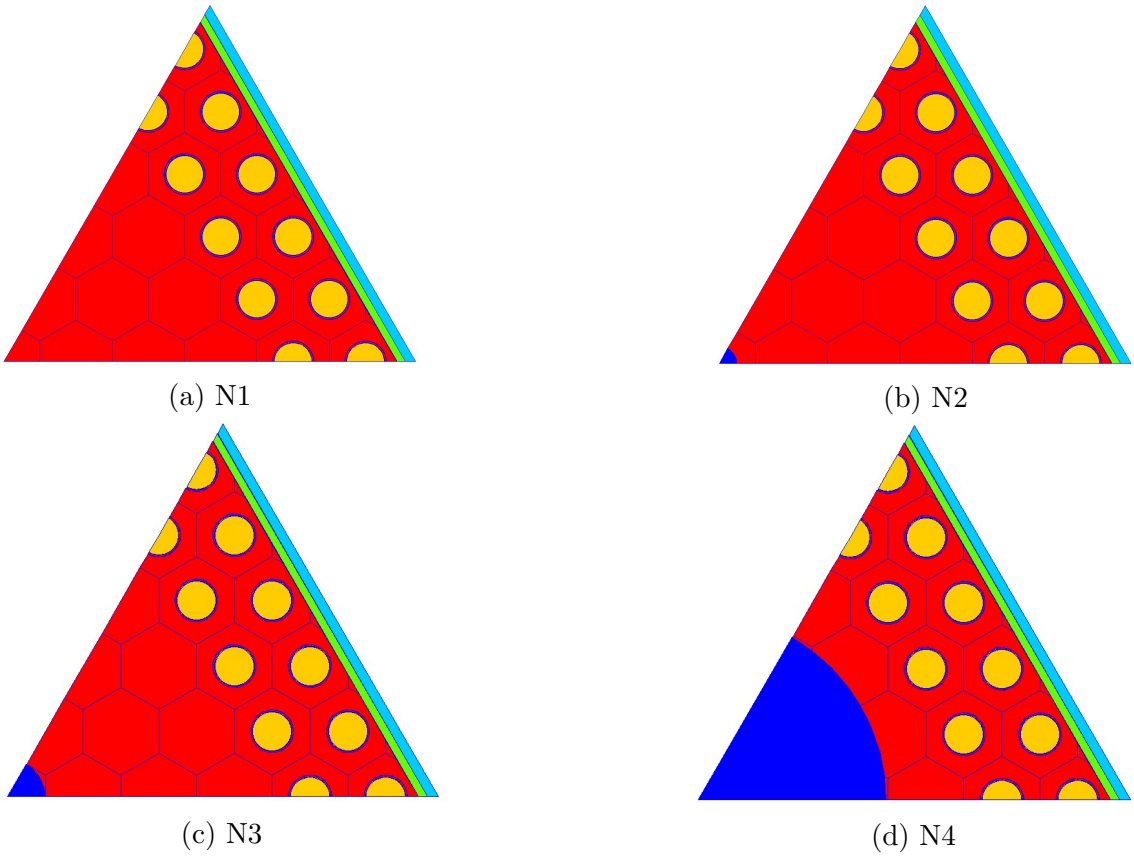

(a) N1 (b) N2

(c) N3 (d) N4

Figure 5.7: Representation of $\frac{1}{6}$ of the assembly

The intermediate handling hole dimension, denoted as $N3$, is chosen to be the reference geometry on which further modifications are done. In the Figure5.8 are represented the geometries varying the sodium thickness layer by 10% (Figure 5.8a and 5.8b) and the third one considering much larger thickness with respect the reference.

In order to undestand and analyse the neutronic behaviour it was considered the reference geometry with one fuel ring in addition. In Figure 5.9 are presented the reference geometry with two outer fuel rings and the geometry with three of them.

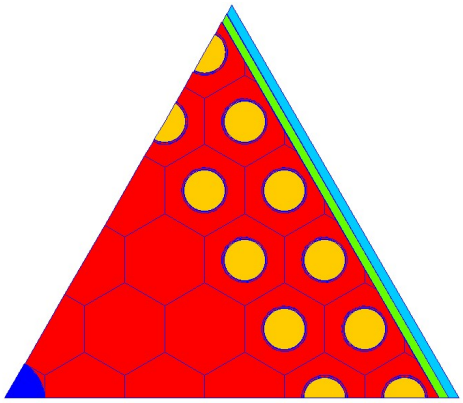

(a) -10%

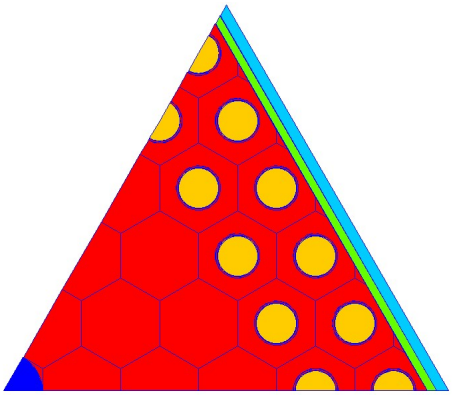

(b) +10%

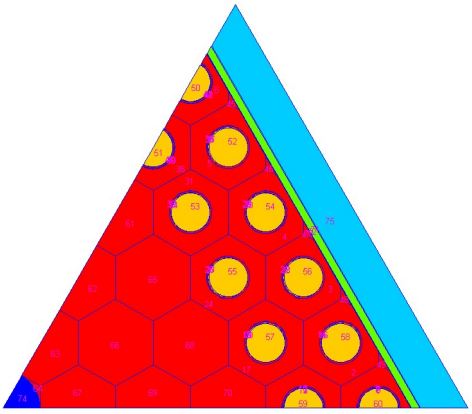

(c) >>reference

Figure 5.8: Sodium thickness layer

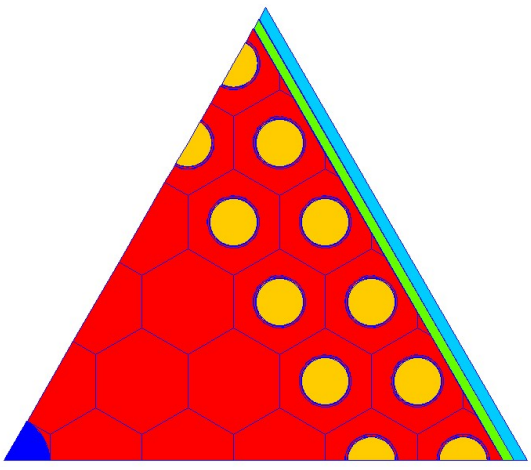

(a) 2 fuel ring

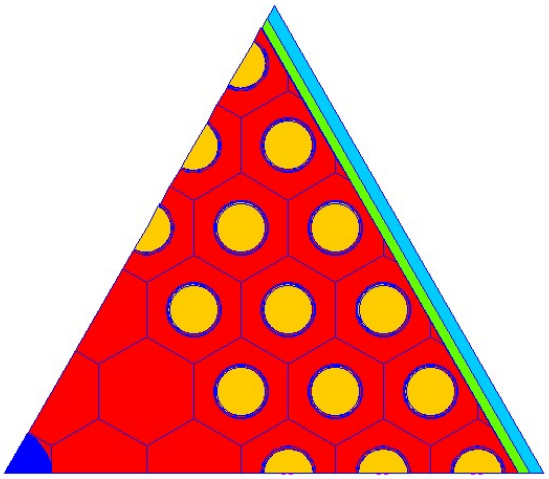

(b) 3 fuel ring

Figure 5.9: Geometries with different number of fuel rings

5.3 Static Calculation Scheme

The static calculation scheme, in combination with the depletion calculation scheme, provides crucial insights into a reactor's behavior, encompassing aspects like neutron transport, cross-section analysis, and the calculation of key neutronic parameters. This comprehensive understanding is foundational for safe and efficient reactor operation. APOLLO2® deterministic code was used to carry on the simulations. The Static scheme in APOLLO2® was adapted from an existing, validated input data set designed for High Temperature Reactors. This adaptation aimed to align it with the new reactor concept. The input data used in the Monte Carlo model for the same type of reactor served as a reference. It is possible to divide the input data script into the following parts:

1. **Material properties**.
2. **Geometry description**.
3. **Self shielding calculation**.
4. **Flux Calculation**.

Material properties
Information about the materials located inside the assembly, including the isotopic composition of each region, is provided in the first part of the input data. Alongside the isotopic composition, the temperature and density are also specified.

Geometry description
Thank to the Silène output TDT file, the information about the entire assembly is transmitted to APOLLO2®. Each medium, created in the previous part, is indicated corresponding to the ones specified in the TDT file.

Self Shielding calculation
Self-shielding calculations were specifically conducted for the isotopes U^{235} and U^{238} due to their prominent resonance absorption cross-sections. In order to conduct this calculation, a new geometry had to be constructed directly in the APOLLO2® input file. This was necessary because self-shielding calculations require a simplified geometry that can be repeated throughout the simulation.

Flux Calculation
The geometry generated through Silène uses the MOC solver TDT. Within the static calculation scheme, a multigroup formalism is applied, which includes a division of 281 distinct energy groups. In the static scenario, the nuclear data library applied is the one from CEA, that involves the library JEFF 3.1.2, a widely accepted compilation of nuclear data. The Joint Evaluated Fission and Fusion File (JEFF) is an evaluated library produced via an international collaboration of NEA Data Bank participating countries.[32]. This library includes a wide spectrum of isotopes and their cross-section data, which is crucial for accurate reactor physics simulations.

Furthermore, in this particular analysis, the self-shielding effect is taken into consideration. This is particularly significant when isotopes with prominent resonance absorption characteristics are involved.

In the Static calculation, several crucial considerations were taken into account. As this scheme was designed for comparison and validation with the Monte Carlo Code, it was essential to ensure coherence with the model developed in Serpent. One significant consideration, in addition to the input data for the material and assembly layout, was to exclude the consideration of neutron leakage not using the axial leakage correction factor. Moreover an infinite medium assumption was adopted.

In the input data file of the static calculation, some options are considered concerning the reactions to take into account. In the macroscopic cross-section library are included: the total cross section considering both the absorption and P0 diffusion cross section, the P0 self-scattering cross section, absorption cross-section, fission cross section, order 0th transport corrected cross section with the transport correction, the diffusion cross sections and the scattering matrices, both of the first order.

5.4 Comparison with Serpent

As mentioned in the Chapter4, a Monte Carlo model was developed in CEA Cadarache with the aim of validate the deterministic scheme developed during this study. A MC model for one assembly was performed considering three different geometries configuration with different handling hole size. In AppendixA is located a brief overview of Serpent code.

It is important to mention that both Serpent and APOLLO2® use the JEFF3.1.2 library[27][33].

The assembly model was built to validate the deterministic model of APOLLO2®. A crucial point is, thus, the differences between these two methods. First of all, as frequently mentioned, the Serpent code is based on Monte Carlo method. It uses statistical sampling techniques to simulate individual histories and tracks neutrons behaviour stochastically. APOLLO2® is a deterministic code and it takes advantages of numerical model to solve the neutron transport equation. Then the nature of the two is completely different and in many cases one is used to validate the other.

To build the static calculation scheme, some approximation were introduced as the energy discretization in multi groups, in particular there were considered **281 energy groups** while Serpent uses a continuous energy approach, meaning that neutrons are treated as having a continuous range of energies. This lead to a more approximated result from the deterministic scheme.

5.4.1 Model and Results

In this subsection, the model created in Serpent will be shown and the resulting physical quantities will be compared.

In Figure 5.10 is shown the Triso particles dispersed in a graohite matrix in the system built in Serpent.

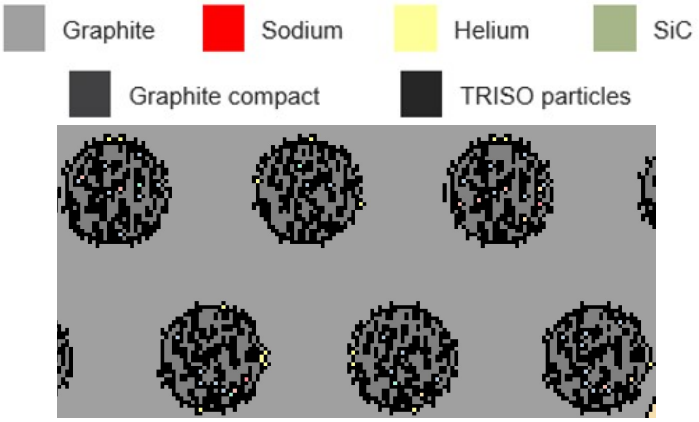

Figure 5.10: TRISO particles dispensed in a graphite matrix

The TRISO particles were created using the "pbed" Serpent card used for explicit stochastic pebble bed geometry definition. A finer description of the method applied is in the AppendixA.

The Serpent model was created considering three geometries with different diameters for the handling hole, as the ones considered in the present study.

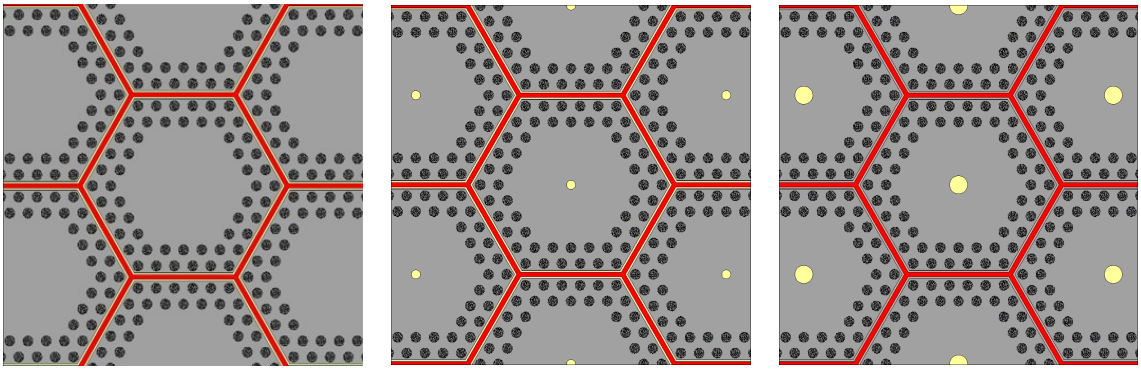

(a) without handling hole (b) with handling hole (c) with larger handling hole

Figure 5.11: Serpent model.

geometry	$\boldsymbol{\rho\,[pcm]}$	$\boldsymbol{k_{eff}}$
N1	26642	1.36318
N2	26592	1.36226
N3	26642	1.36319

Table 5.1: APOLLO2®

geometry	$\boldsymbol{\rho\,[pcm]}$	$\boldsymbol{k_{eff}}$
N1	26847	1.36700
N2	26720	1.36463
N3	26591	1.36224

Table 5.2: Serpent

In the Table 5.1 and 5.2 are shown the reactivity, expressed in pcm, and the effective multiplication factor for each geometries involved.

geometry	$\lvert\rho_{\text{APOLLO2®}} - \rho_{\textbf{Serpent}}\rvert$	**unit**
N1	205	pcm
N2	128	pcm
N3	51	pcm

Table 5.3: Results Comparison

For the sake of clarity and comparison, Table 5.3 presents difference in reactivity of the results to better visualize the discrepancies. Looking the results, it is possible to say that with an increase in the diameter of the handling hole, the discrepancy in reactivity becomes progressively less significant. In conclusion, it is possible to consider the static calculation scheme validated with the Monte Carlo code.

After validating the static calculation scheme, modifications were made to the sodium definition in the input data. This adjustment was necessary due to the implementation of an empirical formula for estimating the sodium density based on temperature and pressure. The input data are the temperature and the pressure. Subsequently, the simulations were re-run to ensure consistency with the analyses. In the Table 5.4 the new results from A2:

geometry	$\rho\,[pcm]$	k_{eff}
N1	27119	1.3721
N2	27070	1.37117
N3	26921	1.36838

Table 5.4: New results of APOLLO2®simulation with the sodium definition in the input data according with the empirical formula

5.5 Depletion calculation scheme

In the evaluation of reactor physics behaviour, one of the key actions is the depletion calculation. The latter includes the evaluation in time of the reactor, in particular it takes into account how the fuel evolves during the normal operation. From those calculations it is possible to evaluate very important physical parameters as the cycle length, the temperature coefficient at the end of life and so on. It gives a very precious overview of how the reactor behaves during operation. In addition the depletion calculations help evaluating the safety of a nuclear reactor. Understanding how the concentrations of fissile and fission products evolve during operation allows for the assessment of safety margins and potential risks. It is possible to collect the concentrations of important fission products as Xe^{135}. From the management point of view, depletion calculations allow to take into account the isotopic composition of spent nuclear fuel. This information is essential for assessing long-term storage and disposal options.

After the construction of the static calculation scheme, the depletion calculation one was performed starting from an input data file suitable for HTR's. The task was to adapt it to the new concept of reactor giving the right information about the medium, geometry, flux calculation, flux normalization, self shielding calculation and evolution of nuclei.

1. Property definitions.
2. Object definitions.
3. Flux calculation and normalization.
4. Self shielding calculation.
5. Burn up step definition.
6. Depletion calculation of a fuel element.
7. Storage of the concentrations.

8. Calculation of fuel concentration at the end of life.

There are some differences to point out between the static calculation scheme and the depletion scheme. First of all, the geometry is defined differently, as each fuel element must have its own name to which the evolution of the fuel will be associated. This takes into account the different position of the fuel element, as the fuel is depleted differently depending on its position in the assembly.
In the Figure 5.12 is shown the depletion geometry, with the reference handling hole size. The medium composition remains identical to that used in the static calculation.

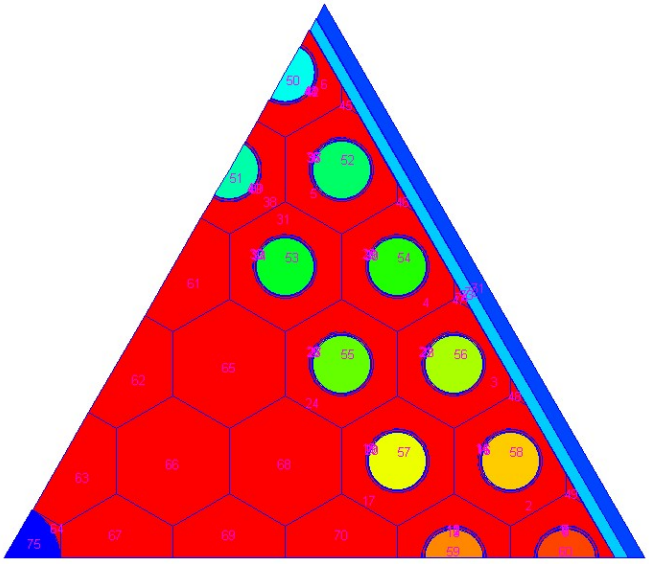

Figure 5.12: Geometry for depletion calculation

5.5.1 Results and validation

For each burn up step considered, the output of the depletion calculation scheme are: infinite multiplicative factor k_{inf}, the migration area $M2$ and the effective multiplicative factor k_{eff}. The latter is imposed to be critic, $k_{eff} = 1$. In the Figure 5.13 is shown the evolution of the infinite multiplicative factor as function of burn up values. A more exhaustive discussion will take place the in Chapter6, when the physical analysis will be carried out.

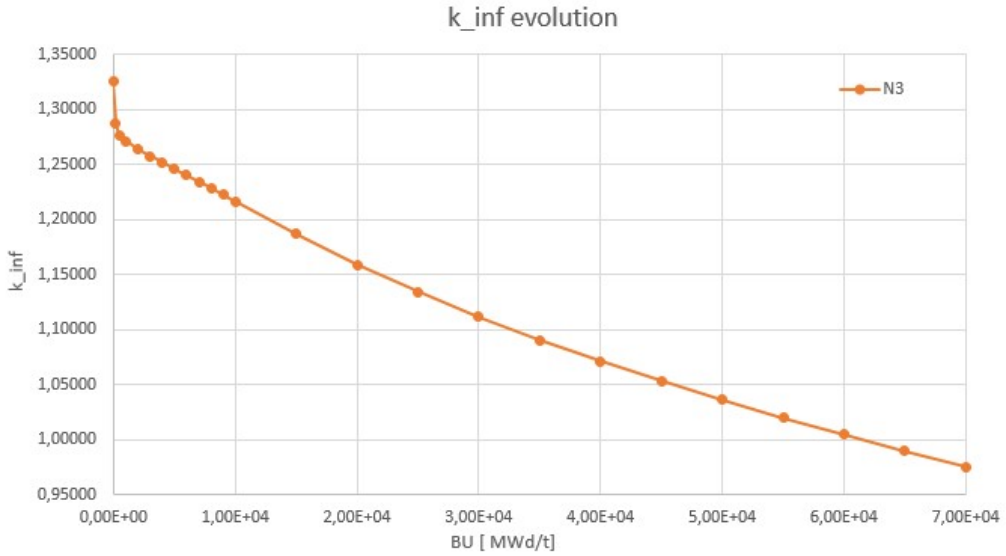

Figure 5.13: Evolution in of k_{inf} for the reference geometry

In depletion calculation the critical buckling B_2 is set to be critical but, to be able to validate it with the static calculation, the option concerning the critical buckling was selected to be coherent with the static calculation.

calculation	$\boldsymbol{B_2}$	**BU [MWd/t]**	$\boldsymbol{k_{eff}}$	$\boldsymbol{k_{\text{inf}}}$
STATIC	NULL	0.0	1.36838	**1.36853**
DEPLETION	NULL	0.0	1.36880	**1.36886**

Table 5.5: Validation Depletion calculation, Critical Buckling imposed Null

As it is possible to see from the table, imposing the Critical buckling B_2 NULL in depletion, the resulting value of k_{inf} is very close to the that found in the static calculation scheme. In this way it is possible to consider the depletion calculation scheme validated.
An important evaluation is performed in the framework of depletion calculation: the verification of the number of burn up steps. With this evaluation the aims is to make sure that the trend of the evolution of the k_{inf} is the same considering the

double of point for the iterations. The calculation was carried out considering the reference number of steps and then doubling them from 10 steps to 20 steps. This was realized by adding 1 step between the burn up point considered. In the Figure 5.14 is represented the trend of the k_{inf} as function of BU considering 10steps and 20steps.

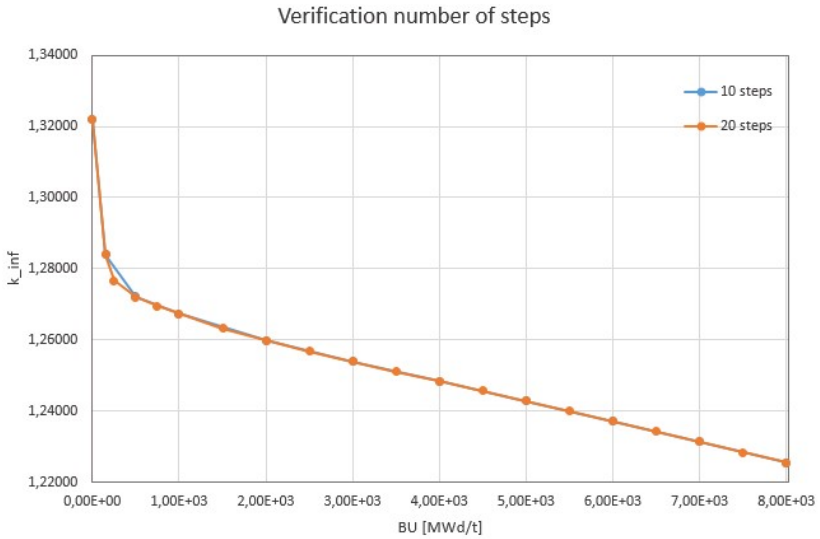

Figure 5.14: Verification number of BU steps in depletion calculation

From the graph above, it is possible to declare that 10 burn up steps are enough to well describe the trend of the infinite multiplicative factor in depletion calculation.

Physical analysis

6.1 Physical analysis goals

In this section are reported all the neutronic parameters evaluated resulting from both static and depletion calculation scheme. The following design configurations are evaluated:

1. The geometries varying the handling hole size.
2. The geometries changing the thickness of the coolant layer surrounding the fuel assembly.
3. Implementation with different fuel isotopic concentrations.
4. The geometries with different number of fuel rings.
5. Replacement of SiC layer with steel and vice versa.

The main goal is to evaluate the reactor behavior considering several design configurations. To be able to understand the reactor behaviour some neutronic parameter were evaluated:

1. Reactivity, effective and infinite multiplication factor.
2. Temperature coefficients for the fuel, moderator and for the coolant.
3. Cycle length.

6.2 Temperature effect definition

The temperature effects play a crucial role in reactor physics, influencing the behavior and safety of nuclear reactors. It quantifies how reactivity changes in response of a variation of the temperature. A positive temperature coefficient means that reactivity increases with temperature, potentially leading to an unstable reactor, while a negative coefficient provides a stabilizing effect. In general a Temperature coefficient is evaluated as:

$$\alpha_f(T_f) = \frac{\partial \rho}{\partial T_f} \tag{6.1}$$

The most important ones are listed[34]:

Doppler Coefficient (α_D): This coefficient measures the reactivity change in response to a sudden increase in fuel temperature. A negative Doppler coefficient is a crucial safety feature. The Doppler effect is linked the Broadening effect regarding the energies at which neutrons are absorbed in resonance.

Moderator Temperature Coefficient (α_M): This coefficient accounts for changes in reactivity due to variations in the temperature of the material used to slow down neutrons (the moderator), such as water or graphite.

Coolant Temperature Coefficient (α_C): It represents the change in reactivity with respect to changes in coolant temperature, considering how coolant properties like density and thermal neutron absorption vary with temperature.

Understanding and accurately predicting these coefficients are essential for reactor safety analysis, transient response studies, and reactor control strategies. In this study Doppler coefficient, Moderator Temperature coefficient and Coolant Temperature coefficient are evaluated for both fresh fuel and depleted fuel, i.e.end of life, in different design configuration.

6.3 Static calculation

In the following sections are listed and commented the neutronic parameters selected to represent the reactor behavior at lattice level. The evaluation were performed considering each design configuration proposed. For the purpose of clarity, the following results interest fresh fuel, with $BU = 0MWd/t$, without considering the neutron leakage, imposing the geometrical buckling to be null.

It is interesting to consider, before going deep in the physical analysis, the average spectra of neutron on the fuel compact.

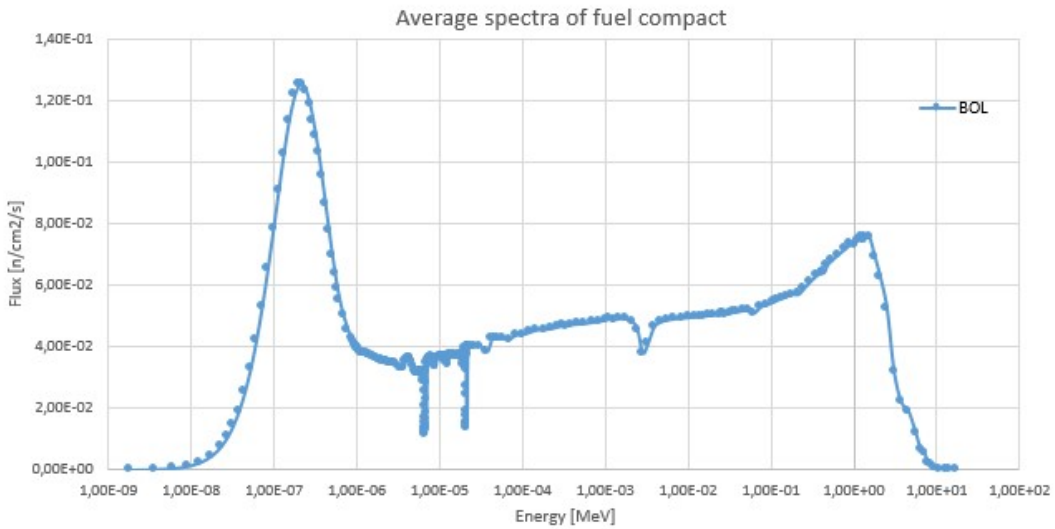

Figure 6.1: Neutron flux at beginning of life (BOL)

The neutron born as fast neutron, then they undergo scattering process within the medium loosing energy. Two strong depressions are visible in the epithermal region due to absorption resonances. Finally the thermal region is visible after the resonances, with energy in the thermal range. To those values of energy the fission event are likelihood to happen.

6.3.1 Reactivity

The first implementation regards the geometries with different handling hole diameters. In the Table 6.1 are listed the reactivity, expressed in pcm, and the effective multiplication factor.

geometry	$\boldsymbol{\rho}\,[\boldsymbol{pcm}]$	$\boldsymbol{k_{eff}}$
N1	27119	1.3721
N2	27070	1.37117
N3	26921	1.36838
N4	20676	1.26065

Table 6.1: APOLLO2® results implementing different handling hole size

As it is possible to see from the Table6.1 the results regarding the first three geometry are very close. The exception is shown for the last geometry, the one with larger central hole diameter. The lower result in reactivity is due to the fact that a big portion of the inner region of the assembly, where the graphite was located, is replaced by helium. This leads to a less fuel thermalization and as consequence a lower value of reactivity.

In the next table are listed the results implementing the geometries in which was been varied the thickness of the sodium layer surrounding the assembly.

geometry	**Na thickness [cm]**	$\boldsymbol{\rho}\,[\boldsymbol{pcm}]$	$\boldsymbol{k_{eff}}$
N3	ref	26921	1.36838
N3	+10%	27101	1.37175
N3	-10%	26750	1.36512
N3	$>> ref$	19845	1.24759

Table 6.2: APOLLO2® results implementing different sodium thickness layer

Considering ±10% of coolant thickness the results change very little, a few hundred of pcm. The interesting result is shown for the geometry with a bigger thickness for the sodium layer. Increasing the layer means increase the amount of sodium within it and couses an increase in the probability for neutron to get absorbed with a consequent reduction in reactivity.

The Table 6.3 is about the same geometry, N3, selected as the reference one, with different fissile content. The fissile content was increased and decreased while keeping the total amount of uranium constant.

geometry	**conc** $[\frac{1}{b\,cm}]$	$\boldsymbol{\rho\,[pcm]}$	$\boldsymbol{k_{eff}}$
N3	ref	26921	1.36838
N3	+10%	27661	1.38238
N3	-10%	26021	1.35173

Table 6.3: APOLLO2® results implementing different fuel isotopic concentration

As it was expected, increasing the fissile content the reactivity increases and vice versa.

The Table 6.4 contains the results considering 2 fuel rings and 3 fuel rings in the outer region of the assembly.

geometry	**n° fuel ring**	$\boldsymbol{\rho\,[pcm]}$	$\boldsymbol{k_{eff}}$
N3	2	26921	1.36838
N3	3	21474	1.27347

Table 6.4: APOLLO2® results considering different number of fuel rings

The results indicate that, despite having the same packing fraction (30%) in both cases, the geometry with three rings exhibits a significant discrepancy compared to the case with two rings. This is likely attributed to the nature of the particle dispersion within the graphite matrix. Having more fissile material located where the graphite was sited leads to a lower reactivity value as the neutrons do not thermalize.

The layers surrounding the fuel assembly are, starting from the inner region towards the outer one: gap of helium, SiC layer, thin steel layer, sodium layer. The last evaluation interested the replacement of the layer of SiC, with steel and vice versa. The aim was to assess the behaviour of the assembly considering either one or the other medium. It's crucial to remember that the self-shielding calculation

was not conducted for the isotopes of steel. This may lead to an underestimation in the subsequent results.

geometry	**material layers**	$\boldsymbol{\rho}\,[\boldsymbol{pcm}]$	$\boldsymbol{k_{eff}}$
N3	Only SiC	27919	1.38733
N3	Only Steel	-10390	0.90588

Table 6.5: APOLLO2® results considering two material for the external layer

In fact, considering only steel in the layers, leads to an under-critical situation. The choice to put a very thin layer of steel between SiC compound and sodium, is due to chemical and structural reasons.

6.3.2 Temperature coefficients

To analyze the temperature coefficients at begging of life, temperature variations were introduced in the static calculation scheme. Specifically, two temperatures were considered relative to the reference temperature: one with +10°C and another with -10°C. The temperature coefficients were calculated in a sequential manner, first by altering the fuel temperature, followed by the moderator temperature, and finally the coolant temperature and density. Furthermore, these computations were conducted for each design configuration, including changes in handling hole size, coolant layer thickness, fuel concentration, rings number as well as substitutions between SiC and steel materials.

First of all is important to assess the sign of the temperature coefficients resulting from these calculation. As is shown in the following sections, the fuel temperature coefficient (or Doppler coefficient) is negative as it was expected. Increasing or decreasing the fuel temperature the reactivity decreases. It is very important to have this behaviour for safety reason. The moderator coefficient is also negative.

Finally, the coolant temperature coefficient is positive. The main reason is related to the fact that having less sodium coolant leads to less absorption of the neutron giving a positive effect.

Taking into account the different the size of the handling hole, in particular increasing the diameter of the central hole, the results in Table6.6, show a bigger Doppler effect for the geometry with the greater handling hole size. This could be due to a less presence of graphite. Since graphite acts as the moderator and is responsible for slowing down (themalizing) neutrons, reducing its presence can result in a greater number of fast neutrons being lost from the system. This can lead to a higher value for the temperature coefficient of reactivity.

Geometry	Fuel conc.	Coolant layer	α_{fuel}	$\alpha_{moderator}$	$\alpha_{coolant}$
N1	ref	ref	**−3.2**	**−0.7**	**0.6**
N2	ref	ref	**−3.2**	**−0.7**	**0.6**
N3	ref	ref	**−3.2**	**−0.7**	**0.6**
N4	ref	ref	**−4.5**	**−0.7**	**0.7**

Table 6.6: Temperature coefficients changing the handling hole size

Geometry	Fuel conc.	Coolant layer	α_{fuel}	$\alpha_{moderator}$	$\alpha_{coolant}$
N3	ref	ref	**−3.2**	**−0.7**	**0.6**
N3	ref	+10%	**−3.2**	**−0.6**	**0.7**
N3	ref	−10%	**−3.2**	**−0.7**	**0.5**
N3	ref	$>> ref$	**−3.4**	**−0.9**	**2.8**

Table 6.7: Temperature coefficients changing sodium layer thickness

Considering different thickness for the sodium layer around the assembly, there aren't strong effect in the the resulting temperature coefficient for the fuel, moderator and coolant except for the last case implemented, with the thickness much larger then the reference one. In fact, as Table6.7 shown, the coolant temperature coefficient tends to rise when it is considered a larger thickness for the sodium layer. This is a predictable effect as increasing the amount of sodium around the assembly, the probability for neutrons to get absorbed became higher.

Geometry	Fuel conc.	Coolant layer	α_{fuel}	$\alpha_{moderator}$	$\alpha_{coolant}$
N3	ref	ref	**−3.2**	**−0.7**	**0.6**
N3	+10%	ref	**−3.1**	**−0.6**	**0.6**
N3	−10%	ref	**−3.3**	**−0.8**	**0.7**

Table 6.8: Temperature coefficients changing the fuel isotopic concentration

The temperature coefficient evaluation is carried out also considering a ±10% of U^{235} fissile amount in the particles keeping the total amount of UO_2 constant, table6.8.Considering a bigger amount of fissile material lead to have a lower fuel temperature coefficient and having lower amount of fissile material leads to a bigger fuel temperature coefficient.

Geometry	**P.f.**[%]	**Fuel conc.**	**Coolant layer**	$\boldsymbol{\alpha_{fuel}}$	$\boldsymbol{\alpha_{moderator}}$	$\boldsymbol{\alpha_{coolant}}$
N3	30	ref	ref	**−3.2**	**−0.7**	**0.6**
N3+1RING	30	ref	ref	**−4.4**	**−0.6**	**0.6**
N3+1RING	22.5	ref	ref	**−3.8**	**−0.8**	**0.6**

Table 6.9: Temperature coefficients changing number of fuel RINGs

The Table 6.9 shows the results about three different calculations, involving the the reference geometry with a reference value of packing fraction, the second calculation including a different geometry, with one rings of fuel in addition (showed in Figure 5.9b in Chapter5). The third calculation is about the same geometry as the latter but with different packing fraction.

In the case with 3 fuel rings and 30% of packing fraction, the fuel temperature coefficient is higher respect the other cases. The reason correlated to this behaviour is due to the presence of more fissile material. This leads to have higher probability for neutron to be absorbed within the assembly and lower chance of escape. The third case instead is performed by considering the same geometry with the packing fraction that leads to the same amount of fuel than in the first case.

The last evaluation regards the substitution of the steel layer with SiC compound and vice versa. It is important to say that the in both static and depletion calculation scheme the self shielding evaluation was not performed considering the isotopes embedded in the steel material. They should be included as most of them have high resonances.

Geometry	**Material**	**Fuel conc.**	**Coolant layer**	$\boldsymbol{\alpha_{fuel}}$	$\boldsymbol{\alpha_{moderator}}$	$\boldsymbol{\alpha_{coolant}}$
N3	only steel	ref	ref	**−4.6**	**−2.2**	**0.6**
N3	only SiC	ref	ref	**−3.2**	**−0.7**	**0.6**

Table 6.10: Temperature coefficients changing material surrounding the assembly

The results concerning the temperature coefficients show a very close behaviour to the reference one when the thin layer of steel is replaced by SiC. On the contrary the considering steel where the SiC were introduced leads to a bigger temperature effect for both fuel and moderator.

6.3.3 Packing fraction

An unexpected behaviour was found in the evaluation of the packing fraction for the reference geometry. The effective multiplication factor and the corresponding reactivity was collected by considering different percentages of the packing fraction. The packing fraction is evaluated as the fraction occupied by TRISO particles in the graphite matrix.

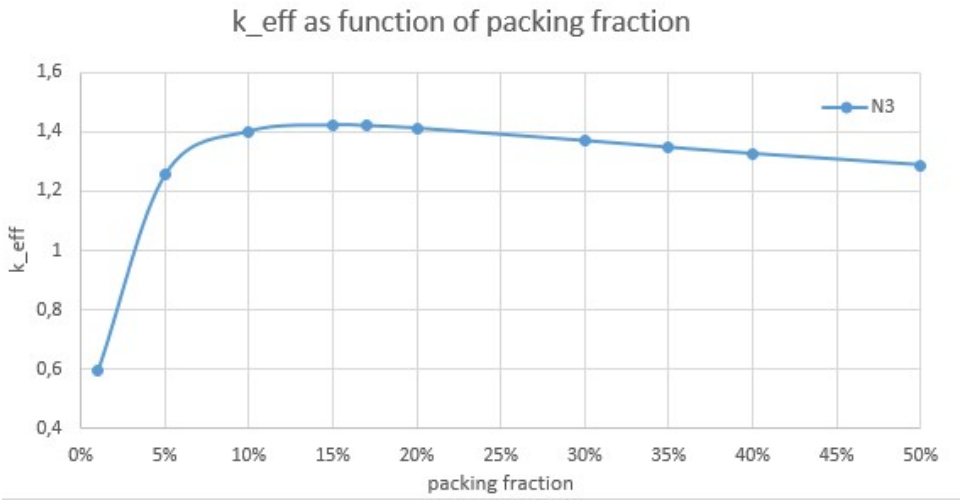

Figure 6.2: k_{eff} as function of the packing fraction

As can be deduced from Figure 6.2, as the number of fuel particles in the fuel compacts increases, the k_{eff} decreases. This is a peculiar behaviour, since a higher value of the effective multiplication factor was expected as the amount of fissile material increases, considering a higher value of the packing fraction. This may be due to the fact that, as the amount of fuel particles within the graphite matrix increases, there is less fuel thermalisation and consequently fewer fission events. This may also be related to the nature of the double heterogeneity of the dispersed particles. After some literature researches, a very important report[35] was found on the Triso particle, in which the effective multiplication factor and the heterogeneity effect, measured in pcm, are compared changing the packing fraction percentage. Considering the Report[35] is possible to assess that the same trend is found during this analysis.

Other evaluations were carried out to assess this behaviour, in particular considering the size of the handling hole and the isotopic concentration of the fuel. The same trend was also found for these evaluations.

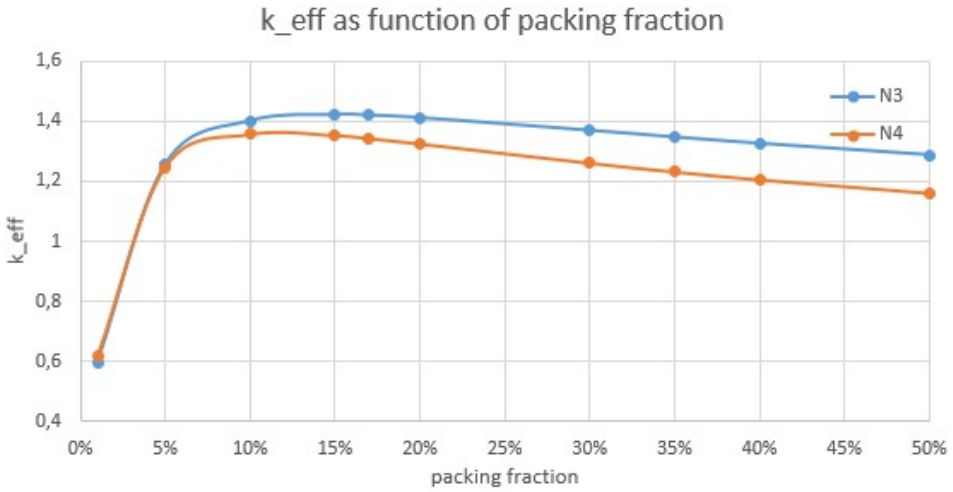

(a) k_{eff} as function of the packing fraction

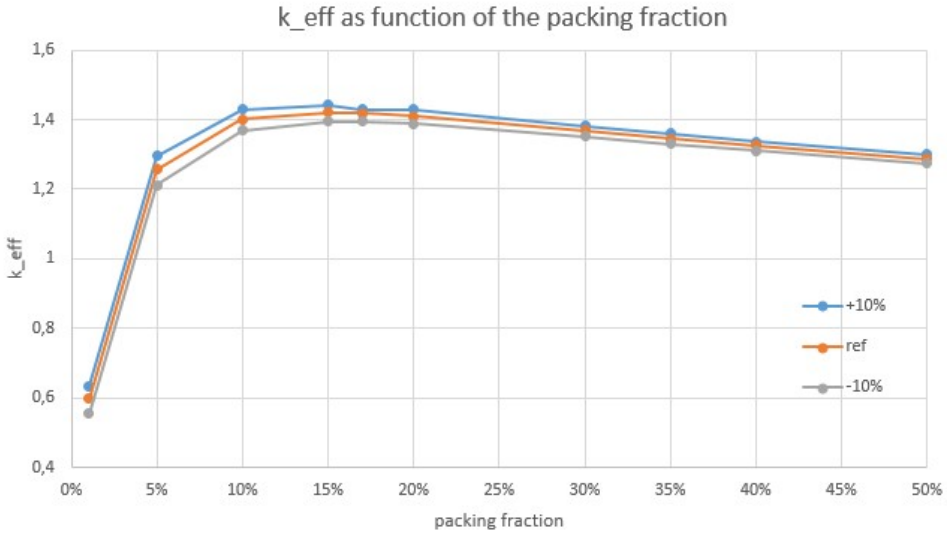

(b) k_{eff} as function of the packing fraction

In both Figure 6.3a and Figure 6.3b, it is possible to observe a distinctive behavior that confirms the variation of the multiplication factor in relation to the packing fraction. This underscores the critical role of packing fraction as a physical and geometric parameter in assembly design. The selection of 30% as the reference value for this parameter is a balance between maximising cycle length and respecting the structural mechanical constraints.

Another two cases were carried out, the fist one, **CASE1**, considering the higher packing fraction while implementing the reference geometry and the second one, **CASE2**, considering the geometry with a fuel ring in addition. Some calculation were done to find the value of packing fraction, for the case 2, such that the amount

of heavy nuclei inside the kernel was the same as the previous case. In the Table 6.11 the results are shown:

CASE	**packing fraction[%]**	**reactivity [pcm]**	k_{eff}
1	50	22316	1.28726
2	37.50	18521	1.22731

Table 6.11: Comparison between 2 and 3 outer ring with the same amount of fuel mass

The Figure 6.4 illustrates the effective multiplication factor plotted vs the mass of heavy nuclei for the two considered cases. The calculations involved the radius and volume of the compact, as well as the packing fraction. This allowed for the determination of the kernel volume by considering the inner and outer layer diameters. The subsequent evaluation of heavy nuclei mass take into account their density. Furthermore, the graph in the Figure 6.4 represents the variation in heavy nuclei mass for different packing fraction values:

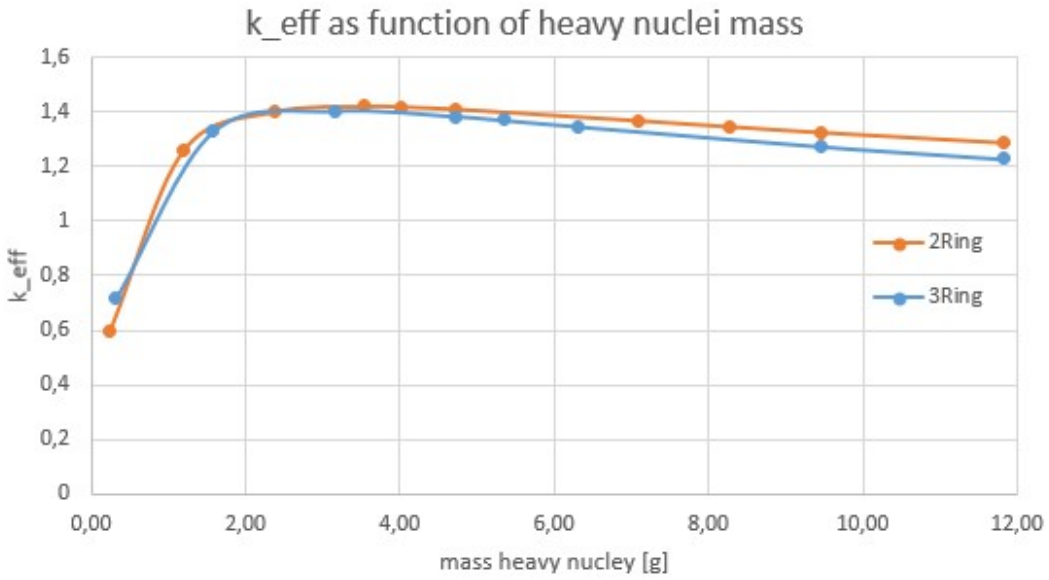

Figure 6.4: Evaluation of the 2cases changing packing fraction

To compare the two results a conversion factor was considered to be able to determine the packing fraction while keeping the same amount of mass. In fact as it is possible to see from the Figure 6.4 the last point for the 2ring case corresponds to 50% of packing fraction and, the blue point for the 3ring correspond to 37.5% one. The result was obtained by considering $(50 * (\frac{9}{12}))$, where 9 and 12 are the number of fuel compacts with respectively 2 and 3 rings.

As the results show, considering a fuel ring in addition with the same amount of fuel mass, the reactivity results lower respect the case with the 2 ring. For information, in the Figure 6.5 is provided the same results in function of the packing fraction.

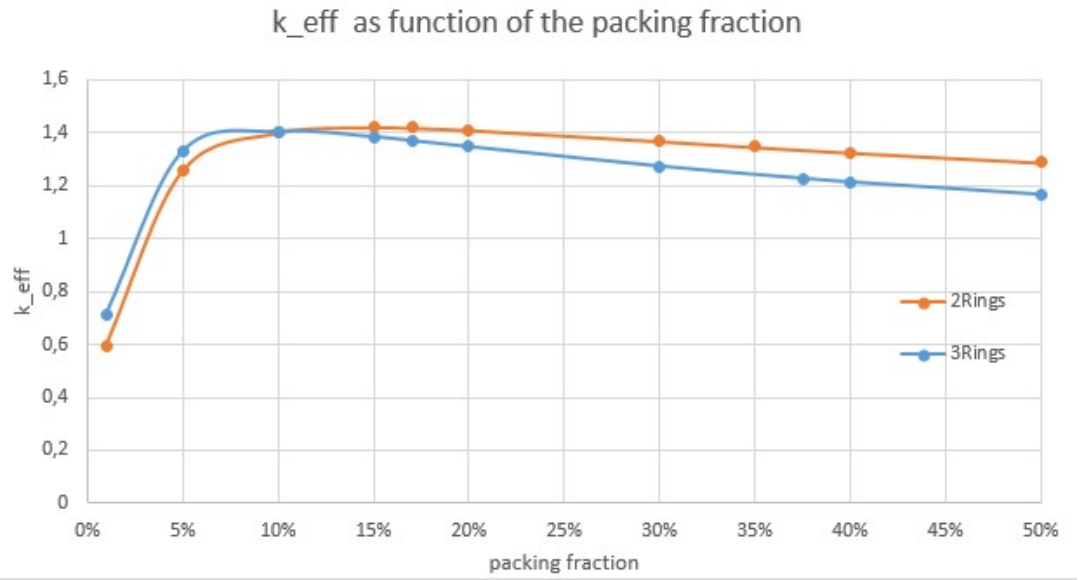

Figure 6.5: Evaluation of the 2cases changing packing fraction

6.4 Depletion calculation

Several evaluations have been performed to assess the behaviour of the assembly considering different geometry configuration and properties condition. In this section is shown all the calculation pointing out the behaviour for each configuration implemented.

Before going on, the average neutron flux is represented in the Figure 6.6 for depleted fuel, at the end of life. In Figure 6.7, instead, a comparison between fresh fuel and end of fuel life is shown.

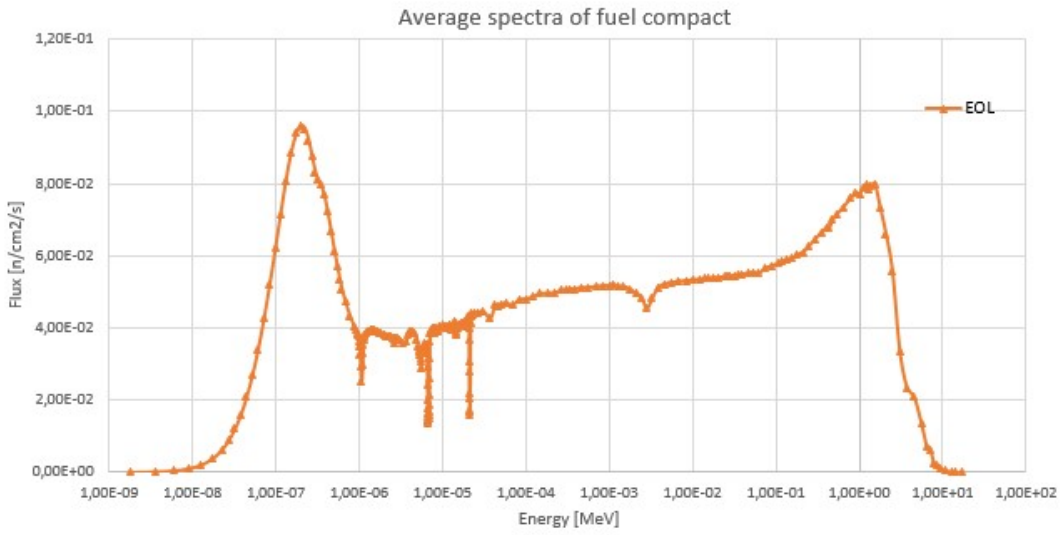

Figure 6.6: Neutron flux at end of life (EOL)

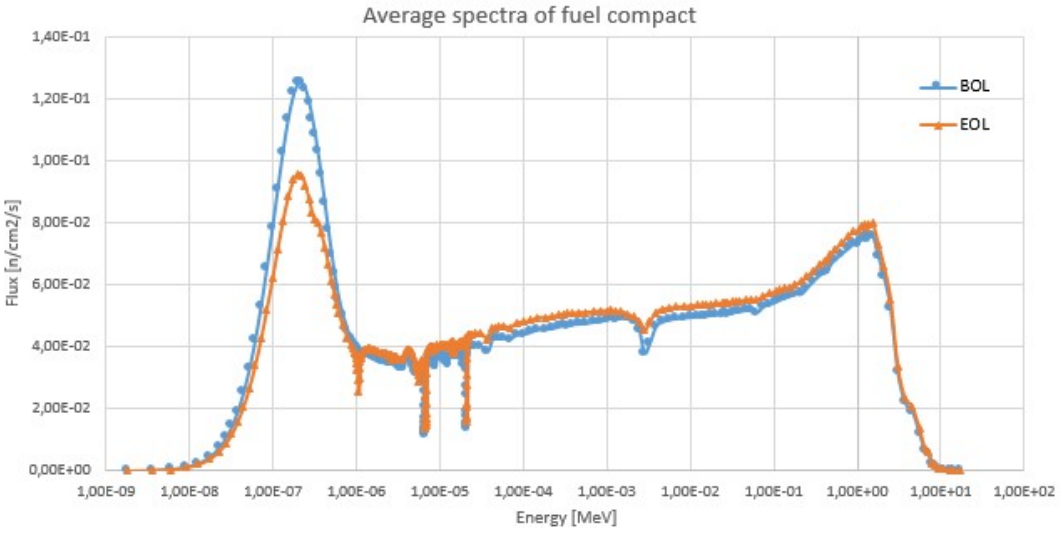

Figure 6.7: Neutron flux comparison BOL and EOL

6.4.1 Evolution of Infinite multiplication factor

In this framework some values of k_{inf} considering the neutron leakages i.e. B_2 imposed to be critical, were collected.. As input for the calculation, the parameter to consider was the **specific power**, imposed to be $200\,W/g_{HN}$ for the reference case. In the Figure 6.8 is represented the evolution of the infinite multiplication factor for different size of the central hole as function of burn up [MWd/t].

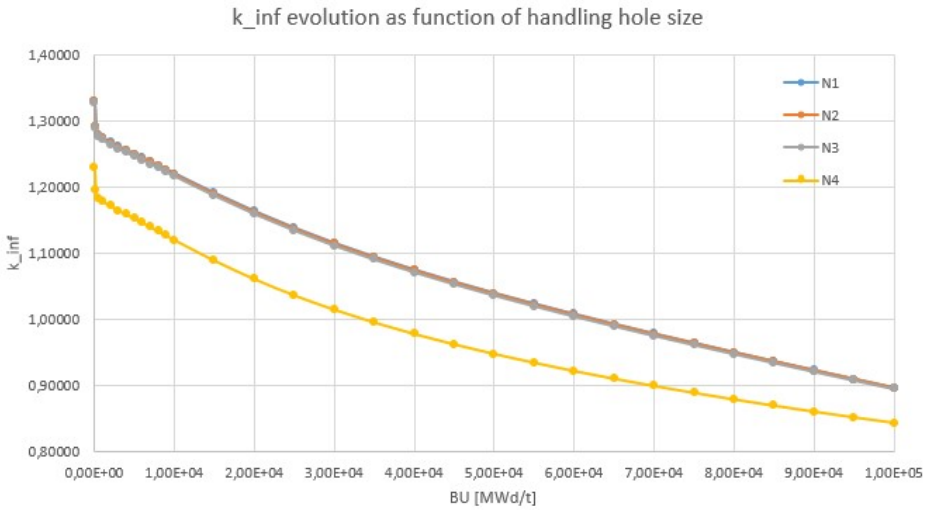

Figure 6.8: Depletion calculation changing handling hole size

Through the graph in Figure 6.8 is possible to understand the behaviour in time, expressed in burn up, of the infinite multiplication factor. The main visible difference is in the geometry N4. The geometry N4, the one with larger diameter for the handling hole, has less graphite material inside the assembly. This contributes to a less effective slowing down process, causing a decreasing in reactivity. Regarding the other geometries, is possible to say that there aren't strong differences as the dimensions are very close to each others.

In the Figre 6.9 the evolution of the k_{inf} as function of the thickness of the sodium (coolant) layer is considered.

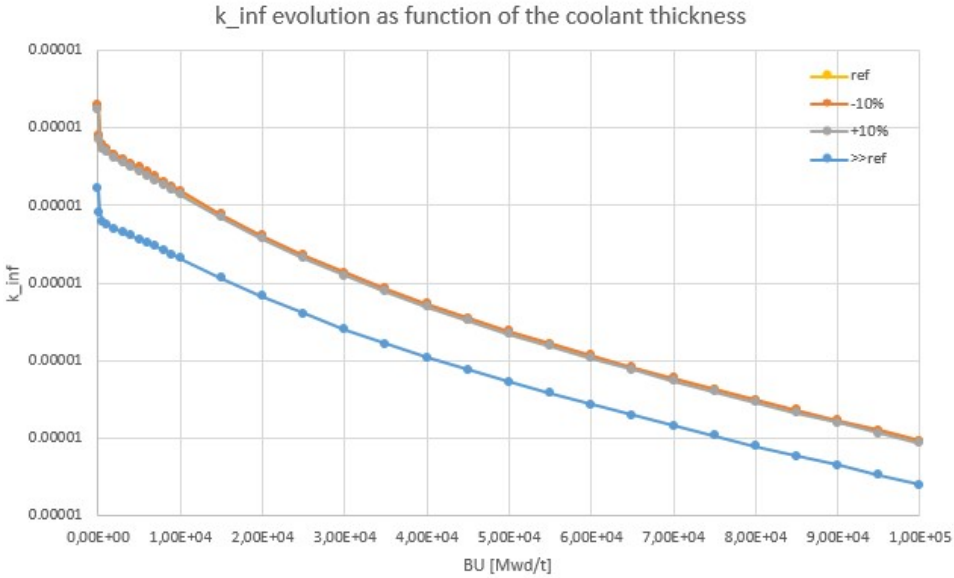

Figure 6.9: Depletion calculation changing the coolant thickness

The results follow the same path as the previous one. A strong impact is visible when a much larger thickness is involved in the geometry. The result is due to a rise in the probability for the neutrons to be absorbed by the sodium nuclei.

The following graph represent the evolution of the infinite multiplication factor considering the reference case, a case with more fissile material and the last one with less fissile content. The calculations were performed while keeping the total amount of uranium constant, in this way a bigger fissile content is followed by a lower fissionable material and vice versa.

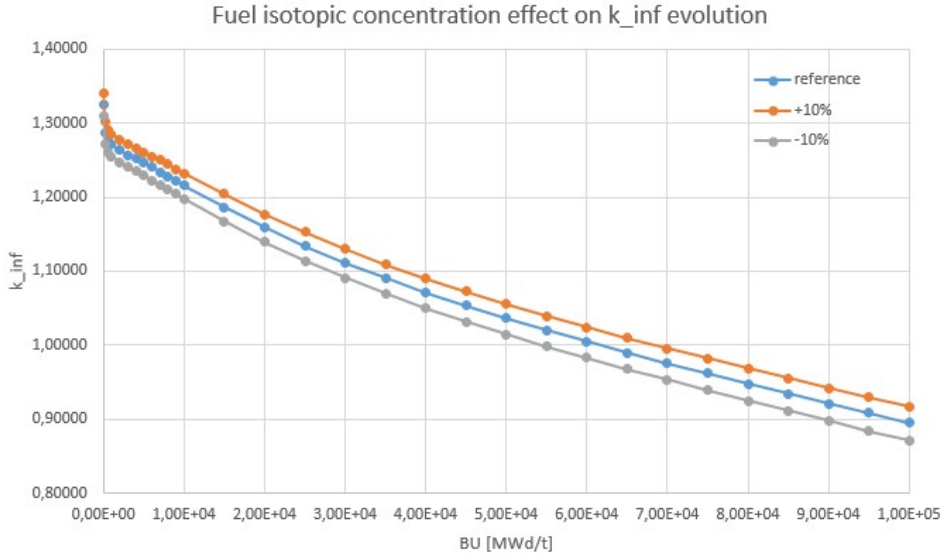

Figure 6.10: Depletion calculation changing fuel isotopic concentration

As it was expected, having less fissile material decreases the probability to have fission event and the results shown an evolution that goes beyond the reference case.

As the exact opposite, the case considering more fissile material, the multiplication factor is higher.

The evaluation of the depletion calculation confronting the reference geometry and the one with 3 rings represented in Figure 5.9b in the Chapter5 is shown. In this case, some considerations about the specific power are necessary. In particular considering the geometry with three fuel rings, it is necessary to adjust the specific power to be able to confront them. To better understand the differences, the Figure **??** shows the evolution of the multiplication factor as function of the burn up step and another as function of the days.

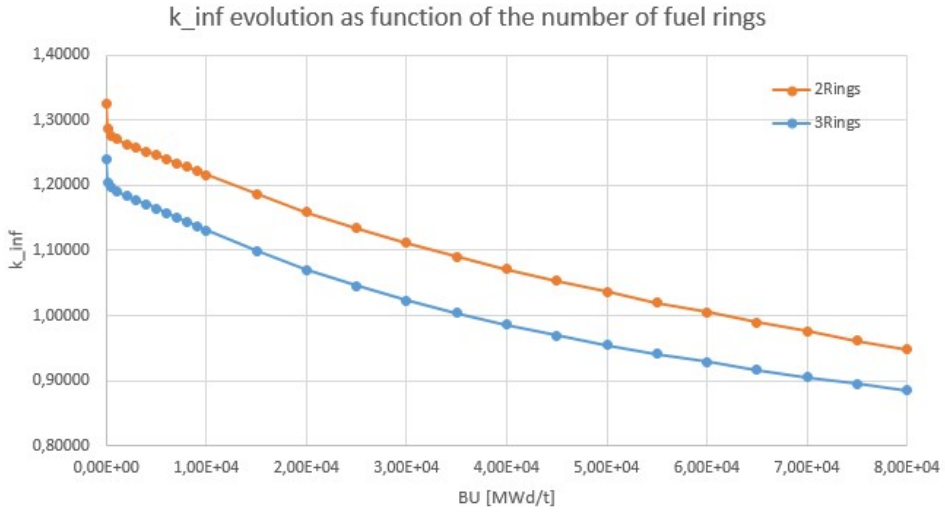

Figure 6.11: Depletion calculation changing the number of rings

The evaluation of the infinite multiplication factor considering different number of fuel rings, same packing fraction and proportional specific power is shown in the Figure 6.11.

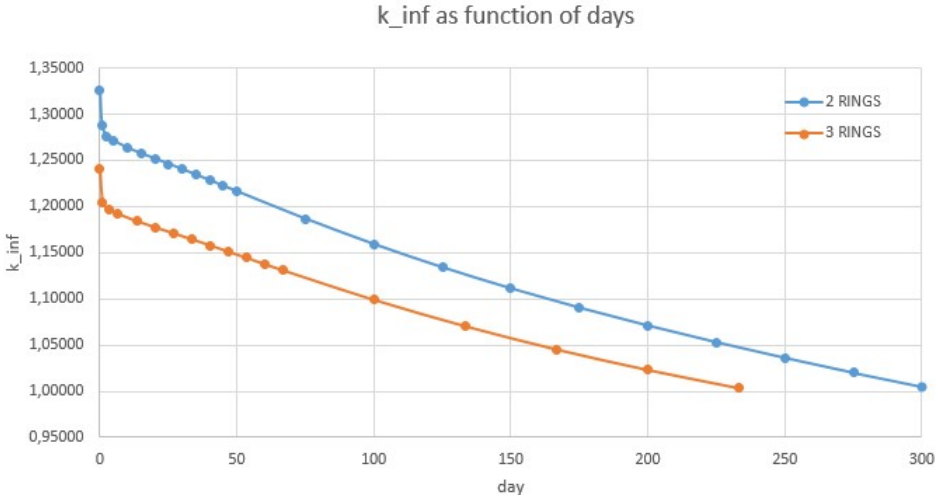

Figure 6.12: Depletion calculation in days changing the number of fuel rings

The last design configuration evaluated interested the replacement of the SiC medium with steel and vice versa in the layers surrounding the fuel assembly. To support the reader, the Figure 5.5 in Chapter5 shown a detail on the layers surrounding the assembly.

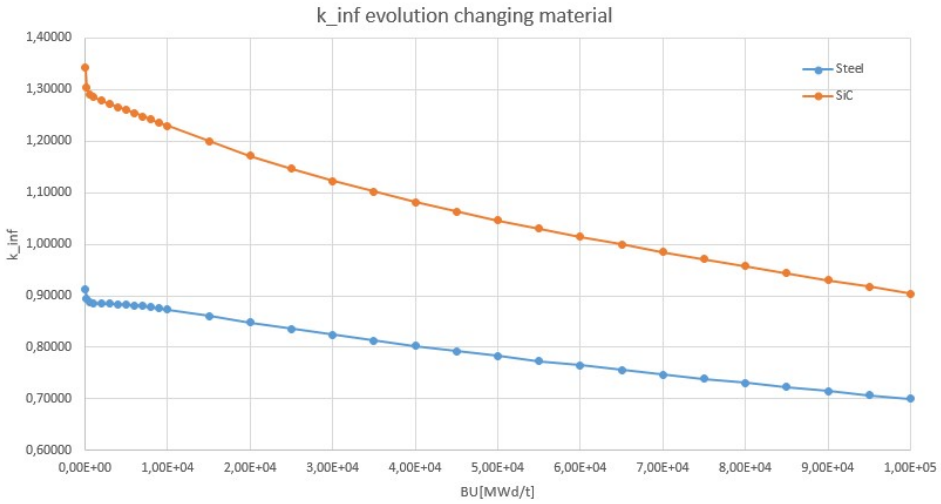

Figure 6.13: Depletion calculation changing the medium in the layers

As discovered during the evaluation of the static calculation scheme evaluation, replacing SiC with steel medium leads to a sub-critical state of the system. This behaviour is also observed in the context of the depletion calculation. It's crucial to recall that, as mentioned earlier, the isotopes of steel were not considered in the self-shielding calculation. This may result in a significant impact on the assessment of reactivity evaluation.

6.4.2 Packing fraction

The further evaluation involves the packing fraction parameter. As already mentioned, the packing fraction parameter has the information about how many particles are embedded into the graphite matrix. Having different packing fraction means that it is necessary to adjust the specific power values to be coherent with the others simulation and to keep constant the total power within the core. For this evaluation were involved three values for the packing fraction. The one chose as reference, 30%, a lower value and a slightly bigger value. The specific power was adapted considering a simple factor: *(reference packing fraction) / (packing fraction to be evaluated)*. It is important, for this evaluation, to consider the conversion between the burn up values and the cycle length, evaluated in EFPD (Equivalent Full Power Day), to better appreciate the differences between the calculations. For this reason, once the value of burn up at the end of fuel life was evaluated, it was possible to calculate the cycle length tanking into account also the specific power. In the Figure 6.14 is represented the evolution of the infinite multiplication factor as function of burn up steps while in Figure 6.12 the same parameter is evaluated as function of the EFPD.

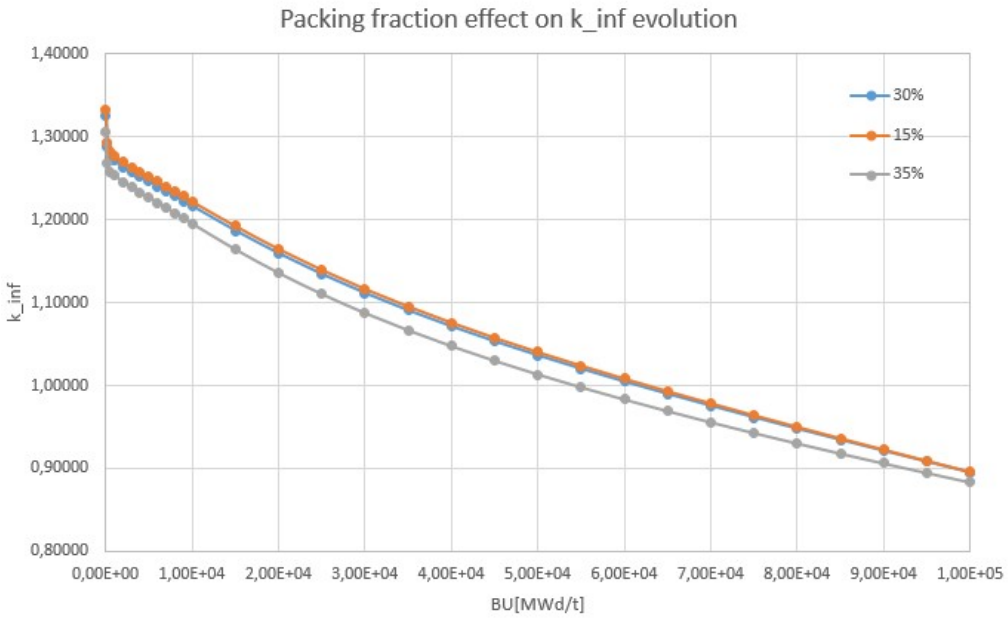

Figure 6.14: Depletion calculation changing the packing fraction

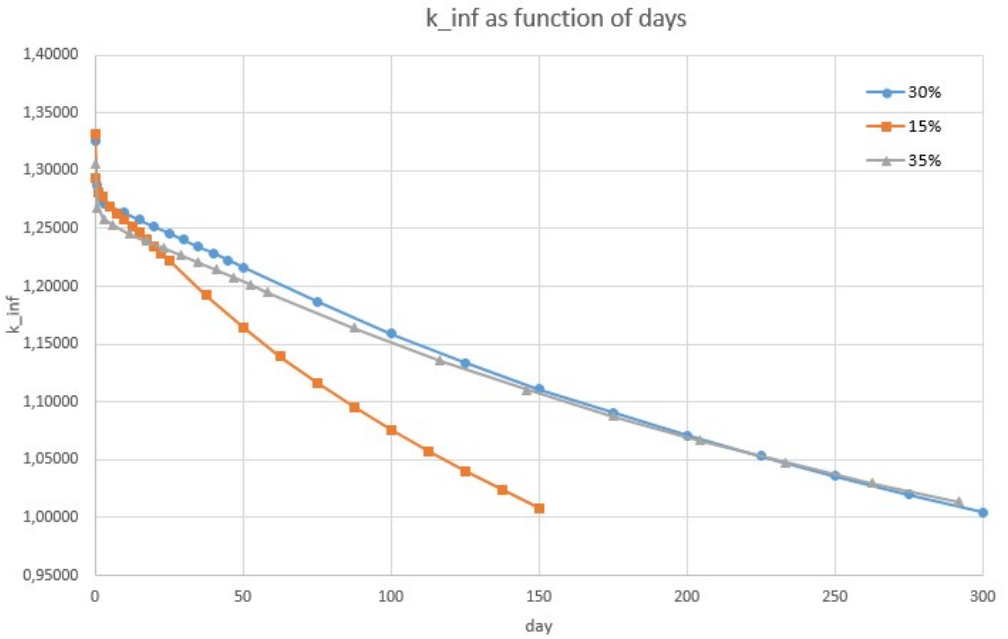

Figure 6.15: Depletion calculation in EFPD changing the packing fraction

As results, the end of fuel life for the case in which the packing fraction of 15% is considered is shorter than for the other two cases. Having lower amount of fuel particles leads to a faster degradation of the matters, resulting in reduced operational time.

6.4.3 Temperature coefficients at EOL

To evaluate the temperature coefficients at end of life, some different schemes were introduced to assess which one of them was the correct one. First of all, since all the results about the evolution of k_{inf} were already performed, the information about the value of burn up at which the reactor goes in under-critical condition was known. Thank to this, some calculation scheme were introduced to try to evaluate different temperature condition at the end of the fuel life. One of these was to perform the flux, after the depletion calculation, recalling the same procedure for the flux calculation imposing different temperature and imposing the neutron leakage to be null as in the static version. This calculation scheme was not the right one as the value of the reactivity was the same after changing the temperature for fuel, moderator and also coolant. The resulting temperature coefficient were all null. After that, another calculation scheme was involved, this time by introducing another input data file in which, as input, where considered all the fission product concentration at the end of life. This new calculation scheme was coupled with a python script to extract for each of the fission product isotopes the correspondent isotopic concentration. Before going on with the evaluation of the temperature coefficient, it was necessary to validate the calculation scheme with the depletion calculation one.
To do so, the same options for the flux calculation were considered, including the neutron leakages and the value of the k_{inf} were compared. The depletion product concentrations were calculated considering a table of burn up in which the number of steps was indicated. This lead to an evaluation of the concentrations not exactly to the value of burn up considered for the flux evaluation. It is an important passage for the understanding of the results. In Table6.12 are shown the result of the two calculations. The new input file is called *Post-processing*.

Scheme	**geometry**	**burn up [MWd/t]**	**fuel conc**	$\boldsymbol{k_{\text{inf}}}$
Depletion	N3	60000	ref	1.00467
Post-processing	N3	61453	EOL	1.00065

Table 6.12: validation of the post processing scheme

As previous mentioned, the concentration of the fuel composition were evaluated considering a value of burn up a bit larger then the one considered for the end of fuel life. It is linked to the different burn up table as input for the depletion calculations. To this is related the difference in k_{inf} values between the calculation. Even with this difference, the values are very close. The Post-processing input file is therefore considered as validated with the depletion calculation scheme.

It was then possible to change the options for the evaluation of the flux to be able to get the effective multiplication factor and the correspondence reactivity. The evaluation of temperature coefficients was performed again by introducing +10°C

and -10°C to the reference temperature. For the sodium density was used the same empiric formula used for the static calculation scheme.

The evaluation interested not all the geometry configurations as in the static one but only for those for which the temperature coefficients for fresh fuel were different with respect in the reference case. So the cases involved in this evaluation were: the reference case, the case with the largest handling hole size, the changes on the fuel isotopic concentration, the larger thickness of the sodium layer and the geometry with three fuel rings.

Geo	**BU**	**IC-BOL**	**IC-EFL**	**Na layer**	$\boldsymbol{\alpha_{fuel}}$	$\boldsymbol{\alpha_{moderator}}$	$\boldsymbol{\alpha_{coolant}}$
N3	6.00E+4	ref	EOL	ref	**−4.4**	**−0.2**	**0.8**
N4	3.00E+4	ref	EOL	ref	**−5.5**	**−0.5**	**0.6**
N3	6.50E+4	+10%	EOL	ref	**−4.3**	**−0.4**	**0.7**
N3	5.00E+4	−10%	EOL	ref	**−4.3**	**0.3**	**0.8**
N3	4.00E+4	ref	EOL	$>> ref$	**−4.2**	**0.7**	**2.9**
N3+1RING	3.50E+4	ref	EOL	ref	**−5.5**	**−0.8**	**0.4**

Table 6.13: Temperature coefficients EOL

Where are indicated: the geometry (Geo), the burn up (BU) value at the end of fuel life, isotopic concentration for fresh fuel (IC-BOL), the isotopic concentration at the end of fuel (IC-EFL), the thickness of the sodium layer, and then the three temperature coefficients respectively for fuel, moderator and coolant. As it possible to appreciate from the Table 6.13, there are some cases in which the moderator temperature coefficient is not anymore negative. This is peculiar of HTGs reactor. Many studies show this behaviours for particular design configuration. It is probable due to the neutron energy spectrum at the end of life.

As the Table 6.14 shown, the results are larger then the ones found for fresh fuel. In the following table the results are compared to the ones evaluated for fresh fuel considering the same design configuration for the reference case.

		BOL	EOL
Ref.case	$\boldsymbol{\alpha_{fuel}}$	$\mathbf{-3.2}$	$\mathbf{-4.4}$
	$\boldsymbol{\alpha_{moderator}}$	$\mathbf{-0.7}$	$\mathbf{-0.2}$
	$\boldsymbol{\alpha_{coolant}}$	$\mathbf{0.6}$	$\mathbf{0.8}$

Table 6.14: Temperature coefficient comparison between fresh fuel and spent fuel for the reference case.

The fuel temperature coefficient at the end of fuel life, is higher than that of fresh fuel.

The temperature coefficient of the moderator is lower at the end of the fuel's life, this behaviour depends on the energy spectrum of the neutrons under these conditions, whereas for the coolant coefficient, there is no actual difference between the two calculations.

Core Calculation

Once the deterministic scheme at the assembly level was built, a core calculation was performed. Before proceeding with the calculation scheme, a preliminary analysis was performed to predict the value of the effective multiplication factor at the core level from assembly calculations. It is important to remind that the assembly calculation scheme was performed using the deterministic code APOLLO2®, instead the core calculation was performed using APOLLO3®. Over the effective multiplication factor, also the cycle length was evaluated.

7.1 Preliminary Core Analysis

This section includes the evaluation of the effective multiplication factor and the cycle length stating from the physical parameters provided as output of the assembly depletion calculation scheme. The analysis will interest different design configuration including: geometry, packing fraction value, fuel isotopic concentration, sodium layer thickness, number of fuel rings.

For each of the design configuration is performed the evolution of the k_{eff} as function of the burn up values. Once the burn up value at which the reactor becomes under-critical is known, the cycle length is evaluated considering the ration between the burn up and the specific core power.

7.1.1 Physical quantities

Before going on describing all the results, it is important to give a brief overview about the physical parameters to evaluate and the ones that are involved for the evaluation.

Geometrical Buckling
The geometrical Buckling is a measure of the neutron leakage. Thanks to this parameter it is possible to quantify the number of neutrons that escape from the core. It is evaluated, for cylindrical core shape, as:

$$B_g^2 = \frac{2.405^2}{R} + \frac{\pi^2}{H} \tag{7.1}$$

where the R is the radius and H the height.[36] As this parameter does not depend on the different design configuration, it is calculated at the beginning and then recall

it for every physical evaluation.

Migration area
The Migration area, also known as the square of the migration length, give the information about the distance between the birth of the neutron and its absorption. In particular it is one-sixth of the square of the average distance between birth and death of the neutron. It is composed by two terms, the *neutron diffusion length* $L^2 = D/\Sigma_a$ that counts the distance between the neutron birth as thermal neutron and its absorption and the *slowing-down length*, often indicated as τ_{th} or L_s^2 and it gives the information about the distance between the neutron's birth as fast neutron and the point where it has become thermalized. It is known also as *Fermi age*. The migration area is an output of the depletion calculation scheme in APOLLO2®, thus depending on the design configuration it assumes specific values for each burn up step.[37]

Core effective multiplication factor
the core effective multiplication factor k_{eff} is estimated starting from the definition of the infinite multiplication factor k_{inf} adding the information about the non leakages probability that is evaluated as:

$$P_{NL} = \frac{1}{1 + M^2 B^2} \tag{7.2}$$

The effective multiplication factor is calculated as:

$$k_{eff} = k_{\text{inf}}\, P_{NL} = \frac{k_{\text{inf}}}{1 + M^2 B^2} \tag{7.3}$$

7.1.2 Geometry

In this first section, the physical analysis considering different geometry configurations is carried out, in particular changing the diameter of the central hole of the assembly. For each geometrical configuration, the evolution of the k_{eff} is evaluated. In Figure 7.1 are summarized all the evaluations, while in Table7.1 are indicated the cycle length values for each geometry. Here also the specific power and the end of life burn up are included.
As pointed out in the physical analysis at the assembly level, the geometry that shows difference with respect the other is the one with the bigger diameter for the handling hole. This behaviour is reflected also at core level. Having less graphite amount leads to have less amount of neutrons that are thermalize. As consequence, the reactivity is lower. Moreover, as it is possible to see from Table7.1, the cycle length for the case in which the geometry N4 is involved, has a very low value with respect the others.

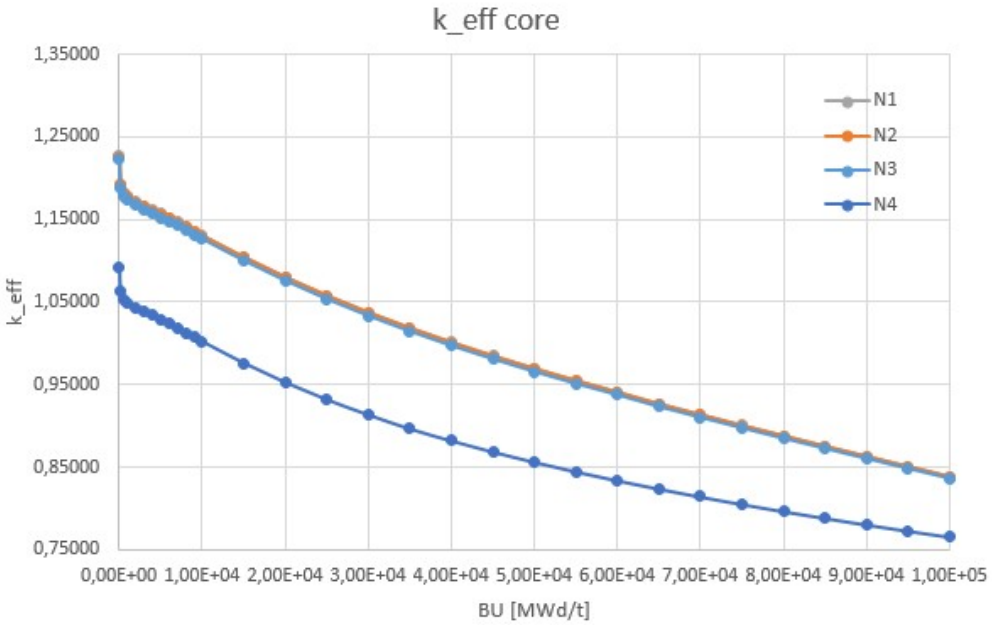

Figure 7.1: k_{eff} evaluation changing the diameter of the handling hole.

Where the trend of the effective multiplication factor cross the ordinate value $y = 1$ the reactor become under-critical. Taking that value, the cycle length is evaluated considering the specific power imposed as 200 W/g. For the geometry N1 and N2 there aren't difference, nether for the burn up at the end of life nor for the resulting cycle length value. Considering though, higher value for the diameter of the handling hole, the cycle length decreases. For the geometry choose as the reference one the cycle length is of 175days.

GEO	**SP [W/g]**	**BU-EOL [MWd/t]**	**CL [EFPD]**
N1	200	4.00E+04	200
N2	200	4.00E+04	200
N3	200	3.50E+04	175
N4	200	1.00E+04	50

Table 7.1: Cycle length changing the diameter of the handling hole.

7.1.3 Packing fraction

For the packing fraction, three different values are evaluated, as were done in the depletion calculation analysis. Selecting 30% as the reference values, 15% and 35% were also evaluated to assess the behaviour of the core effective multiplication factor. As mentioned in the previous chapter, changing the packing fraction value means also adjusting the specific power in order to keep the core power unchanged. Applying this adjustment, in the Table7.2, is possible to appreciate the values of the cycle length, while in the Figure 7.2 the information about the specific power is not visible and it is difficult to catch the differences.

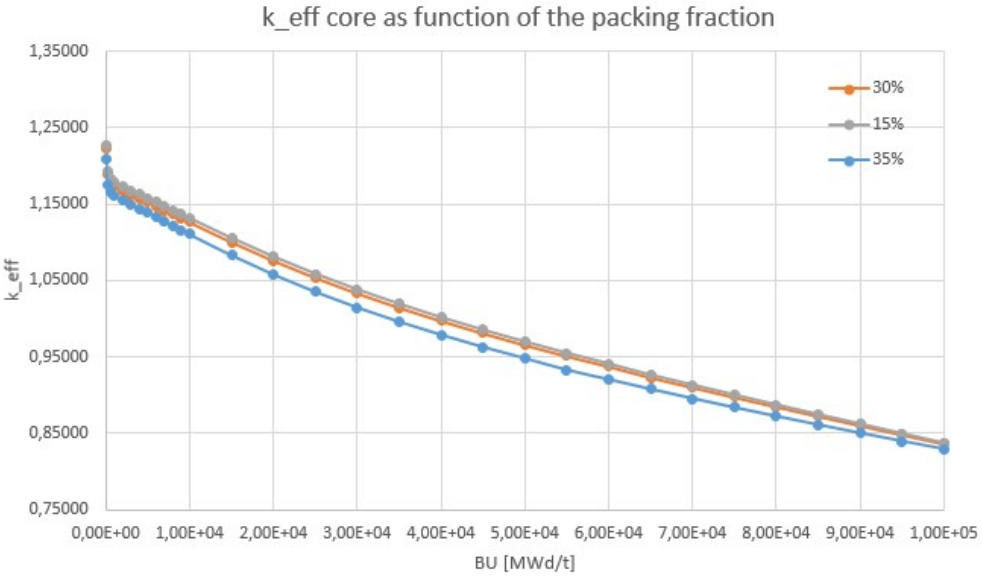

Figure 7.2: k_{eff} evaluation changing the packing fraction values.

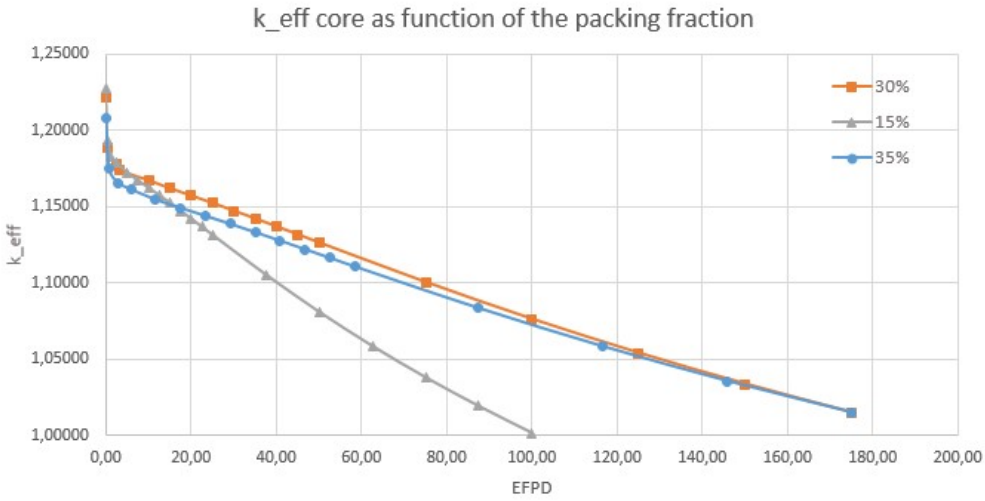

Figure 7.3: k_{eff} evaluation changing the packing fraction values.

GEO	PF[%]	SP [W/g]	BU-EOL [MWd/t]	CL [EFPD]
N3	30	200	3.50E+04	175
N3	15	400	4.00E+04	100
N3	35	171.4	3.00E+04	175

Table 7.2: Cycle length changing the packing fraction

7.1.4 Fuel isotopic concentration

The cases considering more and less content of fissile material, while keeping the total amount of UO_2 constant, is also evaluated. As showed in the physical analysis carried out in the previous chapter, considering more fissile material leads to an increasing in the reactivity and the opposite considering less fissile material. The same behaviour is shown in the Figure 7.4. The cycle length results for the three configuration are showed in the Table7.3.

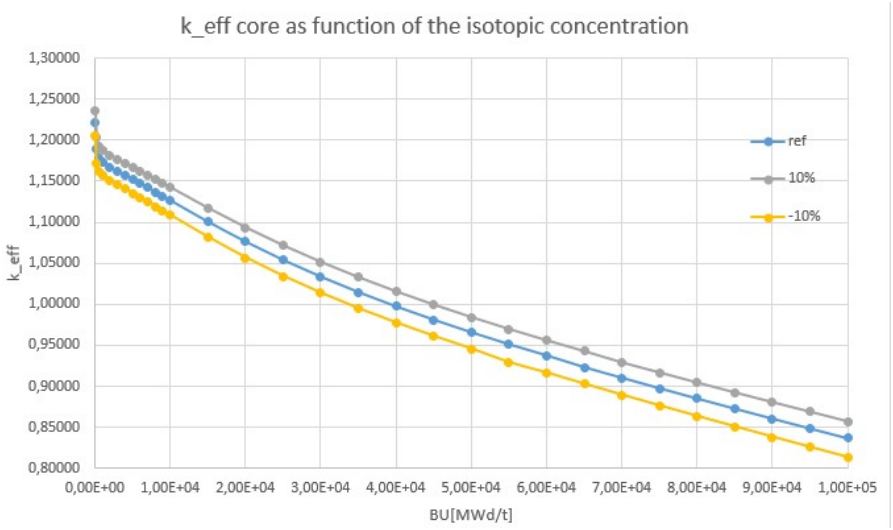

Figure 7.4: k_{eff} evaluation changing the fuel isotopic content.

GEO	IC	SP [W/g]	BU-EOL [MWd/t]	CL [EFPD]
N3	ref	200	3.50E+04	175
N3	+10%	200	4.00E+04	200
N3	−10%	200	3.00E+04	150

Table 7.3: Cycle length changing the fissile content.

7.1.5 Sodium thickness layer

In this subsection are showed the results considering three different configurations regarding the sodium thickness layer surrounding the assembly. As at the assembly level, at the core it is expected to have the same behaviour. In fact as in the Figure 7.5 is shown, the evolution of the effective multiplication factor follow the exact path of the one at assembly level. For the geometry with larger thickness for the coolant region, the reactivity follow a lower trend resulting in a much shorter cycle length. As it is possible to see from the table7.4 all the geometries involved in the calculation shown the same cycle length, the only one that is quite distance is the one with a larger sodium later in between the assembly.

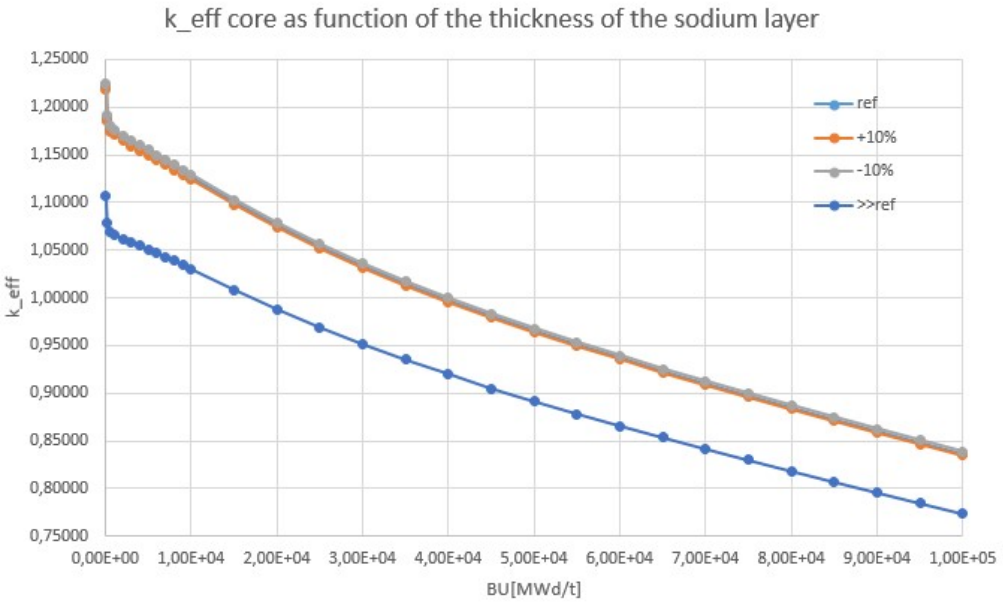

Figure 7.5: k_{eff} evaluation changing the fuel isotopic content.

GEO	Na layer	SP [W/g]	BU-EOL [MWd/t]	CL [EFPD]
N3	ref	200	3.50E+04	175
N3	+10%	200	3.50E+04	175
N3	−10%	200	3.50E+04	175
N3	$>> ref$	200	1.50E+04	75

Table 7.4: Cycle length changing the thickness of the coolant.

7.1.6 Number of fuel rings

In the evaluation of the core effective multiplication factor, in accordance with the depletion calculation scheme, the specif power was adjusted depending on the case evaluated. For this evaluation the geometry involving two fuel rings and the one with three fuel rings are considered. Considering three fuel rings keeping the same packing fraction means lower the specific power. In the Table7.5 are collected the results of the calculation. At core level it is expected to have a lower trend for the effective multiplication factor resulting in a lower value for the cycle length.

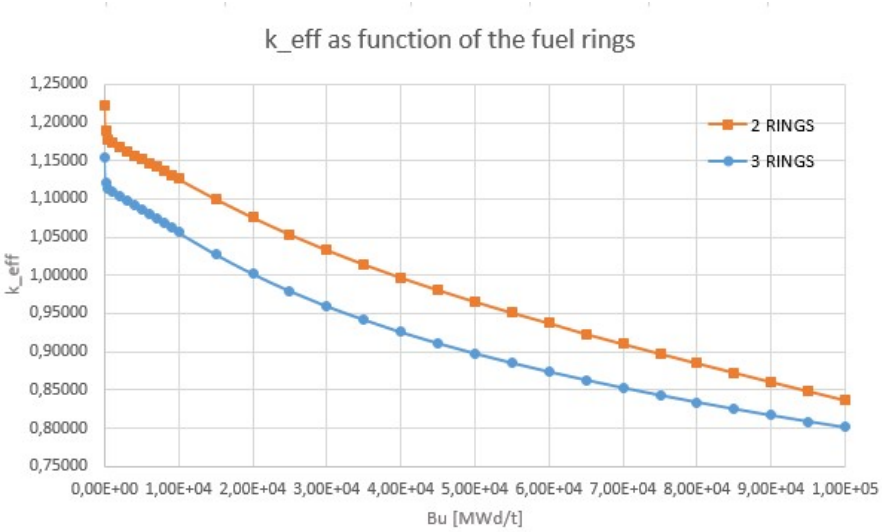

Figure 7.6: k_{eff} evaluation changing the number fuel rings.

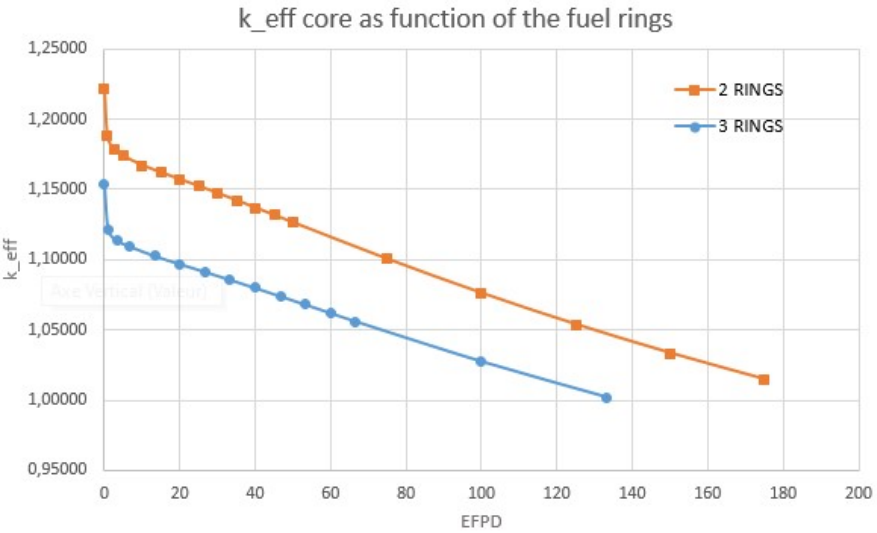

Figure 7.7: k_{eff} evaluation changing the number fuel rings.

GEO	PF [%]	SP [W/g]	BU-EOL [MWd/t]	CL [EFPD]
N3	30%	200	3.50E+04	175
N3+1RING	30%	150	2.00E+04	133

Table 7.5: cycle length changing the packing fraction

7.2 Core calculation

Referring to the logic scheme of this study, in Chapter4, before performing the core calculation, the cross section were created starting from APOLLO2®, creating in this way a bridge between the assembly calculation scheme and the core one. The creation of the cross section libraries of the case studied was performed through the use of the *Saphyb: Module* in APOLLO2®. Thanks to successive call to this module, it is possible to create a library as output containing the a set of elementary APOLLO2® calculation performed under different condition. The output Saphyb libraries can be used for several purposes as the input for other APOLLO2® or APOLLO3® calculations. It is important to know that, given a series of calculation, the results are stored by output regions or macro-regions defined by the user through an output geometry, usually after being collapsed in energy. For each macro-region, the result correlated to particular isotopes selection or groups of isotopes, known as *macros*, are stored indicating which reactions are to be stored for each isotope or macro-group. In general in the input data file the homogenization and condensation process is performed, homogenizing all the media in one and condensing the 281 energy groups in, for this study, 8 groups. For this goal was defined also burnup rate providing the cross section libraries during depletion.[38]

The output file, used then as input for the core calculation performed in APOLLO3®, contain many information[39]. The most important ones are:

1. **General Information**: information about the file and its dimensions.
2. **Physical constants, multigroup mesh**: it contains all the information about the isotopes as their name, radioactive decay constant etc., used in the internal Apolib used in the calculation, together with the multi-groups mesh and the collapsed mesh.
3. **Defining output geometry**: it contains all the output media, their volume and surface values.
4. **Defining the contents**: It contains the isotopes, the definition of the macros and the type of reaction. There are two types of data: the *total macro* contains all of the isotopes for a given medium and the *residual macro* contains all the isotopes that were not selected.

5. **Referencing of cross section**: The multi-groups cross sections (both microscopic and macroscopic) of all the reaction for all the isotopes and macros are stored.

6. **Defining parameters**: in this section are stored all the properties as the temperature, density, concentration of the medium.

7. **Defining an elementary calculation**: it contains all the information about a calculation as the k_{eff}, k_{inf}, B^2.

Once the cross section libraries are created, the core calculation scheme can be built. The core geometry layout was taken from the Serpent model built for comparing the deterministic approach with Monte Carlo code. The core of the HTTR was taken as reference considering one fuel assembly surrounded by control rods. In the Figure 7.8 a sketch of the core is showed.

```
                REF REF REF REF REF REF REF REF
              REF REF REF REF REF REF REF REF REF
            REF REF REF REF REF REF REF REF REF REF
          REF REF REF CTR FAS CTR FAS CTR REF REF REF
        REF REF REF FAS FAS FAS FAS FAS FAS REF REF REF
      REF REF REF CTR FAS CTR FAS CTR FAS CTR REF REF REF
    REF REF REF FAS FAS FAS FAS FAS FAS FAS FAS REF REF REF
  REF REF REF CTR FAS CTR FAS CTR FAS CTR FAS CTR REF REF REF
    REF REF REF FAS FAS FAS FAS FAS FAS FAS FAS REF REF REF
      REF REF REF CTR FAS CTR FAS CTR FAS CTR REF REF REF
        REF REF REF FAS FAS FAS FAS FAS FAS REF REF REF
          REF REF REF CTR FAS CTR FAS CTR REF REF REF
            REF REF REF REF REF REF REF REF REF REF
              REF REF REF REF REF REF REF REF REF
                REF REF REF REF REF REF REF REF
```

Figure 7.8: Core configuration

where with "REF" are indicated the reflectors, with "CTR" the control rods and with "FAS" the fuel assemblies.

It is important to mention that the cross sections for the reflector and the control rods were not created and they were taken from the ones created for HTTR within the SERMA department. The Saphyb files were, instead, created for the fuel assembly, considering the reference configuration with the reference temperature, density and others files varying the temperature by 100°C. The homogenised medium was then implemented in the code together with the information about the reflector and the control rod.

Two distinct schemes were formulated, one for steady state and another for depletion analysis. Several stopping criteria were taken into account, including the one based on k_{eff} to assess the cycle length. The nominal power within the

core was specified as an input parameter. The core evaluation primarily aimed at confronting the results obtained with the preliminary core calculation carried out using the output from APOLLO2®.

7.2.1 Results

The core calculation was carried out to asses the behaviour of the whole core giving the HTTR configuration and replacing the fuel assembly with the new concept design. The reference design configuration is shown in the Table 7.6.

geometry	**PF [%]**	**fuel conc**	**Na layer**
N3	30%	ref	ref

Table 7.6: Fuel assembly configuration

Before going on with the results description, in the APOLLO2® calculations, the specific power value was chosen arbitrary. In the APOLLO3® core calculation scheme, the input is no longer the specific power but rather the nominal core power. The alignment of these two values was necessary to facilitate the complete analysis.

Some calculation were performed in order to evaluate the total core power corresponding to the specific power of $200W/g$ imposed in the assembly calculations. Those calculations included some dimensional parameter as the volume of the kernel in which is located the fuel, the mass and the density of heavy nuclei, the number of active fuel compact and the number of fuel assembly considered in the core. For the latter was considered the core configuration of the HTTRṪhen, the nominal core power found is 88MWth. This values was specified as input data for the core calculation.

In the Figure 7.9 is shown the effective multiplication factor as function of burn up rates for the two calculations, the one performed starting from the output of APOLLO2® at assembly level with non leakage probability factor used and the one performed with Apollo3 for the whole core. The evolution trends show, for both the calculation, a very close behaviour.

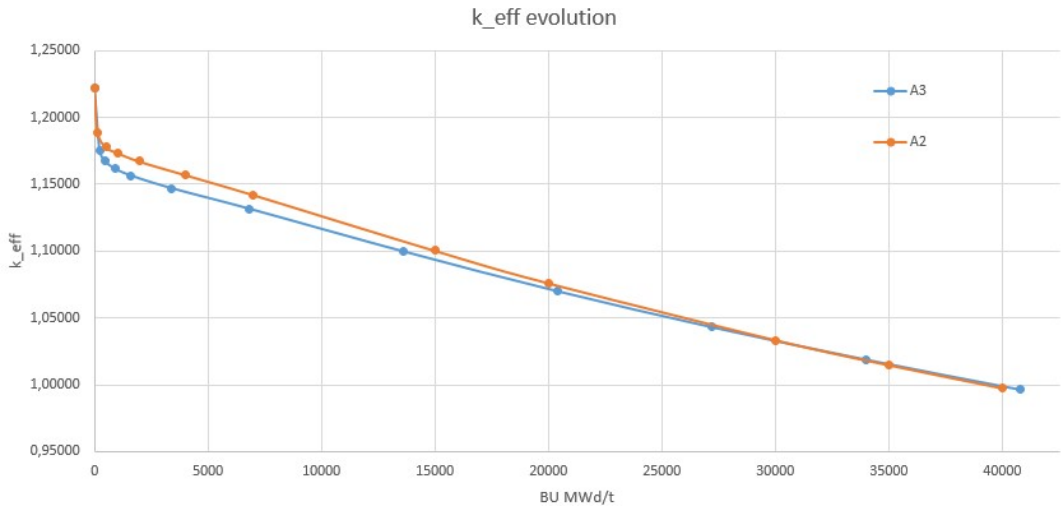

Figure 7.9: k_{eff} core from A2 and A3

After the comparison between the preliminary core calculation and the core calculation itself performed in Apollo3, it is possible to confirm the reactor behaviour at core level.

As mentioned in the previous section, the primary objective of the core calculation is to validate the results derived from APOLLO2® and ultimately determine the cycle length. First of all, starting from the results coming from the preliminary core calculation analysis, a linear interpolation was carried out to assess the value of burnup at which the k_{eff} results to be equal to 1. In the table shown in the Figure 7.10 are listed all the results from the preliminary core calculation.

BU [MWd/t]	k_eff
0,00E+00	1,22205
1,50E+02	1,18857
5,00E+02	1,17801
1,00E+03	1,17376
2,00E+03	1,16719
4,00E+03	1,15715
7,00E+03	1,14214
1,50E+04	1,10038
2,00E+04	1,07606
3,00E+04	1,03341
3,50E+04	1,01469
4,00E+04	0,99734

Figure 7.10: Results from preliminary core calculation for the reference design

Then a linear interpolation was carried out between the last two steps of the

burnup to evaluate the exact value of burnup at which the k_{eff} is critical, resulting:

Average Core Burnup	38633 MWd/t
k_{eff}	1

Table 7.7: Core calculation output

Considering the specific power of $200 W/g$ and the BU at which the k_{eff} is equal to 1, the cycle length was evaluated. In the Table 7.8, the results are shown.

	A2 Core Calculation	**A3 Core Calculation**	**Unit**
Average Core BU	38633	39097	MWd/t
Specific Power	200	200	W/g
Cycle length	**193**	**196**	**EFPD**

Table 7.8: Cycle length comparison preliminary calculation scheme and core calculation

In conclusion, a first evaluation at core level was carried out and the results were compared with the preliminary analysis of the core computed starting from the results at assembly level in APOLLO2®. The effective multiplication factor at core level fits with the one resulting from the core calculation and the resulting values for the cycle length are very close to each other considering the same specific power and evaluating the burnup at the end of life.

Conclusion and perspectives

The objective of this research was to develop a deterministic scheme for an High-Temperature Sodium-cooled reactor. Starting from the core configuration of the HTTR, a new design concept is proposed with the aim to replace the helium coolant, used in the HTGRs, with liquid sodium, to downsize the reactor and to enhance the core density power. A detailed analysis, pointing out the main characteristics of the HTTR, is performed to better understand the advantages, as the use of TRISO particles and the disadvantages, as the non-compactness due to the use of helium coolant. Moreover, special attention is given to the TRISO particles due to their crucial role in retaining fission products and their ability to withstand high temperatures without compromising their integrity.

A static and depletion calculation schemes are developed using the CEA's deterministic code APOLLO2® implementing the MOC, with the aim to have a full understanding of the neutron flux within different assembly configuration and reactor behaviour at assembly level. The designs considered differentiate depending on the size of the handling hole, the thickness of the sodium layer, the fuel isotopic concentration, the number of fuel rings in the assembly and considering a replacement between SiC layer with steel and vice versa. A comprehensive physical analysis was conducted for each implemented design, assessing reactivity, temperature coefficients, and cycle length. This makes possible to understand the dependence of the neutron parameters evaluated considering different configurations. It is important to assess how the reactivity changes considering a larger central hole or considering a less thin sodium layer surrounding the assembly. This information helps in making decisions about which configuration to choose based on specific priorities and objectives.

Important results are collected in this framework, as how the reactivity changes varying the value of the packing fraction. It is demonstrated that increasing the volume fraction of the TRISO particle within the graphite matrix, the reactivity decreases. Such behaviour was completely unexpected. Other important calculations are performed as the temperature coefficients for both beginning and end of fuel life. Though this calculations it is possible to highlight some important aspects, as the positive temperature coefficient of the coolant and the very low value of the temperature coefficient of the moderator. Moreover, a preliminary analysis is considered to predict the effective multiplication factor at core level starting from the results obtained at assembly level. Thought the latter, the cycle length are calculated for each assembly configuration. After assessing the reactor behaviour at assembly level, the

core calculation is performed using the deterministic core APOLLO3®. A comparison between the core calculation results and the preliminary ones was carried out to align the calculation made at assembly and core level using APOLLO2® and later APOLLO3®, allowing the calculation validation.
Further evaluations at the core level could be conducted. This would involve performing calculations to assess the behavior of the reactor, taking into account the entire core, including the fuel assembly, control rods, and reflectors. Additionally, in order to accurately model the design configuration and core layout, it's crucial to determine the cross-section libraries for both reflectors and control rods. Finally, a detailed evaluation of the neutronic feedback effects, such as the temperature coefficient at the core level, would provide a broader understanding of the reactor's behavior.

Serpent

Here a brief overview of what is Serpent code given to the reader. Serpent is a three-dimensional continuous-energy Monte Carlo reactor physics burn up calculation code, developed at VTT Technical Research Centre of Finland since 2004[40][33]. Serpent is a versatile tool primarily designed for lattice physics applications, but it extends its utility to three-dimensional geometries as well. It employs pre-built calculation routines to generate homogenized multi-group constants, crucial for deterministic reactor simulator computations. The standard output encompasses essential parameters such as effective and infinite multiplication factors, homogenized reaction cross sections, scattering matrices, diffusion coefficients, assembly discontinuity factors, point-kinetic parameters, effective delayed neutron fractions, and precursor group decay constants. Furthermore, users can define custom values for computing various integral reaction rates and spectral properties.

One of Serpent's notable capabilities is its internal burnup calculation feature. This empowers the code to simulate fuel depletion as a standalone application. Significant effort has been invested in optimizing the calculation routines, enabling Serpent to execute detailed assembly burnup calculations close to deterministic lattice codes within reasonable time frames. Further reductions in overall computation time can be achieved through parallelization.

Serpent finds application in a range of reactor physics calculations, spanning from pin to assembly and core levels. Its continuous-energy Monte Carlo methodology makes it suitable for modeling several critical reactor types, including both thermal and fast neutron systems.

Serpent best characteristic is that it is continuous-energy[41]. The neutron transport simulation can be carried out imposing a $k - eigenvalue$ or external source. A transient condition can be also simulated.

About the geometry: Serpent is based on a three-dimensional constructive solid geometry (CSG) model, usually used for Monte Carlo particle transport code. The geometry can be built referring to different level of detail. The code is based on universes, transformation and repeated structures as the square and the hexagonal lattice.

For this study is important to mention that an explicit stochastic geometry model is present in the code for handling randomly-distributed particle fuel used in high temperature reactor (HTGR's). The coordinates of individual fuel particle are expressed in another input file and the distribution is modelled without approximation. In Serpent the particles tracking is based on a combination of re-tracing

based surface tracking and the rejection sampling base delta-tracking method. The latter is based on the a rejection sampling algorithm that allows the neutrons to move directly to their next collision without stopping the track at each boundary surfaces. This allows also the a considerable speed-up in the transport simulation. In HTGR's reactor simulation, there is a gain of a factor 10 in performance while for conventional PWRs the factor is of 2.

So the delta-tracking geometry based routine is very well suited for reactor as the high temperature reactor where microscopic fuel particles as the tristructural-isotropic (TRISO) particle fuel.

Bibliography

[1] "Infos génériques CEA et ISAS pour rapport de stage". In: ().

[2] *Nuclear Power in the World Today - World Nuclear Association*. URL: https://world-nuclear.org/information-library/current-and-future-generation/nuclear-power-in-the-world-today.

[3] Stephen M Goldberg and Robert Rosner. "Nuclear Reactors: Generation to Generation". In: *Nuclear Reactors* ().

[4] Redazione. *Sicurezza nei Reattori Nucleari al Sodio: il progetto ESFR-SMART*. Energy — CUENEWS. Sept. 27, 2018. URL: https://www.energycue.it/2018/09/27/sicurezza-reattore-nucleare-sodio/.

[5] Jin Iwatsuki et al. "Overview of high temperature gas-cooled reactor". en. In: *High Temperature Gas-Cooled Reactors*. Elsevier, 2021, pp. 1–16. ISBN: 978-0-12-821031-4. DOI: 10.1016/B978-0-12-821031-4.00001-4. URL: https://linkinghub.elsevier.com/retrieve/pii/B9780128210314000014.

[6] Clement Wong et al. "Helium-cooling in fusion power plants". In: (Jan. 1, 1994).

[7] *Prismatic HTGR*. Ultra Safe Nuclear. Oct. 30, 2023. URL: https://www.usnc.com/prismatic-htgr/.

[8] Kenneth J Geelhood. "PNNL-31427 - TRISO Fuel: Properties and Failure Modes". en. In: ().

[9] Giovanni Bruna et al. *Overview of Generation IV (Gen IV) Reactor Designs - Safety and Radiological Protection Considerations*.

[10] Yuzhou Wang et al. "Thermal properties measurement of TRISO particle coatings from room temperature to 900 °C using laser-based thermoreflectance methods". In: *Journal of Nuclear Materials* 565 (), p. 153721. ISSN: 0022-3115. DOI: 10.1016/j.jnucmat.2022.153721. URL: https://www.sciencedirect.com/science/article/pii/S0022311522002100.

[11] Yusuke Fujiwara et al. "2 - Design of High Temperature Engineering Test Reactor (HTTR)". In: *High Temperature Gas-Cooled Reactors*. Ed. by Tetsuaki Takeda and Yoshiyuki Inagaki. Vol. 5. JSME Series in Thermal and Nuclear Power Generation. Academic Press, Jan. 2021, pp. 17–177. ISBN: 978-0-12-821031-4. DOI: 10.1016/B978-0-12-821031-4.00002-6. URL: https://www.sciencedirect.com/science/article/pii/B9780128210314000026.

[12] Yuji Fukaya et al. “4 - Operation of HTTR”. In: *High Temperature Gas-Cooled Reactors*. Ed. by Tetsuaki Takeda and Yoshiyuki Inagaki. Vol. 5. JSME Series in Thermal and Nuclear Power Generation. Academic Press, Jan. 2021, pp. 257–311. ISBN: 978-0-12-821031-4. DOI: 10.1016/B978-0-12-821031-4.00004-X. URL: https://www.sciencedirect.com/science/article/pii/B978012821031400004X.

[13] International Atomic Energy Agency. *Evaluation of High Temperature Gas Cooled Reactor Performance: Benchmark Analysis Related to Initial Testing of the HTTR and HTR-10*. Text. ISBN: 9789201162038 Publication Title: Evaluation of High Temperature Gas Cooled Reactor Performance: Benchmark Analysis Related to Initial Testing of the HTTR and HTR-10. International Atomic Energy Agency, 2003, pp. 1–352. URL: https://www.iaea.org/publications/6821/evaluation-of-high-temperature-gas-cooled-reactor-performance-benchmark-analysis-related-to-initial-testing-of-the-httr-and-htr-10.

[14] X. RAEPSAET F. DAMIAN. “CALCUL DU BENCHMARK NEUTRONIQUE DE DEMARRAGE DU COEUR HTTR”. In: ().

[15] X Raepsaet et al. “Analysis of the European results on the HTTR’s core physics benchmarks”. In: *Nuclear Engineering and Design*. HTR-2002 1st international topical meeting on High Temperature reactor technology 222.2 (), pp. 173–187. ISSN: 0029-5493. DOI: 10.1016/S0029-5493(03)00026-8. URL: https://www.sciencedirect.com/science/article/pii/S0029549303000268.

[16] Weston M Stacey. “Nuclear Reactor Physics, Second Edition”. In: ().

[17] *Neutron Diffusion Theory — Definition — nuclear-power.com*. Nuclear Power. URL: https://www.nuclear-power.com/nuclear-power/reactor-physics/neutron-diffusion-theory/.

[18] John R. Lamarsh. *Introduction to nuclear reactor theory*. In collab. with Internet Archive. Reading, Mass., Addison-Wesley Pub. Co, 1966. 610 pp. URL: http://archive.org/details/introductiontonu0000lama_v6n7.

[19] Collective participation. *Neutronics*. Internal release from CEA. Section: Energy discretization, pp. 64–65.

[20] I Zmijarevic et al. “Polynomial Characteristics Method for Neutron Transport in 3D extruded geometries”. en. In: (2017).

[21] S Dulla and P Ravetto. “Neutron kinetics equations for APOLLO3 R code and application to noise problems”. en. In: ().

[22] Andrea Gammicchia. “Development and acceleration of a 3D characteristics method including an axial polynomial expansion of cross sections”. en. PhD thesis. Université Paris-Saclay, Sept. 2021. URL: https://theses.hal.science/tel-03406149.

[23] Richard Sanchez. “Renormalized treatment of the double heterogeneity with the method of characteristics”. In: *Proceedings of the PHYSOR 2004: The Physics of Fuel Cycles and Advanced Nuclear Systems - Global Developments* (Jan. 2004).

[24] Masiello Sanchez. "TREATMENT OF THE DOUBLE HETEROGENEITY WITH THE METHOD OF CHARACTERISTICS". In: *PHYSOR 2002* (Oct. 2002).

[25] "Development of neutronic calculation schemes for heterogeneous sodium-cooled nuclear cores in the Apollo3 code : application to the ASTRID prototype". URL: https://theses.fr/2019AIXM0289.

[26] Collective participation. *Neutronics*. Internal release from CEA. Chapter: Main Computer Code, p. 127.

[27] Richard Sanchez et al. "Apollo2 year 2010". In: *Nuclear Engineering and Technology* 42 (Oct. 2010). DOI: 10.5516/NET.2010.42.5.474.

[28] D Schneider, F Dolci, and F Gabriel. "APOLLO3® CEA/DEN deterministic multi-purpose code for reactor physics analysis". en. In: (2016).

[29] Daniele Tomatis et al. "Overview of SERMA's Graphical User Interfaces for Lattice Transport Calculations". In: *Energies* 15 (Feb. 2022). DOI: 10.3390/en15041417.

[30] A. C. Raine and A. W. Thorley. "Reactions between sodium and various carbon bearing compounds". English. In: (May 1980). URL: https://www.osti.gov/etdeweb/biblio/20244555.

[31] Internal release from CEA.

[32] *JEFF-3.3*. URL: https://www.oecd-nea.org/dbdata/jeff/jeff33/index.html.

[33] *SERPENT 1.1.7*. URL: https://rsicc.ornl.gov/codes/ccc/ccc7/ccc-757.html.

[34] John R. Lamarsh and Anthony John Baratta. *Introduction to nuclear engineering*. 3rd ed. Addison-Wesley series in nuclear science and engineering. Upper Saddle River, NJ: Prentice Hall, 2001. 783 pp. ISBN: 978-0-201-82498-8.

[35] Hansol Park et al. *Preliminary Study on TRISO Fuel Cross Section Generation*. English. Tech. rep. ANL/NSE-20/54. Argonne National Lab. (ANL), Argonne, IL (United States), Sept. 2020. DOI: 10.2172/1755935. URL: https://www.osti.gov/biblio/1755935.

[36] *Geometrical and Material Buckling — Definition — nuclear-power.com*. en-us. URL: https://www.nuclear-power.com/nuclear-power/reactor-physics/neutron-diffusion-theory/geometrical-material-buckling/.

[37] *Migration Length - Migration Area — Definition — nuclear-power.com*. en-us. URL: https://www.nuclear-power.com/nuclear-power/reactor-physics/neutron-diffusion-theory/migration-length-migration-area/.

[38] *APOLLO2 : REFERENCE MANUAL FOR VERSION 2.8-5.E*. CEA Internal release.

[39] Igor Wmijarevic. *Structure and content of the Apollo2 output file SAPHYB*. CEA Internal release.

[40] J. Leppaenen. “SERPENT Monte Carlo reactor physics code”. In: INIS Reference Number: 41131393. Hungary: Kiadja and KFKI Atomenergia Kutatointezet, 2010, p. 790. ISBN: 978-963-372-643-3.

[41] Jaakko Leppänen et al. “The Serpent Monte Carlo code: Status, development and applications in 2013”. en. In: *Annals of Nuclear Energy* 82 (Aug. 2015), pp. 142–150. ISSN: 03064549. DOI: 10.1016/j.anucene.2014.08.024. URL: https://linkinghub.elsevier.com/retrieve/pii/S0306454914004095.